NORTHWESTERN UNIVERSITY

Synaptic and Circuit Mechanisms of Orientation Selectivity in Mouse Retina

A DISSERTATION

SUBMITTED TO THE GRADUATE SCHOOL

IN PARTIAL FULFILLMENT OF THE REQUIREMENTS

for the degree

DOCTOR OF PHILOSOPHY

Field of Neuroscience

By

Amurta Nath

EVANSTON, ILLINOIS

September, 2018

Abstract

The mammalian retina harbors more than 30 output channels, each playing a distinct role in processing visual images. A comprehensive understanding of the 'retinal code' primarily relies on the functional knowledge of individual output neurons or retinal ganglion cells (RGCs). Despite recent technical advances in imaging and genetics, the function of some neuron types still remains elusive. We have discovered two new types of RGCs in the mouse retina which perform a fundamental visual computation: orientation selectivity (OS). Reconstructions of dendritic trees of these OS ganglion cells have helped us understand the relation between ganglion cell morphology and OS computation. Furthermore, detailed measurements of synaptic conductances coupled with pharmacological manipulations in these RGCs have shed light into novel circuits in the inner retina. In the process, we have discovered an OS amacrine cell which contributes to feature selectivity in one of the OS RGCs. Overall, this work has discovered new and unconventional mechanisms and offers insights into the mechanism of the OS computation at the earliest stage of the visual system.

Acknowledgements

My graduate school life has been less of a journey and more of an adventure. But before talking about the adventure, I must pay tribute to the people who made it possible. My parents underwent considerable amount of hardships to ensure that I receive quality education and enjoy benefits which they never did. My mother, a research technician, taught me the value of perseverance and discipline at a very young age. Most importantly, it was she who introduced me to the scientific process. I used to observe her working meticulously in lab which developed my inclination towards experimental research. My father, also a research technician, taught me to compete with myself and be a better person everyday. Moreover, he inspired me to be a critical thinker, a hard worker and above all to give back to people who have been the building blocks for what I am today. He also instilled in me a strong sense of optimism which has helped me tremendously in rough times. The bond I share with my parents has made all geographical distances seem negligible. Moreover, I'm incredibly lucky to have close relatives and friends who have been very supportive of my career choices.

Before joining graduate school, Dr. Ron Yu took me under his leadership at Stowers Institute for medical research. I'm forever indebted to him for his immense trust in my abilities and providing me with endless resources for personal and scientific development. His consistent encouragement and motivation really boosted my confidence as a scholar. It is in his lab that I developed an acute interest in systems neuroscience. My exposure to the scientific environment in his lab proved to be an outstanding stepping stone for my academic career.

I recall the first time I met my graduate advisor, Dr. Greg Schwartz in his office; he stated that he wants to "solve the entire retina". Such wild ambition is highly infectious, and it spread like a 'disease' in me. Being Greg's first graduate student, I truly learnt the essential elements of electrophysiology from him and was extremely fortunate to have almost uninhibited access to him whenever necessary. I have often been intrigued by his in-depth knowledge, and his creative yet simple thought processes and experimental design. Over the years, I've tried to imbibe his work ethics and his great attention to detail. He has always strived to bring out the best in me and has praised me for small victories in lab and successes outside. I've constantly felt appreciated as a member of his team and I'll forever be grateful to him for that.

Apart from my mentor, I must credit two postdocs in the lab, Jason and Adam. Jason has taken me under his wing and taught me valuable technical details. Adam has helped me substantially in sharpening my coding and computational skills. For the past few years, I have really enjoyed working with them. They have always lent an ear to my ideas, criticized them and given me valuable feedback. I'm also thankful to our technician Susan, who works tirelessly to keep the lab in shape and is indispensable for the smooth coordination of our experiments. Overall, this lab has become a home away from home for me and I've spent some of my happiest moments here.

"All truths are easy to understand once they are discovered; the point is to discover them." – Galileo Galilei

Table of Contents

Chapter 1. Introduction

A brief history of orientation selectivity

One of the principal goals of systems neuroscience is to understand how various sensory stimuli are integrated in the brain. Most higher-order mammals interact with the external world primarily with the help of visual cues. Visual sensory information undergoes systematic alterations in its representation as it flows along the nervous system because of changes in receptive field (RF) properties of neurons along the pathway. The concept of 'receptive field' first originated in the visual system, where it was defined as the region of sensory space in which a stimulus modifies the response of a neuron (Hartline, 1940). Since then, this concept has been extended to other sensory pathways such as auditory and somatosensory systems. More importantly, the idea of sensory RF has tremendously progressed our understanding of how environmental information is processed and transformed from afferent neurons to the cortex.

In the mammalian retina, incident light is sensed by photoreceptors and undergoes a series of transformations before reaching retinal ganglion cells (RGCs) which are the output neurons. Receptive fields of RGCs are circular with antagonistic center-surround organization (Kuffler, 1953). Although RGCs project to more than 50 retino-recipient brain areas (Martersteck et al., 2017), majority of the axons innervate lateral geniculate nucleus (LGN) and superior colliculus (SC). Almost 90% of the retinal output is received by the LGN in primates (Perry et al., 1984) and is relayed to the first cortical center of visual processing, the visual cortex (V1).

A remarkable set of transformations happen in the neural representation of visual world in V1. Unlike concentric center-surround RFs, V1 neurons exhibit complex RF arrangements. While exploring the uncharted territories of V1, David Hubel and Torsten Wiesel discovered cells which provide null response unless the stimulus orientation matches the neuron's preferred orientation defined by its RF (Fig. 1A, (Hubel and Wiesel, 1962). This dramatic conversion of circularly symmetric to oriented RFs across a single synapse fascinated them and based on their findings, Hubel and Wiesel proposed an elegant feed forward mechanism of OS. According to the model, several LGN neurons with RFs arranged in rows across the visual space provide convergent inputs onto a single simple cell. A stimulus along preferred orientation simultaneously activates more relay cells than a non-preferred stimulus and endows the V1 neuron with the property of OS (Fig. 1B). Since the roots of this striking visual computation emerge at a single synapse between thalamic axons and cortical cells, it is easily tractable and has become a model system for studying synaptic circuitry and neural computation. In the past five decades there has been ample evidence supporting this mechanism in different species (Chapman et al., 1991; Ferster et al., 1996; Lien and Scanziani, 2013; Reid and Alonso, 1995; Tanaka, 1985; 1983).

Besides the feedforward model of cortical OS, several studies have put forward feedback models where intracortical connections serve to sharpen OS tuning (Ben-Yishai et al., 1995) (Adorján et al., 1999; Ben-Yishai et al., 1997; Hansel and Sompolinsky, 1996; Somers et al., 1995). However, according to these models, cortical circuitry rather than LGN relay cells play a central role in OS computation. Supported by experimental evidence (Sclar and Freeman, 1982; Skottun et al., 1987)

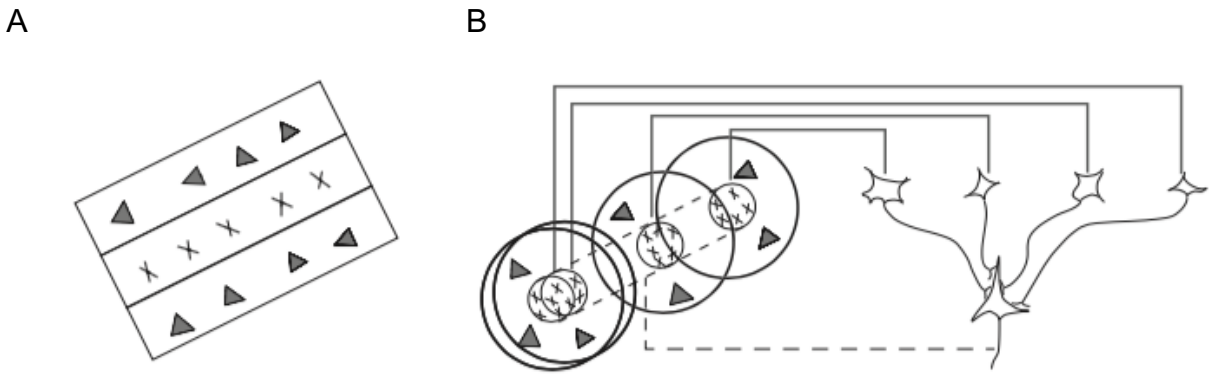

Figure 1. Feedforward model of cortical orientation selectivity.
(**A**) Elongated receptive fields of V1 simple cells with separate ON (black crosses) and OFF (grey triangles) regions. (**B**) The V1 simple cell (right) receives input from multiple LGN relay cells (left) whose ON centers are arranged in a particular orientation in visual space. Adapted from Hubel and Wiesel, 1962.

unsolved by the feedforward model:

(a) The most serious inadequacy of the feedforward model is its inability to account for contrast invariant responses of simple cells to drifting gratings. Feedback models have been able to overcome this (Sclar and Freeman, 1982; Skottun et al., 1987).

(b) Local GABA application for inactivation of a small part of cortical circuit can significantly affect OS of simple cells hundreds of microns away (Crook et al., 1997; Eysel et al., 1990). These observations are easily understood in context of feedback models where cortical inhibition is critical for tuning (Bonds, 1989; Pfleger and Bonds, 1995; Sillito, 1975; Sillito et al., 1980; Tsumoto et al., 1979).

These two models are fundamentally different and the precise mechanism via which cortical orientation selectivity is generated is still being investigated.

Origin of Orientation Selectivity in visual system

While cortex has historically been at the crux of orientation selectivity, there is ample evidence supporting the fact that orientation-selective selective pathways exist in rodents and other mammals upstream of V1. Orientation-selective LGN cells have been reported in cats and primates, including macaques, owl monkeys, and marmosets (Smith et al., 1990; White et al., 1998; Xu et al., 2002), but the tuning is weaker compared to later reports in rodents. Lesions in cat V1 did not significantly alter the tuning or proportion of orientation selective LGN cells (Vidyasagar and Urbas, 1982). A functional imaging study in mouse discovered neurons that encode horizontal axis of motion in dorsal LGN (Marshel et al., 2012). Interestingly, visual cortex was aspirated to expose the thalamus in animals used in this study. Shortly afterwards,

Piscopo et al. (Piscopo et al., 2013) performed extracellular multiunit recordings in LGN and reported both horizontal and vertical OS cells. Based on spatial location of recording sites, it was found that OS units are greatly enriched in the posterior and dorsolateral LGN. In addition to the retinal inputs, LGN cells also receive inputs from several other brain regions, including feedback inputs from layer 6 V1 neurons. Robust OS responses to drifting gratings were recorded in mouse LGN after V1 was silenced by injection of $GABA_A$ antagonist, muscimol (Zhao et al., 2013). Combined with the previous studies, this eliminates the role of cortical feedback in LGN OS computation. Furthermore, this raises the question about the origin of orientation selectivity in V1. Despite clear demonstration of OS in LGN, three counterarguments have been made to challenge its significance in generating cortical selectivity (Ferster, 1987; Ferster and Koch, 1987): (1) only a small percentage of LGN cells are OS cats and monkeys; (2) most cortical cells prefer lower spatial frequencies (Soodak et al., 1987) whereas most LGN cells are only selective at high spatial frequencies; and (3) single cortical cells receive high amount of convergent inputs from LGN relay cells so that any orientation preference in individual LGN cells will probably be averaged out.

At this stage, it is very important to highlight interspecies differences. Firstly, a vast population of LGN cells are OS in mice (Piscopo et al., 2013; Zhao et al., 2013). Secondly, similar spatial frequencies were preferred by mouse V1 and LGN neurons (Zhao et al., 2013). High convergence ratio, however, does not provide any insights into synaptic strengths. Even though a postsynaptic simple cell receives inputs from relay cells tuned to multiple orientations, synaptic strengths may be stronger for inputs that prefer similar orientations, resulting in an

orientation bias. It has been observed that overall orientation preference in individual mouse V1 neurons is dictated by the summation of the heterogeneously tuned synaptic inputs (Jia et al., 2010). This suggests that inputs from orientation selective LGN cells could thus contribute to the overall tuning of simple cells.

The obvious question arises: how does orientation selectivity arise in brain regions receiving postsynaptic inputs from the retina? Marshel et al. (Marshel et al., 2012) proposed a model in which direction-selective (DS) RGCs, long known to exist in mouse retina, converge to form 'axis-selective' LGN cells. A viral trans-synaptic circuit tracing study (Cruz-Martín et al., 2014) demonstrated that DS RGCs send axonal projections to LGN shell in mouse, and further contribute to OS and DS in V1. The convergence of RGC axons to LGN neurons is known to be low (2-3:1; (C. Chen and Regehr, 2000). Any spatial displacement of the presynaptic RGCs' RF centers will potentially lead to an orientation bias in LGN cells. This is probably an unlikely OS mechanism, because more than half of the OS LGN cells have nearly circular RFs (Zhao et al., 2013). Moreover, it has been shown in a recent study (Rompani et al., 2017) that a single LGN cell can receive inputs from up to 91 RGCs! Hence, displacement of receptive fields in visual space is an unlikely mechanism for OS in LGN cells. Blocking GABAergic transmission in LGN dramatically weakened orientation selectivity (Vidyasagar, 1984), and the authors interpreted the data to support the idea that local inhibitory circuits generate LGN orientation selectivity. However, this type of pharmacological manipulation saturates the postsynaptic cell's responses. Inhibition may just play a permissive role in expanding the cell's dynamic range, while the bias to specific stimulus orientations may still be established by excitatory inputs. Zhao et al. (Zhao et al., 2013) instead suggested that OS might originate in the retina and identified putative OS

RGCs in multielectrode array recordings, as did two other groups (H. Chen et al., 2014; Pearson and Kerschensteiner, 2015).

Orientation selectivity has also been reported in the superficial layers of mouse superior colliculus (SC), another brain region that receives direct input from the retina (Ahmadlou and Heimel, 2015; Feinberg and Meister, 2015; Wang et al., 2010). In the zebrafish, orientation selectivity is both inherited from the retina as well as generated locally in the tectum (Hunter et al., 2013). It is not yet known whether the orientation selectivity in the mouse SC is inherited from the retina or computed locally.

Orientation selectivity in the retina

The foundations of OS in the retina were laid shortly afterwards Hubel and Wiesel's seminal work in the cortex. Maturana and Frenk (Maturana and Frenk, 1963) described horizontal edge detectors in pigeons which respond maximally to vertical motion of a horizontal bar or edge (Fig. 2A). Levick (Levick, 1967) documented the responses of two distinct populations of ON and OFF-center RGCs in rabbit (Fig. 2B, C). One class preferred both static and moving bars aligned with the visual streak (horizontally oriented), and a second class preferred vertically oriented stimuli. From loose patch clamp recordings, Levick proposed a simple feedforward model where the inhibitory surround was absent along the preferred orientation axis, leading to (1) flanking inhibitory inputs that only suppressed spiking along null orientations (2) asymmetric excitatory inputs. The circuit mechanisms of OS in rabbit RGCs were first studied by (Caldwell and Daw, 1978), who showed that the $GABA_A$ and $GABA_C$

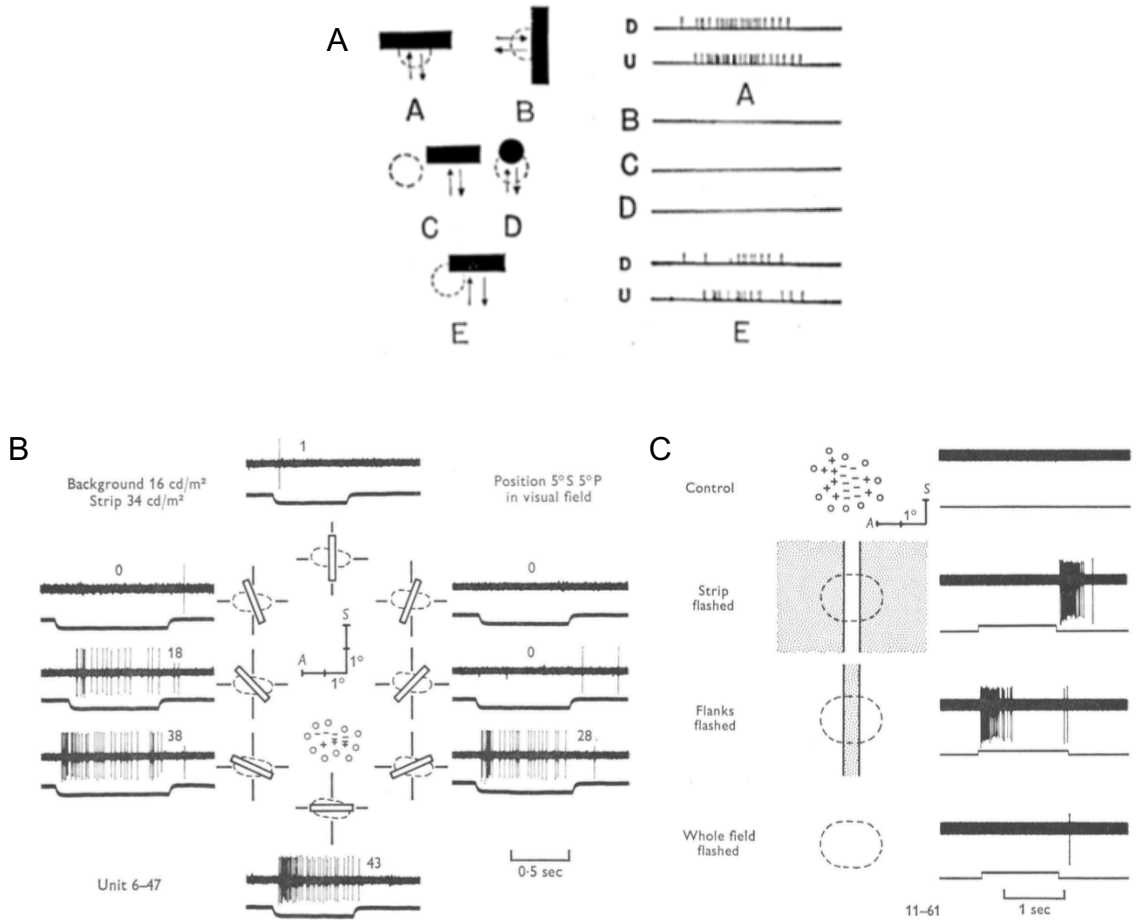

Figure 2. Earliest studies of Orientation selective ganglion cells in the mouse retina. (**A**) Discovery of horizontally tuned OSGCs in the pigeon retina by Maturana and Frenk (1963). In A (right side), the firing of a pigeon OSGC in response to a horizontal bar moving downward (D) or upward (U) is represented. As shown in B, C and D, the same cell does not respond to a vertically oriented bar moving leftward or rightward (B), nor to a horizontal bar presented over the receptive field surround (C), or to a small spot moving over the receptive field center (D). Adapted from Maturana and Frenk (1963). (**B**) Characterization of OSGCs in the rabbit retina by Levick (1967). Spiking responses of a horizontally tuned RGC to light bars of different orientations flashed on the receptive field center. The receptive field center is also represented at the center of the schematic. The '+' symbol indicates responses to a stationary spot at light ON; '–', at light OFF; '±', at both light ON and OFF; 'o', no response detected. The traces show the spiking responses elicited by the bars. (**C**) Spiking responses of a vertically tuned RGC to ON, OFF flashed bars and full field light stimuli. Adapted from Levick, 1967.

receptor antagonist picrotoxin abolished OS spike responses; consistent with Levick's notion. Subsequent work combined intracellular recordings with dye fills of OS amacrine and ganglion cells in rabbit retina and suggested that oriented dendrites could give rise to OS excitation, which could combine with OS inhibition tuned to the orthogonal orientation to enhance selectivity (Amthor et al., 1989; Bloomfield, 1994). Finally, a more recent study used voltage-clamp recordings to show that OS in horizontal and vertical OFF OS RGCs in rabbit relies on presynaptic GABAergic inhibition, but that the two cell types differ in that horizontal OFF OS RGCs receive direct OS inhibition (tuned to the null orientation), whereas vertical OFF OS RGCs are instead influenced by a disinhibitory circuit that reduces tonic inhibition in the preferred orientation (Venkataramani and Taylor, 2010).

Retinal orientation selectivity has been reported in a myriad of other vertebrate species. These include macaque (Passaglia et al., 2002), cat (Levick and Thibos, 1982; 1980; Shou et al., 1995), turtle (Sernagor and Grzywacz, 1995), goldfish (Damjanović et al., 2011; Damjanović et al., 2012; Johnston et al., 2014; Johnston and Lagnado, 2015), and zebrafish (Nikolaou et al., 2012; Antinucci et al., 2013; Antinucci et al., 2016; Lowe et al., 2013).

There exists an enormous body of literature based upon genetic, morphological and functional classification of mouse RGCs (Badea and Nathans, 2004; Coombs et al., 2006; Doi et al., 1995; Farrow and Masland, 2011; Kong et al., 2005; Sanes and Masland, 2015; Sun et al., 2002; Sümbül et al., 2014; Völgyi et al., 2009). A recent study identified several functional RGC clusters showing OS, but did not assign these clusters to putative RGC types (Baden et al., 2016). OS RGCs are notably absent from a large-scale physiological classification of mouse RGCs (Farrow and Masland, 2011) and no cell type with consistently oriented dendrites was found in

two large morphological RGC classifications (Sümbül et al., 2014; Völgyi et al., 2005). Three other groups (H. Chen et al., 2014; Pearson and Kerschensteiner, 2015; Zhao et al., 2013) found OS responses in multielectrode array recordings from mouse retina, but were not able to attribute the responses to a particular RGC type or to discount the possibility that some of the recorded units were displaced, spiking amacrine cells (ACs).

In the rabbit retina, three OS amacrine cell classes have been found. Bloomfield (Bloomfield, 1994; 1991) characterized two classes of ACs showing tuning for cardinal orientations. One group comprises wide-field ACs with long, radially extending neurites in which OS appears to arise through an asymmetric inhibitory mechanism. The second group consists of medium-field ACs with highly asymmetric and elongated dendritic tree that were classified as 'orientation-biased'. A third class of OS cells was characterized recently by Murphy-Baum and Taylor (Murphy-Baum and Taylor, 2015) which consists of polyaxonal, wide-field ACs with ON response polarity and cell bodies displaced in the ganglion cell layer. They are consistently tuned to horizontally oriented visual stimuli. Antinucci et al. (Antinucci et al., 2016) found two types of OS amacrine cells in the larval zebrafish retina. These cells exhibit highly elongated dendritic fields and cardinal and oblique orientation preferences are represented in both types. Finally, we have reported a type of OFF OS amacrine cells in the mouse retina (Nath and Schwartz, 2017; chapter 3) which prefers vertical orientations and shares morphological homology to previously reported rabbit and fish ACs (H. J. Wagner and E. Wagner, 1988; Famiglietti, 1989; Bloomfield, 1994; 1991; Hoshi and Mills, 2009).

We have studied the light response profiles of various mouse RGCs to different stimuli and found ON (Chapter 2) and OFF OS (Chapter 3) RGCs tuned to both stationary and moving

stimuli. Moreover, we were able to demonstrate that these RGCs form distinct functional cell types. With the help of cell-attached, whole cell electrophysiological recordings and two-photon and confocal imaging techniques we have unraveled novel mechanisms of orientation selectivity in the retina.

The outline of the rest of the dissertation is as follows. Chapter 2 focusses on the light response profiles, morphology and mechanism of OS computation in ON OS RGCs based on a published paper (Nath and Schwartz, 2016). A novel OS mechanism is reported in chapter 3 based on work on OFF OS RGCs (Nath and Schwartz, 2017).

Chapter 2. Cardinal Orientation Selectivity is Represented by Two Distinct Ganglion Cell Types in the Mouse Retina

Introduction

Orientation selectivity (OS) is one of the fundamental computations of the mammalian visual system. In 1962, Hubel and Wiesel (Hubel and Wiesel, 1962) discovered neurons in primary visual cortex (V1) of the cat that respond selectively to bars of light in a particular orientation. They proposed a mechanism in which several concentric receptive fields in lateral geniculate nucleus (LGN) converge onto a single neuron in V1 and the specific wiring patterns of these feedforward connections endows the V1 neuron with OS. Although both classic and modern work (Lien and Scanziani, 2013) has identified an OS mechanism in selective wiring from lateral geniculate nucleus (LGN) to primary visual cortex, OS responses have now been found upstream of cortex in mouse LGN and superior colliculus, suggesting a possible origin in the retina.

OS retinal ganglion cells (RGCs) have been reported in rabbit (Amthor et al., 1989; Bloomfield, 1994; Caldwell and Daw, 1978; He et al., 1998; Levick, 1967; Venkataramani and Taylor, 2010) (Venkataramani and Taylor, 2016) and also in macaque midget and parasol RGCs (Passaglia et al., 2002). A recent study identified several functional RGC clusters showing OS, but did not assign these clusters to putative RGC types (Baden et al., 2016). OS RGCs are notably absent from a large-scale physiological classification of mouse RGCs (Farrow and Masland, 2011) and no cell type with consistently oriented dendrites was found in two large

morphological RGC classifications (Sümbül et al., 2014; Völgyi et al., 2005). A distinct functional OS RGC type has not yet been characterized in the mouse retina.

We have discovered two OS RGC types in the mouse retina that represent the horizontal (nasal–temporal) and vertical (dorsoventral) axes of the visual field. We have characterized the response properties and morphology of these RGC types and explored the synaptic mechanisms giving rise to the OS computation in the retina. Our studies thus prove the existence of a dedicated OS circuit in the mouse retina and form the basis for future investigations of how retinal OS signals influence downstream brain areas and behavior.

Results

Functional characterization of ON OS RGCs

We performed a large-scale screen of the light response properties of mouse RGCs recorded individually in cell-attached configuration. In total, we report recordings from 146 RGCs from 67 retinas (41 mice). As part of our functional screen, we encountered a set of RGCs with a distinct spiking pattern to a 1 s step of light from darkness confined to the RF center (see Methods). These newly identified RGCs responded with a sustained volley of spikes at light onset, but details of the spike pattern were distinct from two other known sustained ON RGCs (Fig. 1A). These cells responded with a brief burst of spikes followed by a pause and then a sustained discharge throughout the step. The details of this light response, most notably the pause between transient and sustained spike responses, were unique to these RGCs. For all ON and ON-OFF RGCs recorded, we measured the peak transient firing rate (within the first 200 ms) and the maximum interspike interval (ISI) (averaged over trials, Methods) during the 1 s light

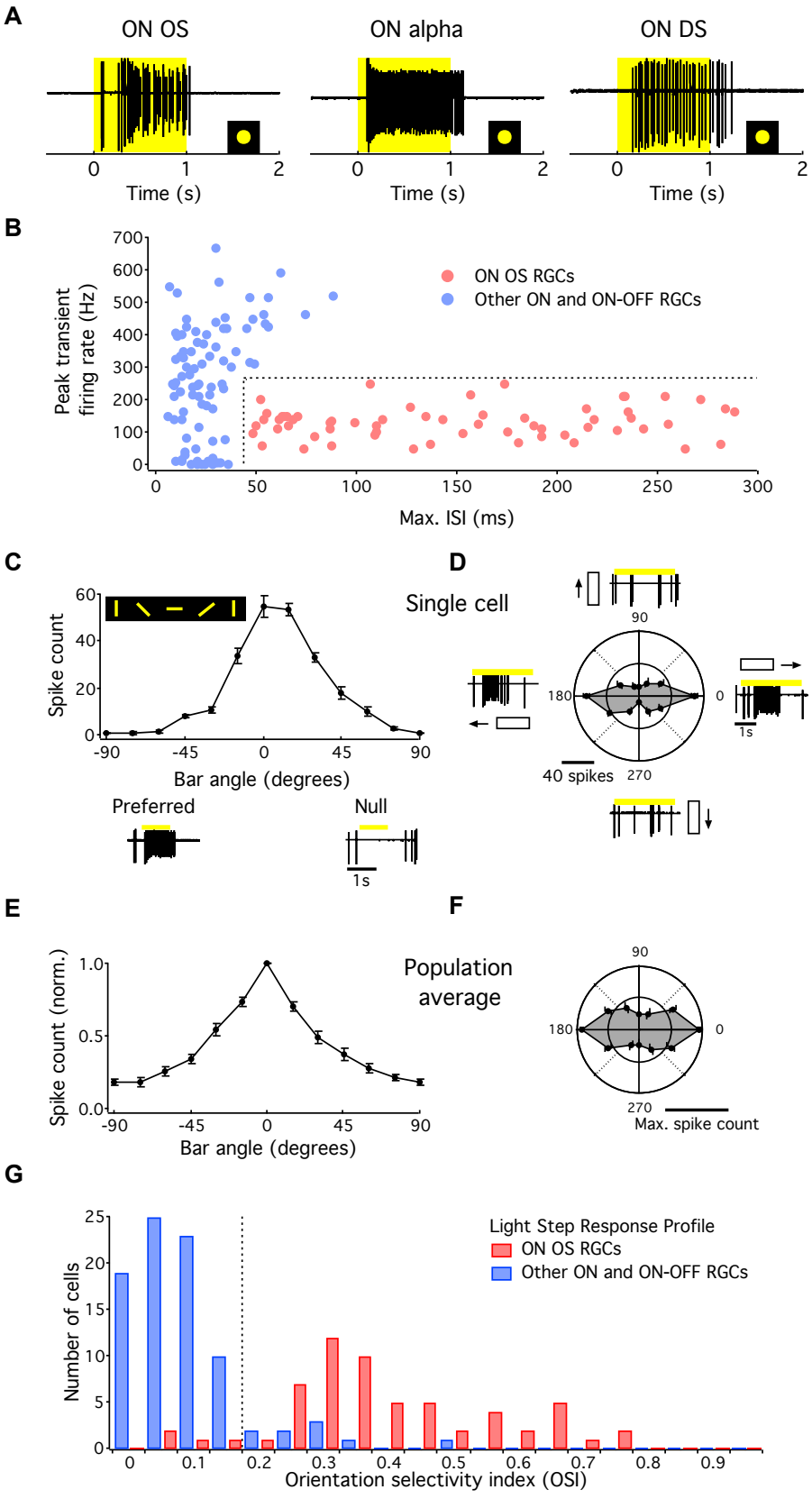
A
ON OS
ON alpha
ON DS
0
1
2
Time (s)
B
Peak transient firing rate (Hz)
700
600
500
400
300
200
100
0
ON OS RGCs
Other ON and ON-OFF RGCs
0
50
100
150
200
250
300
Max. ISI (ms)
C
Spike count
60
40
20
0
-90
-45
0
45
90
Bar angle (degrees)
Preferred
Null
1s
D
Single cell
90
180
0
270
40 spikes
1s
E
Spike count (norm.)
1.0
0.5
0.0
-90
-45
0
45
90
Bar angle (degrees)
F
Population average
90
180
0
270
Max. spike count
G
Number of cells
25
20
15
10
5
0
0
0.1
0.2
0.3
0.4
0.5
0.6
0.7
0.8
0.9
Orientation selectivity index (OSI)
Light Step Response Profile
ON OS RGCs
Other ON and ON-OFF RGCs

Figure 1. ON OS RGC is a distinct functional cell type. (A) Responses of ON OS (left), ON alpha (middle) and ON direction selective (right) RGCs to a 1 s flash of 200 μm diameter circular light spot. Yellow rectangle indicates period of light stimulus. **(B)** Peak transient firing rate plotted against peak ISI for ON OS (n = 60) and non-OS (n = 86) RGCs. Dotted lines indicate peak transient firing rate = 260 Hz and peak ISI = 45 ms. **(C)** Spike responses of an example ON OS RGC to oriented light bar stimuli (800 μm x 50 μm, 12 angles). Preferred and null orientation responses are shown below. Error bars indicate SEM across five trials at each orientation. **(D)** Polar plot of an example ON OS RGC's response to moving bar stimuli (1000 μm/s, 12 directions) with responses along preferred and null orientations. Direction of bar movement is shown along with the responses. Error bars indicate SEM across three trials in each direction. **(E)** Population average normalized orientation tuning curve (see Methods). Responses were aligned to 0° representing their peak selectivity. Error bars indicate SEM across cells (n = 60). **(F)** Population average tuning curve for moving bars aligned as in E. Error bars indicate SEM across cells (n = 21). **(G)** Histogram of OSI of ON OS (n = 60) and non-OS RGCs (n = 86) as identified by their light-step response profile. Dotted line indicates OSI = 0.2. Error bars indicate SEM.

step. These RGCs formed a distinct cluster in this 2D space and were formally classified by a peak transient firing rate < 260 Hz and a maximum ISI > 45 ms (Fig. 1B).

After locating the center of the RF at a resolution of 20 μm (Methods), we first investigated orientation selectivity by presenting flashed light bars presented across the RF center at 12 different orientations. The newly identified ON-sustained RGCs responded preferentially to bars at particular orientations (Fig. 1C), so we will henceforth refer to these cells as ON OS RGCs. Orientation selectivity was also apparent in the responses of ON OS RGCs to moving bars passing through the RF center and selectivity followed the direction of motion (Fig. 1D). Orientation selectivity index (OSI) was computed as the vector sum of the spike responses to the flashed bar stimuli (Piscopo et al., 2013); Methods). Population average response profiles for the flashed and moving bar stimuli are shown in (Figure 1E, F).

Unlike the response to a circular spot, which included the characteristic pause (Fig. 2A, C), responses to flashed bars lacked this feature (Fig. 2B, D). For circular spots, the temporal dynamics of the responses of ON OS RGCs depended on spot size. The initial transient component of the response showed more surround suppression than the sustained component after the pause (Fig. 2E). The unique temporal dynamics of the light response were used to target

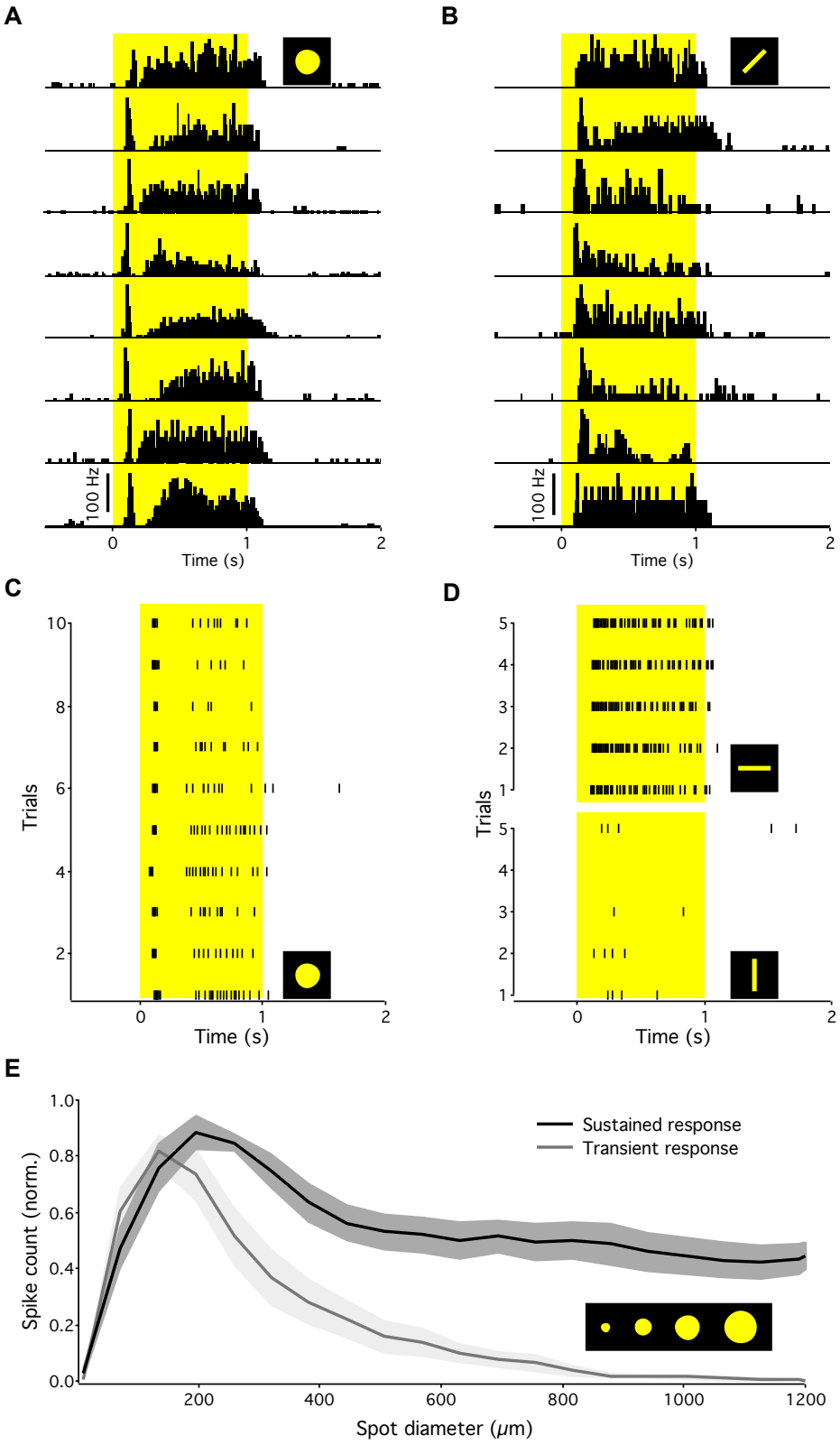
A
B
100 Hz
Time (s)
C
D
Trials
E
Spike count (norm.)
Spot diameter (μm)
Sustained response
Transient response

Figure 2. Temporal dynamics of light responses of ON OS RGCs. (A) Peristimulus time histograms (PSTHs) of light-step responses of 8 representative ON OS RGCs. PSTHs are calculated across 10 trials for each cell. Yellow rectangle indicates period of light stimulus. **(B)** PSTHs of responses to a flashed bar along preferred orientation for each of the eight ON OS RGCs in **(A)**. PSTHs are calculated across five trials for each cell. **(C)** Raster plots of responses of a single ON OS RGC to 1 s flashes of 200 μm diameter circular light spot. **(D)** Raster plots of responses of the same cell as in **(C)** to bars flashed along preferred (top) and null (bottom) orientations. **(E)** Spike count in the transient and sustained portions the light response of ON OS RGCs (n = 8) to spots of varying diameters. Responses are normalized to their maximum for each cell and averaged across cells. Shaded regions indicate SEM.

ON OS RGCs and they provided a classification scheme for ON OS RGCs that was independent of their OS. Based on this classification (Fig. 1B), ON OS RGCs exhibited significantly larger OSIs compared with other ON and ON-OFF RGCs (Fig. 1G, two-sample Kolmogorov–Smirnov test, $p < 10^{-23}$). Ninety-three percent (56/60) of recorded RGCs matching the light-step response profile of ON OS RGCs had an OSI = 0.2. 10% (9/86) of ON and ON-OFF RGCs with different light- step response profiles exceeded this OSI threshold.

Do ON OS RGCs prefer particular orientations in visual space (as has been shown for direction-selective RGCs and OS RGCs in rabbit (He et al., 1998; Levick, 1967; Oyster and Barlow, 1967; Venkataramani and Taylor, 2010) or are all orientations represented as in visual cortex (Blasdel and Salama, 1986; Hubel and Wiesel, 1974; Weliky et al., 1996; Yacoub et al., 2008)? We measured the preferred orientations of ON OS RGCs in retinas in which we had marked the cardinal axes during dissection (Wei et al., 2010); Methods). We found two separate populations of ON OS RGCs, which preferred either horizontal (nasal–temporal) or vertical (dorsoventral) cardinal orientations (Fig. 3A). Preferred orientations showed a clear bimodal distribution (Hartigan's dip test, $p < 0.001$, n = 48 cells). A position map of horizontal and vertical ON OS RGCs averaged across 27 preparations showed no evidence for a bias in the representation of the two axes across visual space (Fig. 3B, two-sample Kolmogorov–Smirnov test, $p = 0.66$ for nasal–temporal axis; $p = 0.16$ for dorsoventral axis). Both horizontal and

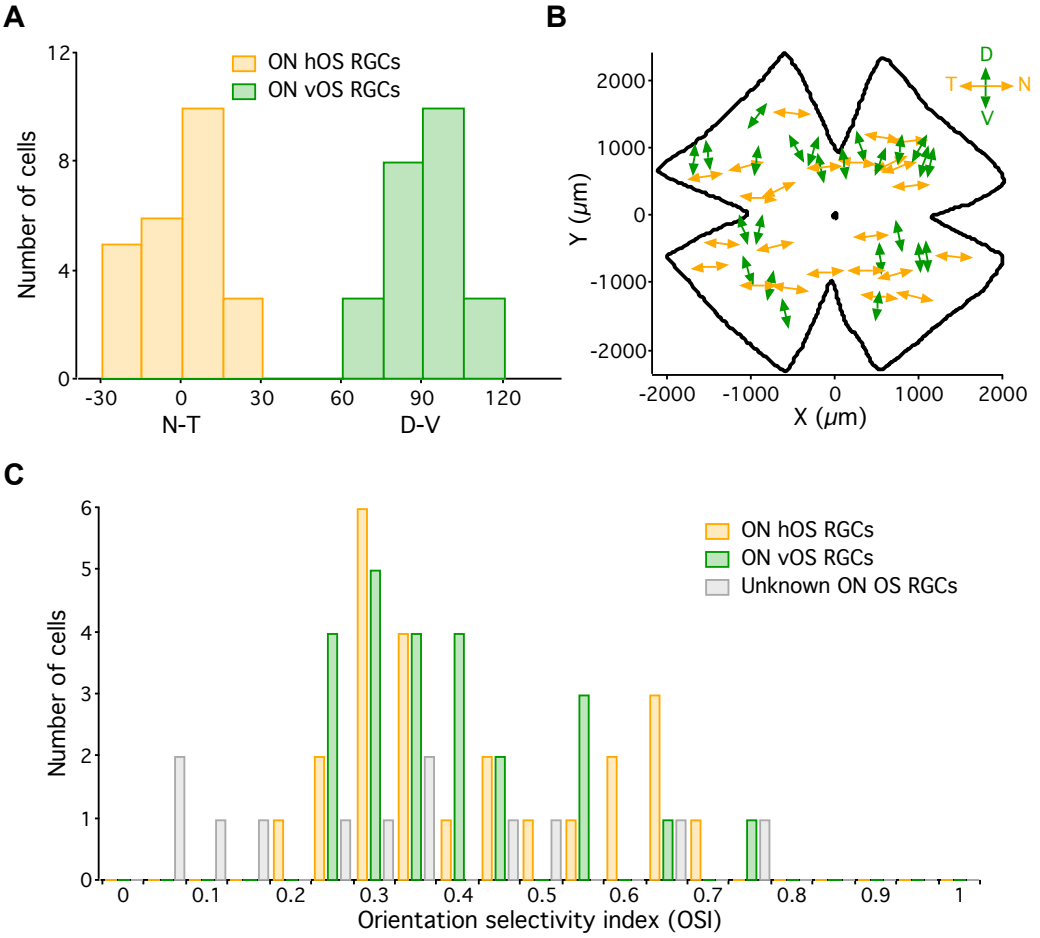

Figure 3. ON OS RGCs represent horizontal and vertical cardinal axes. (A) Angle histogram of preferred orientation of ON OS RGCs (n = 48 cells, 27 retinas, 20 mice) in whole-mount retina. Angles here and in subsequent figures represent real angles in visual space. Two distinct populations are evident; nasal–temporal (horizontal, orange) and dorsoventral (vertical, green). **(B)** Positional map of the ON OS RGCs (n = 48) in the whole retina. **(C)** Same histogram as in Figure 1G separated into horizontal and vertical ON OS RGCs. Unknown ON OS RGCs were recorded from retinal pieces without information about cardinal axes. Non-OS RGCs are not shown.

vertical OS cells had similar OSI distributions (Fig. 3C, two-sample Kolmogorov–Smirnov test, $p = 0.29$), and we observed no differences in their light-step response (two-sample Kolmogorov–Smirnov test, $p = 0.86$ for peak transient firing rates and $p = 0.62$ for peak sustained firing rates). Together, these results identify a new functional RGC class: ON OS RGCs. Like ON-OFF DS RGCs, ON OS RGCs share light response characteristics but can be subdivided into horizontal (ON hOS RGC) and vertical (ON vOS RGC) types based on orientation preference.

Morphology of ON OS RGCs

In addition to direction preference, some of the subtypes of ON- OFF DS RGCs differ in morphological properties. Dendritic asymmetry in one subclass of ON-OFF DS RGCs contributes to the DS computation (Trenholm et al., 2011). We imaged both ON hOS RGCs and ON vOS RGCs to determine whether there are morphological differences between the two subtypes and whether dendritic asymmetries could contribute to the OS computation. During whole-cell recordings, we filled ON OS RGCs with fluorescent dye and visualized their morphological structure after recording using a two-photon laser scanning microscope. In separate experiments, we filled ON OS RGCs with Neurobiotin, fixed the retinas, and stained with Alexa Fluor 488-conjugated streptavidin and an antibody against choline acetyl transferase (ChAT) to mark starburst amacrine cell processes. Although axons were lost in several cells (Fig. 4A), many had axons pointing toward the optic disk, thus confirming that they were RGCs (Fig. 4B). Both subtypes of ON OS RGCs had bistratified dendritic fields (in the ON and OFF sublamina of the inner plexiform layer (IPL); Fig. 4A–D) despite their pure ON functional polarity (Fig. 1A). The dendrites stratified proximal to the inner ChAT band and distal to the

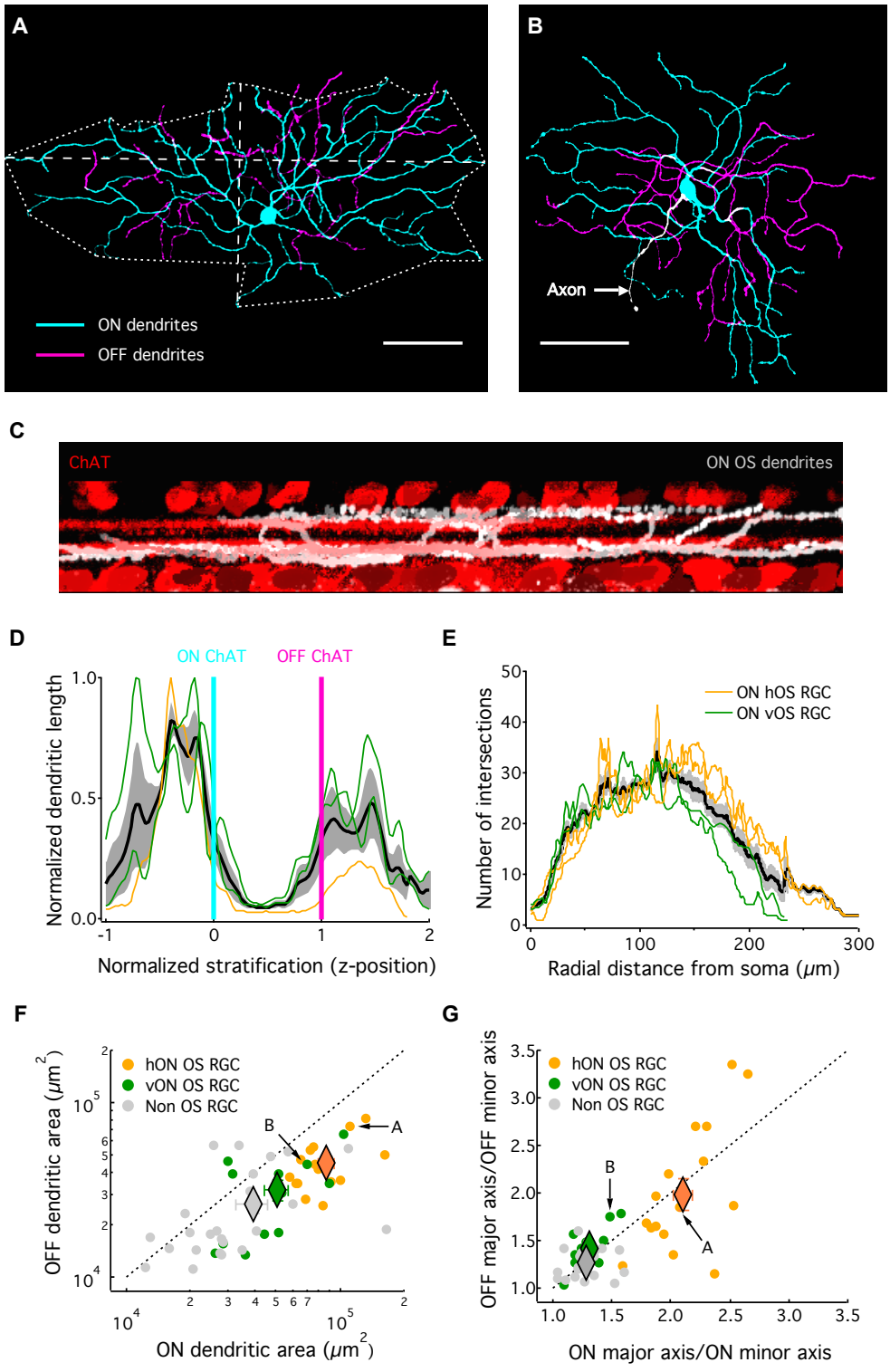

Figure 4. Dendritic morphology of ON OS RGCs. (A, B) Dendritic morphologies of horizontal ON OS RGC **(A)** and vertical ON OS RGC **(B)**. Dendrites in ON and OFF sublaminae of the IPL are colored in cyan and magenta,

respectively. Major and minor axes and polygon fit for ON dendrites are shown as dotted lines. **(C)** Stratification of ON OS cell dendrites relative to ChAT bands. **(D)** Z-profiles of ON OS dendritic arbor stratification. Orange and green lines indicate profiles of individual ON hOS and ON vOS cells, respectively. Black line represents mean. Cyan and magenta lines indicate ON and OFF starburst planes respectively. The inner nuclear layer (INL) is located to the right and the ganglion cell layer (GCL) is located to the left. Shaded region indicates SEM across three cells (one ON hOS and two ON vOS). **(E)** Sholl analysis of ON OS RGCs. Orange and green lines indicate radial profiles of individual ON hOS and ON vOS cells, respectively. Black line represents mean. Shaded region indicates SEM across four cells (two ON hOS and two ON vOS). **(F)** Dendritic field areas of OFF arbors plotted against dendritic field areas of ON arbors for ON OS RGCs (n = 29) and non-OS RGCs (n = 25). Dotted line indicates unity. (G) OFF dendritic axes ratio plotted against ON dendritic axis ratio for ON OS RGCs (n = 29) and non-OS RGCs (n = 25). Dotted line indicates unity. Horizontal ON OS RGCs (n = 16) have a significantly higher axes ratio compared with vertical ON OS (n = 13) and non-OS RGCs (two-sample Kolmogorov–Smirnov test, ON dendrites: $p < 10^{-6}$ for ON hOS vs ON vOS, $p < 10^{-8}$ for ON hOS vs non-OS and $p = 0.57$ for ON vOS vs non-OS; OFF dendrites: $p < 0.002$ for ON hOS vs ON vOS, $p < 10^{-5}$ for ON hOS vs non-OS and $p = 0.1$ for ON vOS vs non-OS). Error bars indicate SEM. Cells in **(A)** and **(B)** are marked with arrows in **(F)** and **(G)**.

outer ChAT band (Fig. 4C, D). Stratification patterns were the same for ON hOS RGCs and ON vOS RGCs (interstrata distance = 18.92 ± 0.54 μm, n = 15 for ON hOS, 17.53 ± 0.66 μm, n = 13 for ON vOS; two-sample Kolmogorov–Smirnov test, p = 0.26). Dendritic branching patterns (Sholl analysis) of ON hOS and ON vOS as a function of radial distance from soma revealed no obvious differences be- tween the two types (Fig. 4E). We fit polygons to the ON and OFF strata of each RGC to measure dendritic area and asymmetry within a plane of the IPL. The area of the ON stratification was significantly larger than that of the OFF stratification for both ON OS RGC subtypes (paired t test, $p < 10^{-4}$ for ON hOS and $p < 0.002$ for ON vOS). ON hOS RGCs had larger ON stratifications than both ON vOS RGCs and non-OS-bistratified RGCs (Fig. 4F, two-sample Kolmogorov–Smirnov test, $p < 10^{-3}$ for ON hOS vs ON vOS and $p < 10^{-6}$ for ON hOS vs non-OS). No relation was found between the size of ON OS RGCs and retinal eccentricity ($R^2 = 0.04$).

The most striking morphological difference between the sub- types of ON OS RGCs was the oriented morphology evident in ON hOS RGCs but not in ON vOS RGCs. We quantified this difference by measuring the ratio of the longest axis through the dendritic polygon to the

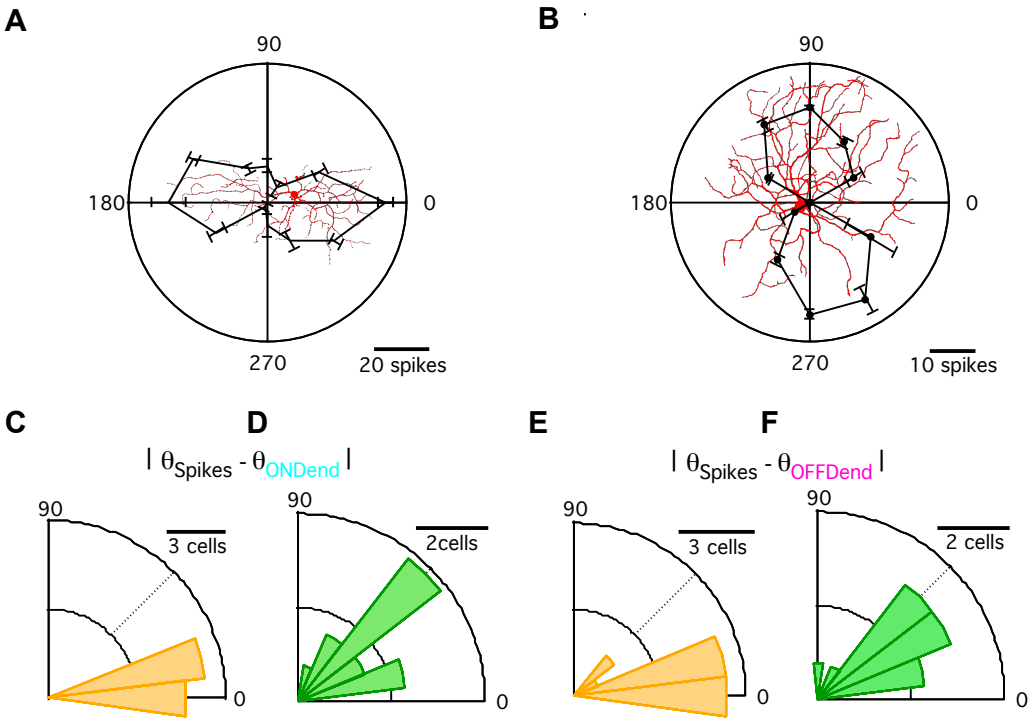

Figure 5. Correlation between dendritic morphology and orientation selectivity. (A, B) Responses of horizontal ON OS RGC **(A)** and vertical ON OS RGC **(B)** to moving bar stimuli. Images of the cells are overlaid on the polar plots. **(C, D)** Rose plots of absolute differences between spikes OS angle (θ_{Spikes}) and ON dendritic OS angle (θ_{ONDend}) of ON h OS RGCs (n = 15; C), and ON vOS RGCs (n = 13; D). **(E, F)** Rose plots of absolute differences between spikes OS angle (θ_{Spikes}) and OFF dendritic OS angle ($\theta_{OFFDend}$) of ON h OS RGCs **(C)** and ON vOS RGCs **(D)**. OS angles were calculated as described in Methods. Error bars indicate SEM across three trials in each direction.

perpendicular axis through the center of mass (major/minor axis ratio; Methods; Fig. 4G). This measure indicated a 2:1 elongation of the dendrites of ON hOS RGCs in both the ON and OFF strata. ON hOS RGCs had significantly more oriented ON and OFF dendrites than either ON vOS RGCs or non-OS bistratified RGCs, which were not different from each other.

Next, we wanted to determine whether the orientation of the dendrites of OS RGCs was related to their functional orientation preference. We measured the difference angle between the preferred orientation of the light response and the orientation of the dendrites (Fig. 5). In ON hOS RGCs, the dendrites were well aligned to the preferred orientation and this alignment was stronger for the ON stratum than the OFF stratum (angle difference = 6.25 ± 1.41° and 14.09 ± 3.37° for ON and OFF strata, respectively, n = 15). Both these relations were significantly different from a random uniform distribution but not different from each other (two-sample Kolmogorov–Smirnov test, $p < 10^{-8}$ and 10^{-4} for ON and OFF strata, respectively; paired t test, p = 0.14 for ON vs OFF strata). ON vOS RGCs had more symmetric dendrites (Fig. 4) and there was no significant relationship between the preferred orientation of spike responses and dendrites in either the ON or OFF strata and a uniform distribution (angle difference = 39.27 ± 5.75° and 46.26 ± 10.42° for ON and OFF strata, respectively, n = 13, two-sample Kolmogorov–Smirnov test, p = 0.27 for ON strata and p = 0.26 for OFF strata). The major/minor axis ratio was related to OSI for ON hOS RGCs, but we found no such relationship for ON vOS RGCs (data not shown). Therefore, although asymmetric dendritic morphology is likely to contribute to OS in ON hOS RGCs, ON vOS RGCs are orientation selective despite symmetric morphology.

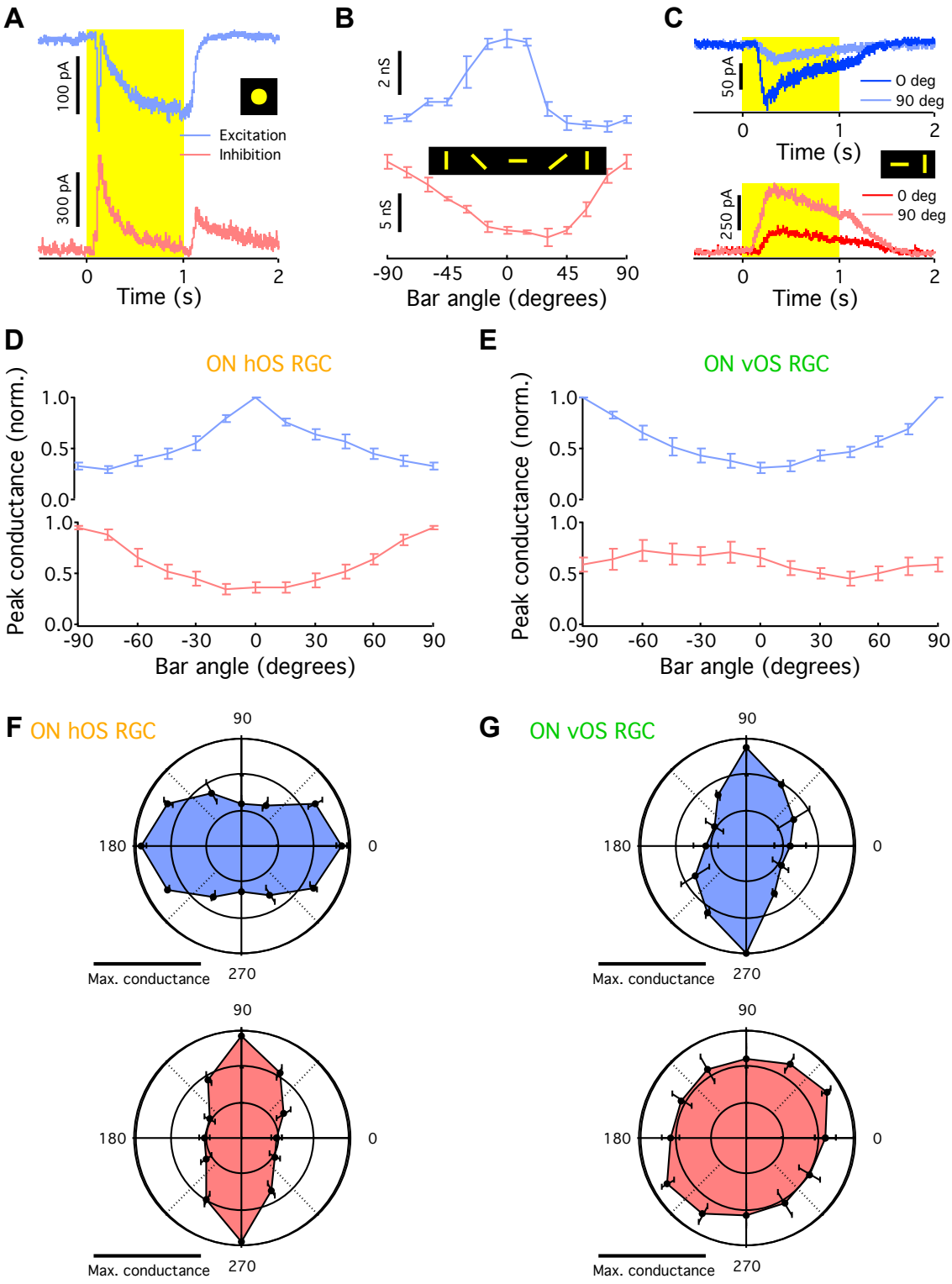
A
100 pA
300 pA
Excitation
Inhibition
0
1
2
Time (s)
B
2 nS
5 nS
-90
-45
0
45
90
Bar angle (degrees)
C
50 pA
0 deg
90 deg
Time (s)
250 pA
0 deg
90 deg
Time (s)
D
ON hOS RGC
Peak conductance (norm.)
1.0
0.5
0.0
-90
-60
-30
0
30
60
90
Bar angle (degrees)
E
ON vOS RGC
Peak conductance (norm.)
Bar angle (degrees)
F ON hOS RGC
90
180
0
270
Max. conductance
G ON vOS RGC
Max. conductance

Figure 6. Excitatory and inhibitory synaptic inputs to ON OS RGCs. (A) Responses of an ON OS RGC to a 1 s flash of 200 μm diameter circular light spot. Cell voltage clamped at -60 mV, the reversal potential for inhibition (top trace, blue). Cell voltage clamped at 20 mV, the reversal potential for excitation (bottom trace, red). Yellow rectangle indicates period of light stimulus. **(B)** Responses of ON hOS RGC to flashed bar stimuli (top trace) and excitation (bottom trace) inhibition. Error bars indicate SEM across five trials at each orientation. **(C)** Traces of excitation (top) and inhibition (bottom) at 0° and 90° bar orientations for cell in **(B)**. **(D, E)** Population averaged responses of horizontal (n = 9; **D**) and vertical (n = 11; **E**) ON OS RGCs to oriented light bar stimuli (top traces) and excitation (bottom traces) inhibition. Error bars indicate SEM across cells. **(F, G)** Population-averaged responses of horizontal (n = 3; **F**) and vertical (n = 3; **G**) ON OS RGCs to moving bar stimuli; excitatory currents (top traces), inhibitory currents (bottom traces). Error bars indicate SEM across cells.

ON OS RGCs receive OS excitation and inhibition

Based on previous studies in rabbit, the synaptic framework of OS in the retina has been built upon three main mechanisms: (1) uniform excitation received by an oriented dendritic tree, (2) tuned direct GABAergic inhibitory input to RGCs along the null orientation, and (3) tuned presynaptic inhibitory input along the null orientation to bipolar axon terminals resulting in OS excitatory input (Amthor et al., 1989; Bloomfield, 1994; Caldwell and Daw, 1978; Venkataramani and Taylor, 2010). Each of these mechanisms has been identified in different OS RGC populations in rabbit retina, but it remains unclear which exist in the mouse, how they interact, and if there are additional OS mechanisms. We sought to identify the OS inputs to ON OS RGCs with specific emphasis on two new areas of investigation: the contribution of GABAergic and glycinergic circuits in OS inhibition and whether OS excitation is always the result of presynaptic OS inhibition.

To begin to explore the circuit mechanisms of OS in the retina, we measured synaptic conductances in ON OS RGCs using whole-cell voltage-clamp recordings. A light step from darkness elicited an ON excitatory current with distinct transient and sustained components and both ON and OFF inhibition (Fig. 6A). It is notable that we measured no excitatory current at

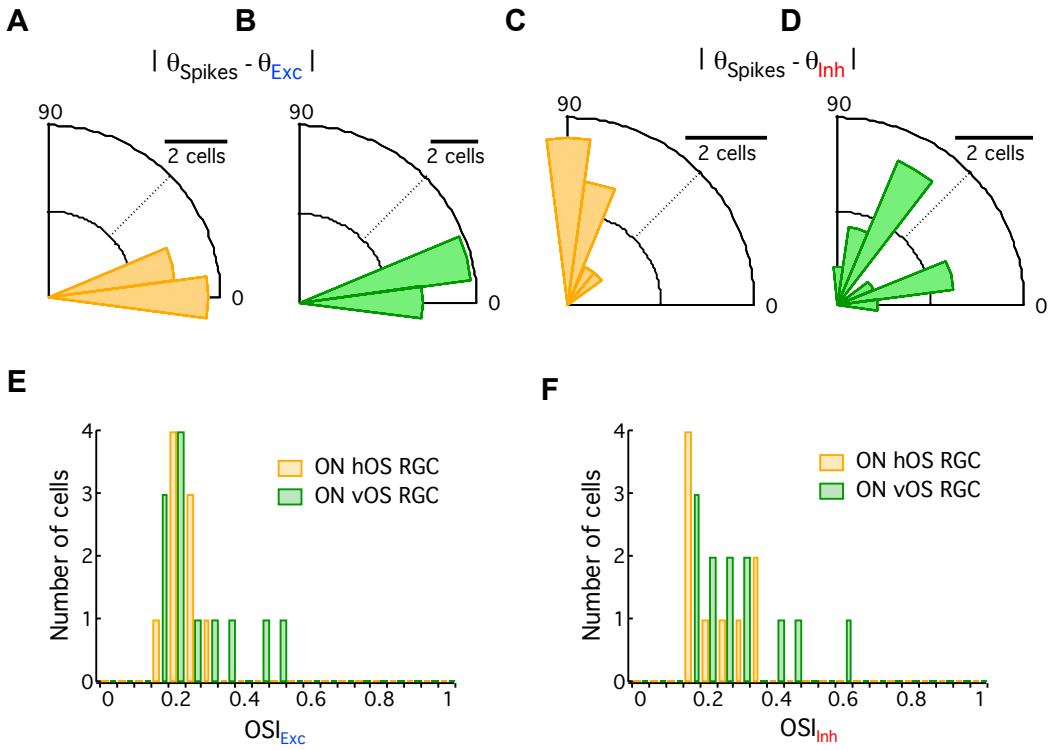

Figure 7. Correlation between synaptic inputs and orientation tuning. (A, B) Rose plots of absolute differences between spikes OS angle (θ_{Spikes}) and excitation OS angle (θ_{Exc}) of ON hOS RGCs (n = 9; **A**) and ON vOS RGCs (n = 12; **B**). **(C, D)** Rose plots of absolute differences between spikes OS angle (θ_{Spikes}) and inhibition OS angle (θ_{Inh}) of ON hOS RGCs (C) and ON vOS RGCs **(D)**. **(E, F)** OSI histograms for excitatory and inhibitory inputs received by horizontal and vertical ON OS RGCs.

light offset despite the bistratified morphology of ON OS RGCs, suggesting that the OFF-stratifying dendrites do not receive excitation from OFF bipolar cells. An OFF stratification with no excitatory input has also been observed in the suppressed-by-contrast RGC (Jacoby et al., 2015).

Both excitatory and inhibitory conductances were orientation selective when probed with flashed bars and, remarkably, preferred orthogonal orientations (Fig. 6B, C). At the population level, we measured oppositely orientation-tuned excitation and inhibition for ON hOS RGCs, but OS excitation and non-OS inhibition for ON vOS RGCs (Fig. 6D, E). Moving bars gave similar results at the population level (Fig. 6F, G).

In ON hOS RGCs, the preferred orientation for excitation was well aligned to that of the spike response and inhibition was aligned to the orthogonal (null) orientation (Fig. 7A, C). Despite untuned inhibition in the population, individual ON vOS RGCs also showed OS excitation and inhibition with OSIs not significantly different from ON hOS RGCs (Fig. 7E, F, two-sample Kolmogorov–Smirnov test, $p = 0.97$ for excitation OSI and $p = 0.99$ for inhibition OSI). Although excitatory orientation preference for ON vOS RGCs was well aligned to spike responses, inhibition was tuned along apparently random orientations (Fig. 7B, D). We found no statistical difference between our measured distribution of inhibitory tuning preference for ON vOS RGCs and a uniform distribution ($p = 0.64$, two-sample Kolmogorov–Smirnov test).

Pharmacology of OS conductances

Amacrine cells provide inhibition (onto RGCs, bipolar cells, and each other) in the inner retina by releasing GABA or glycine and GABAergic starburst amacrine cells are known to play

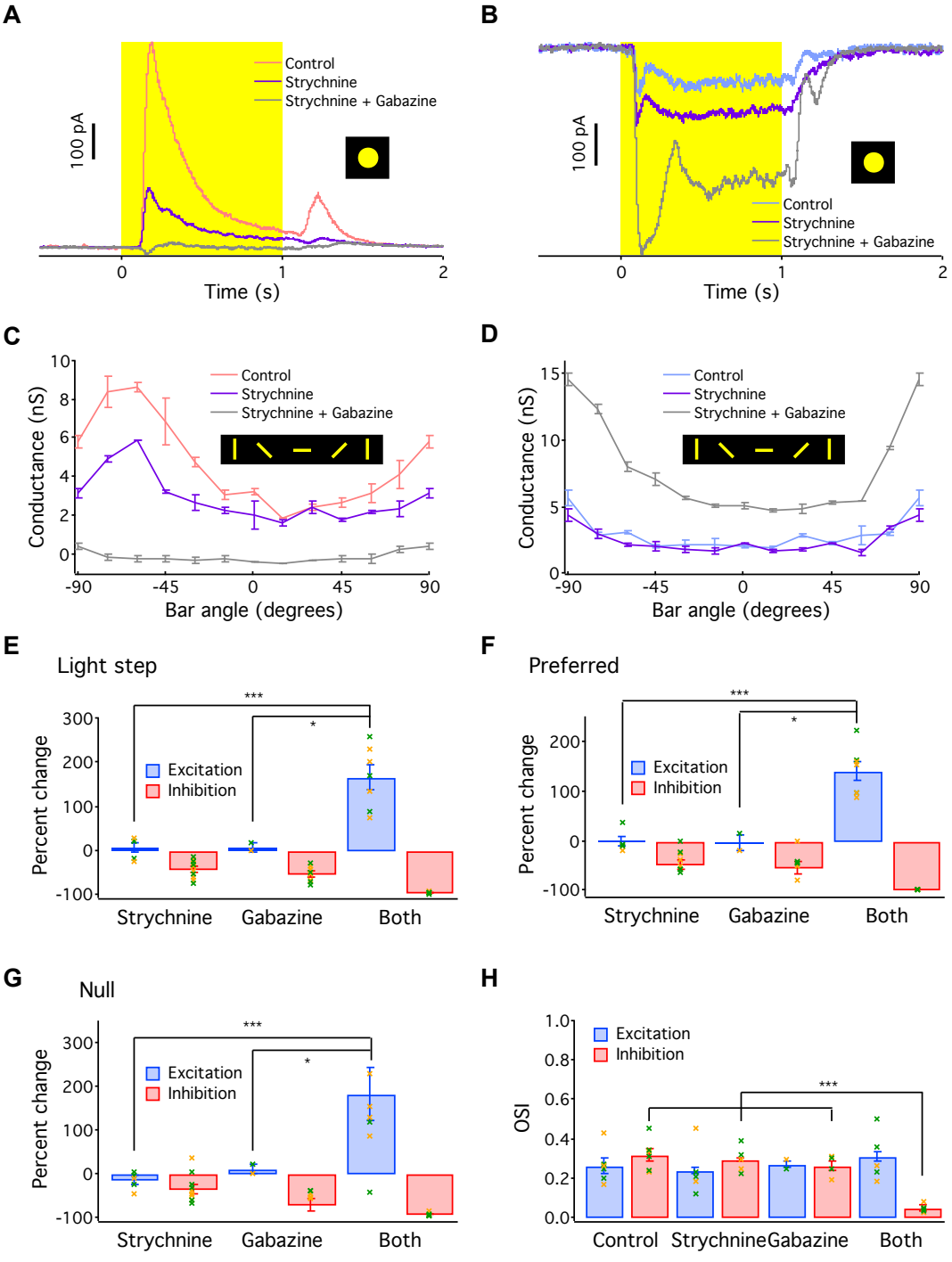

Figure 8. Pharmacological characterization of synaptic inputs. (A, B) Effect of GABA and glycine antagonists on light-step responses of ON OS RGCs. **(A)** Inhibition, **(B)** Excitation. Yellow rectangle indicates period of light stimulus. **(C, D)** Flashed bar responses of a vertical ON OS RGC in presence of inhibitory blockers. **(C)** Inhibition, **(D)** Excitation. Error bars indicate SEM across five trials at each orientation. **(E–G)** Percentage change in excitatory and inhibitory peak amplitudes in inhibitory antagonists for light step **(E)**, preferred orientation **(F)**, and null

orientation **(G)**. Orange and green crosses indicate data from individual ON hOS and ON vOS cells, respectively. **(H)** Effect of inhibitory blockers on OSI of excitatory and inhibitory inputs. Error bars indicate SEM (n = 4 for strychnine, n = 4 for gabazine, and n = 8 for both drugs). Orange and green crosses indicate data from individual ON hOS and ON vOS cells, respectively. ***$p < 0.001$, *$p < 0.05$.

a major role in DS circuits (Euler et al., 2002; Fried et al., 2002; S. Lee et al., 2010; Yonehara et al., 2011). To explore the source(s) of the OS conductances that we measured in ON OS RGCs, we bath applied antagonists for subtypes of GABA receptors or for glycine receptors (Methods).

Both GABAergic and glycinergic circuits provide inhibition to ON OS RGCs (Fig. 8A, E) and application of antagonists to both receptor types completely abolished inhibition. To determine which of these circuits provides OS inhibition, we blocked them sequentially (in both orders). Surprisingly, OS inhibition persisted in presence of either gabazine or glycine but was eliminated in the presence of both antagonists, suggesting that both GABAergic and glycinergic amacrine cells supply OS inhibition (Fig. 8C, F, G, H). Tetrodotoxin (TTX), $GABA_B$ and $GABA_C$ receptor antagonists had no effect on OS inhibition.

Bipolar cells relay excitatory information from photoreceptors to RGCs. Receptive fields of bipolar cells are 50 μm in diameter (Berntson and Taylor, 2000; Schwartz et al., 2012). Compared with the spatial scale of ON OS RGC dendrites and our flashed bar stimuli, these cells can be considered as small, non-oriented sources of excitation. Previous reports have indicated that presynaptic inhibition of bipolar cell axon terminals by amacrine cells might lead to OS excitation in RGCs (Caldwell and Daw, 1978; Venkataramani and Taylor, 2010). Excitatory input remained unaffected by a single inhibitory blocker (either gabazine or strychnine), but was significantly amplified in the presence of both drugs (Fig. 8 B, E, two-sample Kolmogorov–Smirnov test). None of the antagonists eliminated OS excitation when applied individually.

Surprisingly, OS excitation was not diminished in the presence of both drugs (Fig. 8D, F, G, H). OS excitation was also unchanged by adding $GABA_B$ and $GABA_C$ receptor antagonists to the mixture of blockers. In summary, our data show for the first time that both GABAergic and glycinergic amacrine cells contribute to OS inhibition and that the retina has OS excitation that is independent of inhibitory drive.

Discussion

Our discovery and characterization of ON OS RGCs in mouse retina raises a number of questions both about the mechanisms of OS in the retina and the role of these RGCs in downstream visual processing. Although selective genetic access to ON OS RGCs, which is not presently available, will be critical in answering many of these questions, it is important to discuss the following: (1) the relationship between dendritic morphology and direction or orientation selectivity, (2) the origin of OS excitatory and inhibitory conductances in the retina, and (3) the roles and possible interactions between multiple OS pathways in the early visual system.

Relationship between dendritic morphology and DS/OS computation

The correspondence between the dendritic morphology of RGCs in the plane of the IPL and their receptive fields is well documented (Kier et al., 1995). The simplest mechanism by which a RGC could achieve OS is by developing asymmetric dendrites so that a greater number of bipolar cells making excitatory synapses on the RGC are activated for stimuli in the preferred orientation than for stimuli in the null orientation. Both symmetric and asymmetric morphologies

have been reported among rabbit OS RGCs and OS amacrine cells and asymmetric morphologies have shown a correspondence with orientation preference in some studies (Amthor et al., 1989; Bloomfield, 1994; Murphy-Baum and Taylor, 2015), but not in others (Venkataramani and Taylor, 2010). Asymmetric dendritic morphology has also been implicated in the computation of direction selectivity both within dendritic branches of starburst amacrine cells (J. S. Kim et al., 2014; S. Lee and Zhou, 2006) and in some types of DS RGCS (I.-J. Kim et al., 2008; Trenholm et al., 2011), but another study reported asymmetric morphology in DS RGCs with no correspondence to direction preference (Kay et al., 2011).

We found that ON hOS RGCs have asymmetric dendrites aligned with the orientation preference of the response (Fig. 5). Although this morphology likely contributes to the OS computation, this simple mechanism is an incomplete explanation for the selectivity of ON OS RGCs because ON vOS RGCs receive OS excitation (Fig. 6) despite symmetric dendrites (Fig. 4) and both ON OS RGC types receive OS inhibition (Fig. 6) that is not aligned to the orientation of the dendrites (Fig. 7).

Origin of OS conductances in the retina

Both excitatory and inhibitory conductances in ON OS RGCs were orientation selective. OS inhibition was resistant to either GABA or glycine receptor antagonists applied alone—a combination of both antagonists eliminated all inhibition—whereas OS excitation was resistant to all inhibitory receptor blockers tested (Fig. 8). These results suggest that multiple OS pathways converge onto ON OS RGCs.

Our pharmacology experiments also both agree with aspects of the rabbit data and reveal new OS circuit components. OS inhibition is likely carried by a combination of glycinergic and GABAergic amacrine cells, but it is unclear whether the amacrine cells themselves are OS or if OS arises though selective connectivity with particular neurites of the amacrine cells, as is the case in the starburst amacrine cell to ON-OFF DS RGC circuit (Briggman et al., 2011). The origin of OS excitation remains more elusive because it was resistant to a full inhibitory block even in ON vOS RGCs, which have symmetric dendrites. We can envision three circuit configurations to account for OS excitation: (1) one of the ON bipolar cell types carries OS information, presumably type 8 or type 9 given the stratification profile of ON OS RGCs (Helmstaedter et al., 2013; Wassle et al., 2009); Fig. 4C, D); (2) bipolar cells themselves are not OS, but selective connectivity with the dendrites of ON OS RGCs (more numerous or stronger excitatory synapses along the preferred orientation) endows the postsynaptic cell with OS; or (3) OS excitation is not carried by a bipolar cell but instead by an OS, glutamate-releasing amacrine cell. The existence of such excitatory connections from amacrine cells has been shown recently in a different retinal circuit (S. Lee et al., 2014).

Our voltage-clamp recordings provided clear evidence for OS conductances in ON OS RGCs, but we cannot rule out a role for active conductances in enhancing OS. Dendritic spikes have been shown to play a role in the DS computation in ON-OFF DS RGCs (Oesch et al., 2005).

Multiple OS pathways in the early visual system

Orientation selectivity is a major response property of visual cortex across mammalian species (Chapman et al., 1991; Hubel and Wiesel, 1968; 1962; Niell and Stryker, 2008) and there is substantial evidence in favor of Hubel and Wiesel's model of OS emerging from selective wiring from LGN to V1, including in mouse (Lien and Scanziani, 2013). However, a body of recent evidence has shown that this is not the only OS pathway in the mouse visual system. OS responses have been recorded in both LGN (Marshel et al., 2012; Piscopo et al., 2013; Zhao et al., 2013) and SC (Ahmadlou and Heimel, 2015; Feinberg and Meister, 2015; Wang et al., 2010) in conditions designed to minimize the influence of cortical feedback. Recently, OS cells have also been reported in the koniocellular layers of primate LGN (Cheong et al., 2013). Therefore, separate OS pathways exist in parallel in the early visual system. A similar picture has emerged for DS pathways in the mouse, in which retinal DS information is transmitted to a substructure within dorsal LGN and then onto the superficial layers of cortex (Cruz-Martín et al., 2014). This pathway coexists with more traditional DS circuits in the input layers of cortex (S.-H. Lee et al., 2012; "Mechanisms of Direction Selectivity in Macaque V1," 1998; "Parvalbumin-Expressing Interneurons Linearly Transform Cortical Responses to Visual Stimuli," 2012).

Do the different OS pathways subserve different behaviors or perceptions? One clue lies in the distribution of orientation preferences. OS cells in cortex represent all orientations in a fairly uniform distribution (Blasdel and Salama, 1986; Hubel and Wiesel, 1974) and this representation has been linked to the perception of continuous edges defining object boundaries (Swindale et al., 2000). OS cells in LGN may be tuned to cardinal orientations (Marshel et al.,

2012; Piscopo et al., 2013), as we found in the retina (but see (Zhao et al., 2013). In SC, preferred orientation appears to be linked to retinotopic position, perhaps to represent optic flow (Ahmadlou and Heimel, 2015). Future work will be needed to determine whether these different representations of orientation information are indeed tied to different behaviors and if they interact given that LGN, SC, and V1 are interconnected structures (Bickford et al., 2015). Marshel et al. (Marshel et al., 2012) proposed selective connectivity of oppositely tuned ON-OFF DS RGCs as the source of cardinal OS in LGN. The two cardinal ON OS RGCs that we identified here offer a more parsimonious explanation for cardinal OS in LGN, but tracing studies will be needed to determine their projection patterns within the brain and the possible transformations of OS information in postsynaptic cells.

Subsequent evidences of ON OS RGCs

Since the publication of this work (Nath and Schwartz, 2016), a similar ON OS RGC has been discovered in the rabbit retina (Venkataramani and Taylor, 2016). The authors identified a horizontal orientation preferring RGC possessing similar asymmetric dendritic morphology as ON hOS RGC in mouse. However, the rabbit ON OS RGC is monostratified and has only ON dendrites. Moreover, the excitatory and inhibitory conductances to this RGC are OS along the preferred and null orientations respectively. Furthermore, pharmacological experiments revealed that OS in inhibitory inputs was dependent on GABAergic transmission. Despite clear anatomical and physiological differences, the substantial degree of homology between horizontal orientation preferring ON OS RGCs in mouse and rabbit suggests that conserved mechanisms are principal towards generating retinal orientation selectivity across mammalian species.

In the past few years, remarkable technical advances have been made in the field of imaging. This has led to several studies electron microscopy (EM) studies on ganglion, amacrine and bipolar cell types in the inner retina (Helmstaedter et al., 2013; Sümbül et al., 2014; Bae et al., 2017) and discovery of novel circuits (Briggman et al., 2011). One such EM study (Bae et al., 2017) confirmed the presence of ON OS RGCs in the mouse retina both morphologically and via functional imaging (Fig. 9). The anatomical and physiological data is also available in a 'digital museum' (http://museum.eyewire.org). According to their classification, type 72 and 82wi correspond to ON hOS and ON vOS respectively. Type 72 cells exhibit a denser mosaic than type 82wi (Fig. 9A, D) which is probably the reason why we encountered more ON hOS RGCs in our recordings. Both these cell types were bistratified with ON and OFF dendrites stratifying blow and above the ON and OFF starburst planes respectively (Fig. 9B, E). Moreover, functional imaging revealed OS responses of these cells to moving bars (Fig. 9C, F).

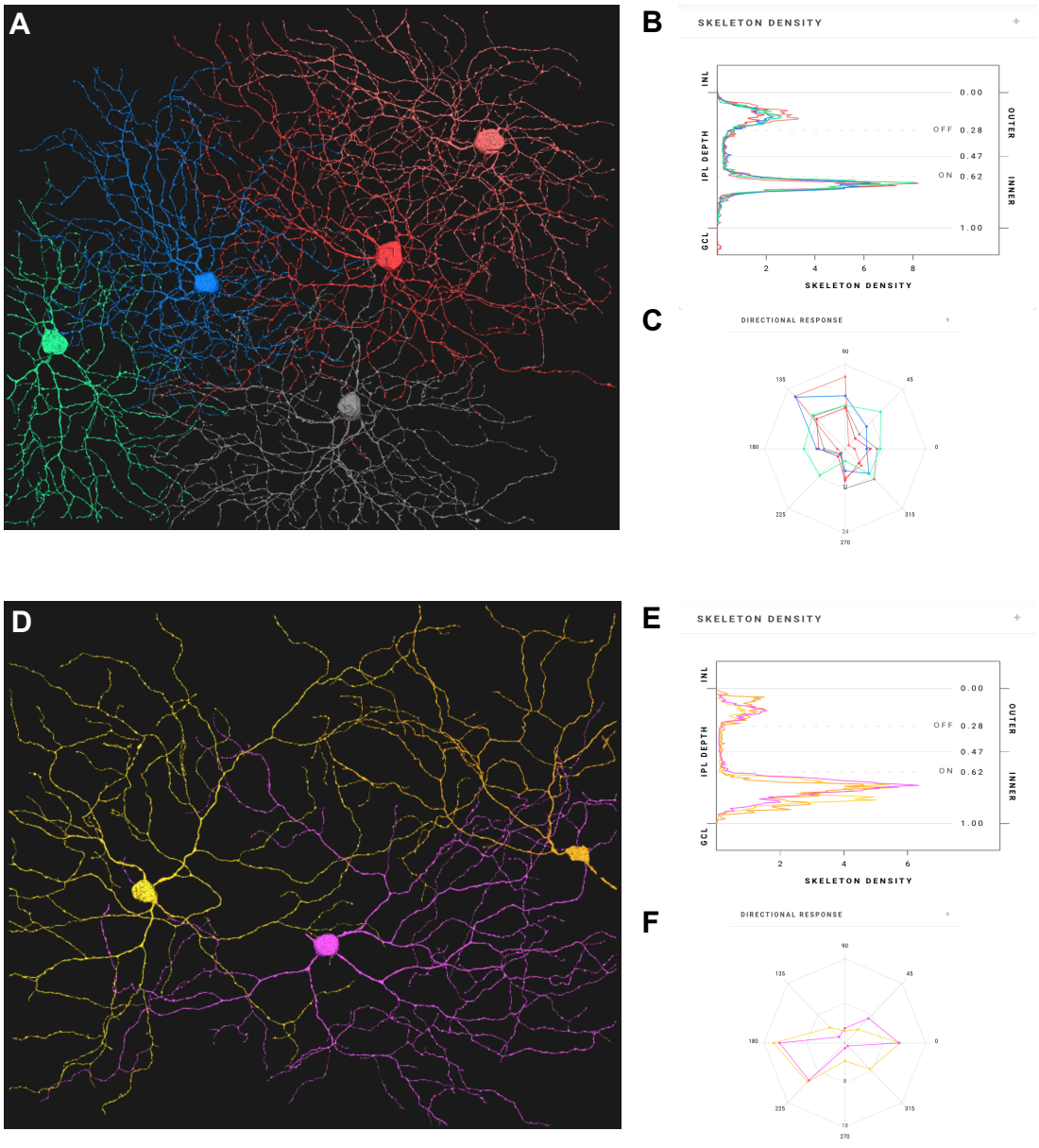

Figure 9. Morphological and physiological confirmation of ON OS RGCs. (A) Dendritic morphology of type 72 RGCs. Different RGCs are in different colors. **(B)** Z-profiles of dendritic arbor stratification of type 72 cells in IPL. Dotted lines indicate ON and OFF sublamina boundaries. **(C)** Polar plot of fluorescence change (ΔF/F) of calcium reporter in type 72 cells in response to moving bar stimuli. **(D-F)** Same as in **(A-C)** but for type 82wi RGCs. Adapted from http://museum.eyewire.org. Please note that retina was not aligned to cardinal directions.

Methods

Electrophysiology: Wild-type mice (C57BL/6) of either sex (37 male and 4 female) were dark adapted overnight. Animals were killed following animal protocols approved by the Center for Comparative Medicine at Northwestern University. Retina dissections were conducted under IR light (940 nm) with assistance from IR visible light converter (night vision) goggles and separate IR dissection scope attachments (BE Meyers). Cardinal directions were identified using scleral landmarks (Wei et al., 2010). Relieving cuts were made along cardinal directions and the whole retina was mounted ganglion cell side up on a 12 mm poly-D-lysine-coated glass coverslip (BioCoat Cellware; Corning) that was secured to a recording dish via grease. The dish was placed on the electrophysiology rig (SliceScope Pro 6000; Scientifica) and superfused with carbogenated Ames medium (Sigma-Aldrich, A-1420; 9 ml/min) warmed to 32°C. Tissue was illuminated at 950 nm for visualization. Cell-attached recordings were obtained with a 2-channel patch-clamp amplifier (MultiClamp 700B; Molecular Devices) using pipettes (2–3 MΩ) filled with Ames solution. For voltage-clamp experiments, pipettes (4–6 MΩ) were filled with an intracellular solution composed of the following (in mM): 105 Cs methanesulfonate, 10 TEA-Cl, 20 HEPES, 10 EGTA, 2 QX-314, 5 Mg-ATP, and 0.5 Tris-GTP at ~ 270 mOsm, pH ~ 7.3 with CsOH. To isolate excitatory and inhibitory synaptic inputs, each ganglion cell was held at the reversal potential for inhibition (~ -60 mV) and excitation (~ 20 mV), respectively. Absolute voltage values were not corrected for a liquid junction potential of -8.58 mV in the Cs-based intracellular solution. Pharmacological reagents were purchased from Sigma-Aldrich (gabazine, strychnine, TPMPA, saclofen) and Tocris Bioscience (TTX). Drug concentrations were as

follows: strychnine, 1 μM; gabazine, 10 μM; TPMPA, 50 μM; saclofen, 100 μM; TTX, 500 nM. Other recording details are as in Jacoby et al. (2015).

Visual stimuli: A custom-designed light projection device (DLP Light- Crafter; Texas Instruments) capable of controlling patterned visual stimulation at frame rates up to 1.4 kHz was used to display visual stimuli. All spatial stimuli patterns were displayed on a 1280 x 800 pixel array with pixel size of 2–3 μm and were focused onto the photoreceptor layer through the microscope condenser. The device used blue LED illumination with a peak spectral output at 450 nm. Photon flux was attenuated to suitable levels using neutral density filters (Thorlabs) and light intensity values were measured in rhodopsin isomerizations per rod per second (R*/rod/s). During cell-attached recording, the RGCs' responses to horizontal and vertical bars (200 x 40 μm) across 11 locations along each axis spaced by 40 μm were measured to obtain the spatial position of receptive field (RF) center. Subsequent stimuli were delivered at the RF center. Circular spots of 200 μm diameter on a dark background were used to identify light-step profiles of RGCs. Spots of diameters ranging from 10 to 1200 μm were used to characterize the temporal dynamics of RGC responses (see Fig. 2E). Bars (800 x 50 μm) were flashed for 1 s at 12 different angles to characterize ON OS RGCs. Moving bar stimuli consisted of rectangular bars (600 x 50 μm) moving at 1000 μm/s for 3 s across the RF of RGCs. All such stimuli were presented at 200 R*/rod/s. Full-field sine wave drifting gratings were presented from a background intensity of 500 R*/rod/s at a Weber contrast of 100%. All stimuli with varying parameters were presented in pseudorandom order.

Immunohistochemistry: Tissues were fixed overnight in 4% paraformaldehyde (Electron Microscopy Sciences). Fixed retinas were incubated in PBS containing 3% normal donkey serum (blocking agent), 0.05% sodium azide, 0.5% Triton X-100, and primary antisera against ChAT (Millipore, AB144P, goat anti-ChAT, 1:500) for 5 nights at 4°C. Afterward, tissues were rinsed in PBS and incubated overnight at 4°C with secondary antibody against goat IgG (Jackson ImmunoResearch, 705–475-147, donkey anti-goat DyLight 405, 1:500) and streptavidin (Pierce Biotechnology, 21832, DyLight 488, 1:500). After immunostaining, retinas were mounted on slides with p-phenylenediamine medium.

Imaging: Before whole-cell recordings, patch pipettes were filed with Alexa Fluor 488. After recording, RGC morphology was imaged using two-photon microscopy (920 nm, MaiTai HP; SpectraPhysics) under a 60X water-immersion objective [Olympus LUMPLan FLN 60X/1.00 numerical aperture (NA)]. Emission was collected by a 520–540 nm band-pass filter.
For dendritic stratification, target RGCs were injected via patch pipettes containing Neurobiotin tracer (Vector Laboratories, SP-1150, 3% w/v and 280 mOsm in potassium aspartate internal solution).

Fixed tissues were imaged on a Nikon A1R laser scanning confocal microscope mounted on a Nikon Ti ZDrive PerfectFocus micro- scope stand equipped with an inverted 60X oil-immersion objective (Nikon Plan Apo VC 60X /1.4 NA). RGC dendrites and ChAT labeling were imaged at 488 and 405 or 647 nm excitation, respectively. All confocal images were collected with spacing of 0.2 μm in the z-axis. Confocal imaging was performed at the Nikon Imaging Center at Northwestern University's Feinberg School of Medicine using Nikon

Elements software. Dendritic arbors were traced using the Fiji software Simple Neurite Tracer plugin and subsequent Sholl analysis was performed. For dendritic stratification profiles, similar program and methods were used as described in (Sümbül et al., 2014).

Data analysis. The light-step response profiles of ON OS and other ON and ON-OFF RGCs were subdivided into transient (0 –200 ms) and sustained (200 –1000 ms) temporal time windows. Peak firing rates in these time windows were calculated from peristimulus time histograms of light-step responses. Peak interspike interval (ISI) was calculated in a 100 –500 ms time window and was averaged across all light-step trials for a single cell. Orientation selective index (OSI) and preferred orientation angle were calculated based on a standard metric of the circular variance. Vector sum of the responses across orientations is given by the following:

$$\frac{\Sigma\, R(\theta) e^{2i\theta}}{\Sigma\, R(\theta)}$$

where R(θ) is the response for orientation across the entire stimulus time window for both flashed bars and moving bars. Absolute value and half the phase of the resultant complex number give the values of the OSI and OS angle, respectively.

For population average tuning curves (see Fig. 1E, F), each flashed bar or moving bar response was normalized to maximum, the maximum responses were circularly shifted to the same preferred angle across cells, and the response was averaged across every bar angle. In Figure 1, 0° was chosen as the common preferred angle. For subsequent figures, no circular shift was performed, and angles are reported in visual space.

For computing the axis ratio, the RGC dendritic field was fitted with a polygon using a custom-written MATLAB package (github.com/ SchwartzNU/SymphonyAnalysis). The maximum distance of two points lying on the polygon perimeter was used as the major axis length. Minor axis length was calculated as the longest line segment perpendicular to the major axis with ends lying on the polygon perimeter. Axis ratio was the fraction of these two lengths. Axis ratio was calculated separately for ON and OFF dendrites. The polygon perimeter was resampled into 1000 points and the centroid was computed. Vectors were constructed from the centroid to the perimeter points and the vector sum calculated similarly using the above equation. Half of the complex phase of the sum gives the preferred orientation of the dendrites.

All electrophysiological data were analyzed with a custom open-source MATLAB analysis package described above and figures were constructed in Igor version 6.36 (Wavemetrics).

Chapter 3. Electrical Synapses Convey Orientation Selectivity in the Mouse Retina

Introduction

Neural circuits rely on both chemical and electrical synapses for inter-neuronal communication (Pereda, 2014). Electrical synapses are most commonly present in dendrites and often aid in lateral signal spread and synchrony among functionally similar cells (Christie and Westbrook, 2006; Detwiler and Hodgkin, 1979; DeVries et al., 2002; Galarreta and Hestrin, 2001; Vervaeke et al., 2012). Gap junctions have many known functions in the central nervous system, including increasing sensitivity of sensory systems (Pereda et al., 1995), participating in escape behaviour (Herberholz et al., 2002), generating persistent firing (Sheffield et al., 2011), contributing to expansion of receptive fields (Elyada et al., 2009), compensating for sublinear dendritic integration (Vervaeke et al., 2012), and regulating interneuron excitability (Apostolides and Trussell, 2013).

Gap junctions are particularly prevalent in the retina, where all five major cell classes are connected by electrical synapses (Bloomfield and Völgyi, 2009). In vertebrates, retinal ganglion cells form homologous gap junction networks with other RGCs of the same type and/or heterologous gap junction networks with amacrine cells (Vaney, 1991; Völgyi et al., 2009; Xin and Bloomfield, 1997)). As in other parts of the central nervous system, both homologous and heterologous electrical networks have been implicated in increasing spike timing synchrony among RGCs (Ala-Laurila et al., 2011; Brivanlou et al., 1998; DeVries, 1999; Hu and Bloomfield, 2003; Mastronarde, 1983; Shlens et al., 2008; Völgyi et al., 2013). Other reported

functional roles of RGC gap junctions involve modulation or support of computations that are principally carried by chemical synapses. The directional tuning of ON direction selective (DS) RGCs is strengthened via coupling to polyaxonal amacrine cells (Ackert et al., 2006). One population of ON-OFF DS RGCs combines chemical and electrical synaptic input to compute lag normalization (Trenholm et al., 2013a; 2013b). OFF transient alpha RGCs receive electrical synaptic inputs from four distinct populations of amacrine cells (Völgyi et al., 2005), contributing to their transient response following the offset of dim flashes (Murphy and Rieke, 2011). Heterologous gap junctions have also been implicated in crossover excitation, in which OFF RGCs receive ON input via electrical synapses (Farajian et al., 2011).

Two of the best-studied computations in RGCs are their selectivity for the direction of movement or the orientation of a visual stimulus. Direction selectivity relies principally on inhibition from starburst amacrine cells (Demb, 2007; Pei et al., 2015; Vaney et al., 2012; Vlasits et al., 2014). Orientation selectivity has been reported to rely on both excitatory and inhibitory synaptic inputs (Caldwell and Daw, 1978; Nath and Schwartz, 2016; Venkataramani and Taylor, 2016; 2010). Here we identify two types of OFF OS RGCs in the mouse retina, and we show that electrical synapses carry OS information to the RGC. Our anatomical and physiological experiments suggest a morphological substrate of this OS signal in a coupled amacrine cell. These results uncover a surprising new function of electrical synapses in conveying feature selectivity to a sensory neuron, and they establish an amacrine cell-RGC circuit critical to the computation of OS.

Results

Functional characterization of OFF OS RGCs

During our large-scale survey of the responses of mouse RGCs, we found OFF RGCs with a distinct response to a 200 μm diameter circular spot of light presented from darkness at the receptive field center for 1 s. (Fig. 1A, left). These OFF cells had a low baseline firing rate and were completely suppressed at light onset. Following light offset, the firing rate gradually reached baseline level and, in some cases, overshot the baseline rate. This type of response was distinct from the two well-known OFF alpha RGCs (Fig. 1A). For all OFF RGCs recorded, we measured the average baseline firing rate and the peak firing rate at light offset (Methods). These low baseline and low peak firing rate RGCs formed a distinct cluster in the two-dimensional response space and were formally classified by an average baseline firing rate < 50 Hz and a peak light offset firing rate < 120 Hz (Fig. 1B).

We stimulated OFF RGCs with drifting gratings (spatial frequency = 0.1 cycles per degree, temporal frequency = 2 Hz), at 12 different orientations to test for OS responses. Cells classified based on their light step responses by the criteria above (Fig. 1B) were strongly OS, with significantly larger OS indices (OSIs) than other OFF RGCs (Fig. 1F, two-sample t test, $p < 10^{-43}$). We will henceforth refer to these RGCs as OFF OS RGCs. 95% of OFF OS RGCs (87/92) had an OSI > 0.2; 4% (4/89) of other OFF RGCs exceeded this OSI threshold.

In one experiment, we encountered two OFF OS RGCs with neighboring somata (Fig. 1C). Both exhibited OS responses (Fig. 1D, E), however, their preferred angles were orthogonal ($\Delta\theta = 85°$). Since RGCs of the same type form mosaics across the entire retina (Rodieck, 1991; Wassle et al., 1981), the presence of proximate OFF OS RGCs suggested that

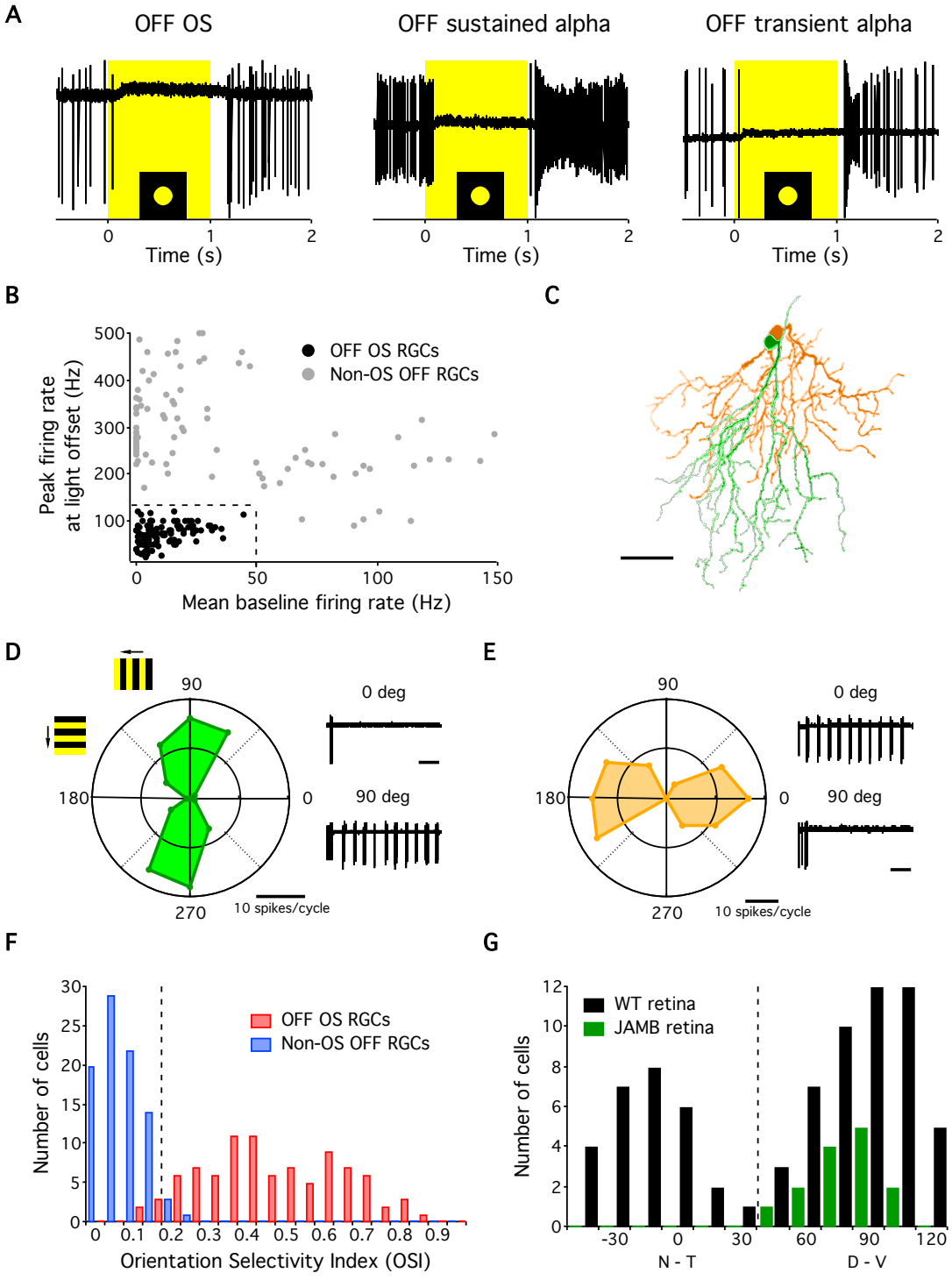

Figure 1. OFF OS RGC is a distinct functional cell type. (A) Responses of OFF OS (left) OFF sustained alpha (middle) and OFF transient alpha (right) RGCs to a 1 s flash of 200 µm diameter circular light spot from darkness. Yellow rectangle indicates light stimulus. **(B)** Peak firing rate at light offset plotted against mean baseline firing rate

for OFF OS (n = 92) and non-OS (n = 84) RGCs. Dotted lines indicate peak firing rate = 135 Hz and mean baseline firing rate = 50 Hz. **(C)** Dendritic morphology of two neighboring OFF OS RGCs. Scale bar = 50 µm. **(D, E)** Polar plots of drifting grating responses of OFF OS RGCs colored in green **(D)** and **(E)** orange, respectively. F1 response amplitudes and grating angles are plotted in radial axes and angle axes, respectively. F1 cycle average responses are calculated from three trails in each angle. **(F)** Histogram of OSI of OFF OS (n = 92) and non-OS RGCs (n = 84) as identified by their light step response profile. Dotted line indicates OSI = 0.2. **(G)** Angle histogram of preferred orientations of OFF OS RGCs recorded in WT retina (black, n = 78) or labelled cells in the JAM-B line (green, n = 14). Dotted line indicates 45° angle.

they might be further separated into multiple, functionally distinct subtypes. We sampled the preferred angles of OFF OS RGCs and found a bimodal distribution (Hartigan's dip test p = 0.008, n = 92 cells, Fig. 1G). We classified cells with preferred orientations between [–45°, 45°] and [45°, –45°] as OFF horizontal (h) OS (nasal-temporal) and OFF vertical (v) OS RGCs (dorsoventral), respectively. We found no significant differences in light step responses, strength of orientation tuning or spatial distribution across the retina between these two OFF OS RGC types (Fig. 2).

We tested the robustness of OS in OFF OS RGCs across a range of temporal and spatial frequencies and light levels. Both vertical and horizontal OFF OS RGCs displayed strong OS responses but had somewhat different spatiotemporal tuning properties (Fig. 3A-D). OS responses were conserved across 7 log units of light intensity (Fig. 3E). Direction selectivity was much weaker than OS across the entire range of spatial and temporal frequencies we tested (Fig. 3F, G).

We noted morphological similarity between some of the OFF OS RGCs and a previously reported RGC type, JAM-B (I.-J. Kim et al., 2008)Fig. 1C and Fig. 4). We therefore recorded from a transgenic line in which JAM-B RGCs are fluorescently labelled. All labelled RGCs recorded in this mouse line (n = 14 cells) were classified as OFF vOS RGCs when probed with drifting gratings (Fig. 1G), indicating that JAM-B RGCs are orientation selective. There was no

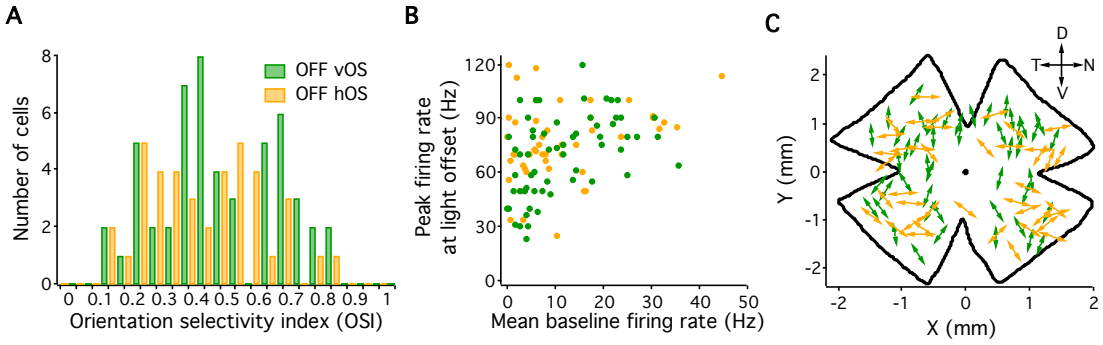

Figure 2. OFF vOS and OFF hOS RGCs have similar light response profiles. (A) Peak firing rate at light offset plotted against mean baseline firing rate for OFF vOS (n = 52) and OFF hOS (n = 40) RGCs. **(B)** Histogram of OSI of OFF vOS (n = 52) and OFF hOS RGCs (n = 40). **(C)** Positional map of the OFF OS RGCs (n = 92) in the whole retina.

significant difference between OSIs of JAM-B RGCs (n = 14, average OSI = 0.47 ± 0.05) and OFF vOS RGCs recorded in WT retina (n = 38, average OSI = 0.48 ± 0.03, p = 0.83, two-sample t test). We return to interpret how OS might interact with the other reported functional properties of JAM-B RGCs in the Discussion.

Morphology of OFF OS RGCs

Perhaps the simplest mechanism by which a RGC can compute OS is by aligning its dendrites along the preferred orientation so that it receives more excitation from bipolar cells in the preferred than in the orthogonal orientation. Dendritic asymmetry is part of the mechanism of some retinal OS cells (Bloomfield, 1994; Murphy-Baum and Taylor, 2015; Nath and Schwartz, 2016; Venkataramani and Taylor, 2016), but it is absent in others (Nath and Schwartz, 2016; Venkataramani and Taylor, 2010). We examined the morphology of OFF OS RGCs and its relationship to their orientation preference.

Our measurements of the morphology of OFF vOS RGCs were consistent with previous reports of JAM-B RGCs (Joesch and Meister, 2016; I.-J. Kim et al., 2008). OFF vOS RGCs were characterized by their highly asymmetric dendrites pointing toward ventral retina (Fig. 4A). OFF hOS RGCs displayed more symmetric dendritic morphologies than OFF vOS RGCs (Fig. 4B). However, we did encounter 2 of 22 OFF vOS RGC with symmetric dendrites. OFF vOS cells stratified distal to the OFF choline acetyltransferase (ChAT) band (Fig. 4C). OFF hOS RGCs stratified in similar locations (Fig. 4D; p = 0.56, Mann–Whitney U-test). Comparing our morphological measurements with an online database of mouse RGC morphologies

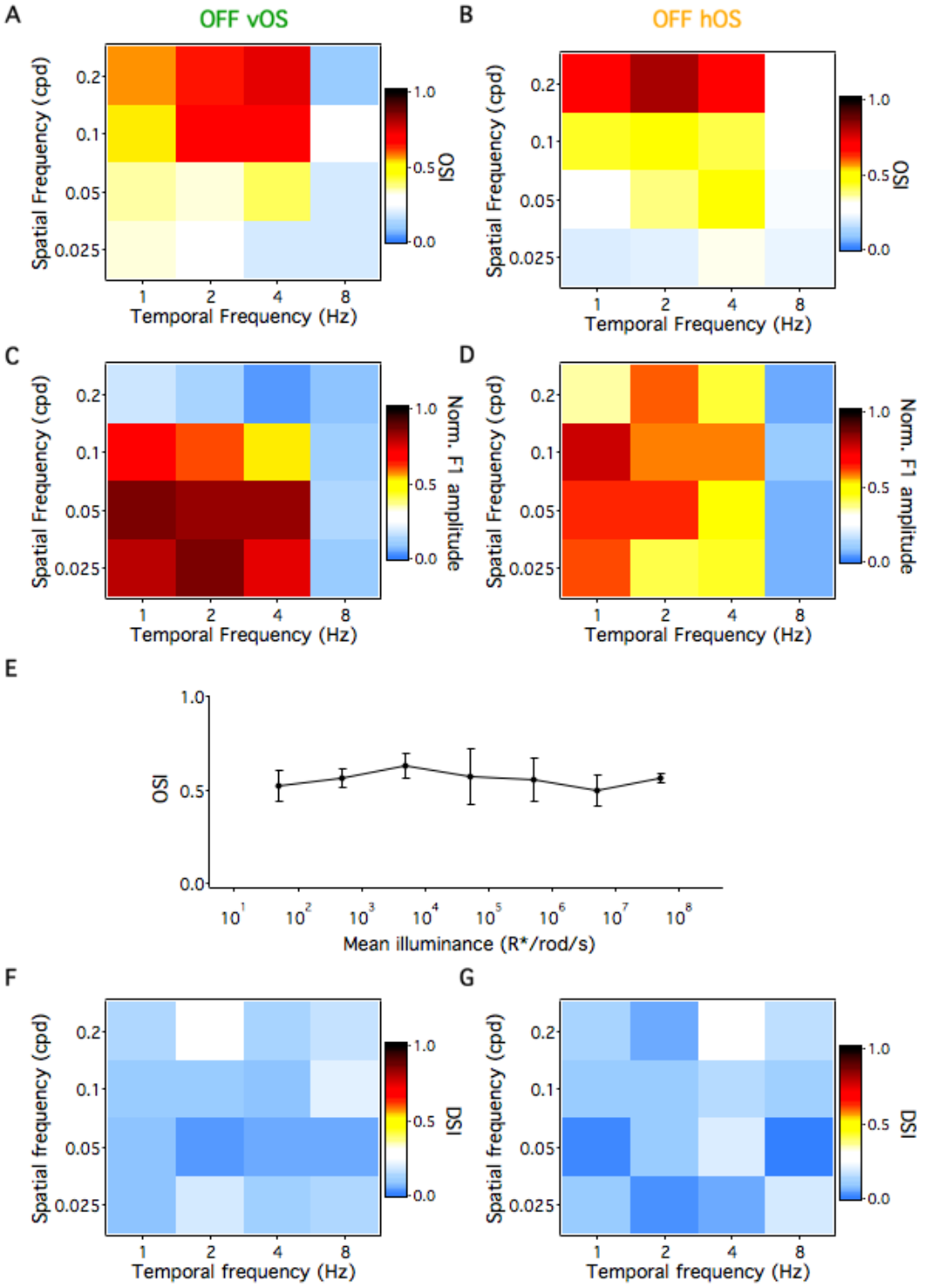

Figure 3. Spatiotemporal tuning of OFF OS RGCs to drifting gratings. (A, B) Heat maps of OSI of OFF vOS RGCs (n=3) **(A)** and OFF hOS RGCs (n=3) **(B)**. (C, D) Heat maps of normalized F1 response amplitudes of OFF vOS RGCs (n=3) **(C)** and OFF hOS RGCs (n=3) **(D)**. **(E)** OSIs of drifting grating responses of OFF OS RGCs across 7 different mean background illumination levels. Error bars indicate SEM across n=8 cells. **(F, G)** Heat maps of DSI of same OFF vOS RGCs (n=3) **(F)** and OFF hOS RGCs (n=3) **(G)** as in **(C)** and **(D)**.

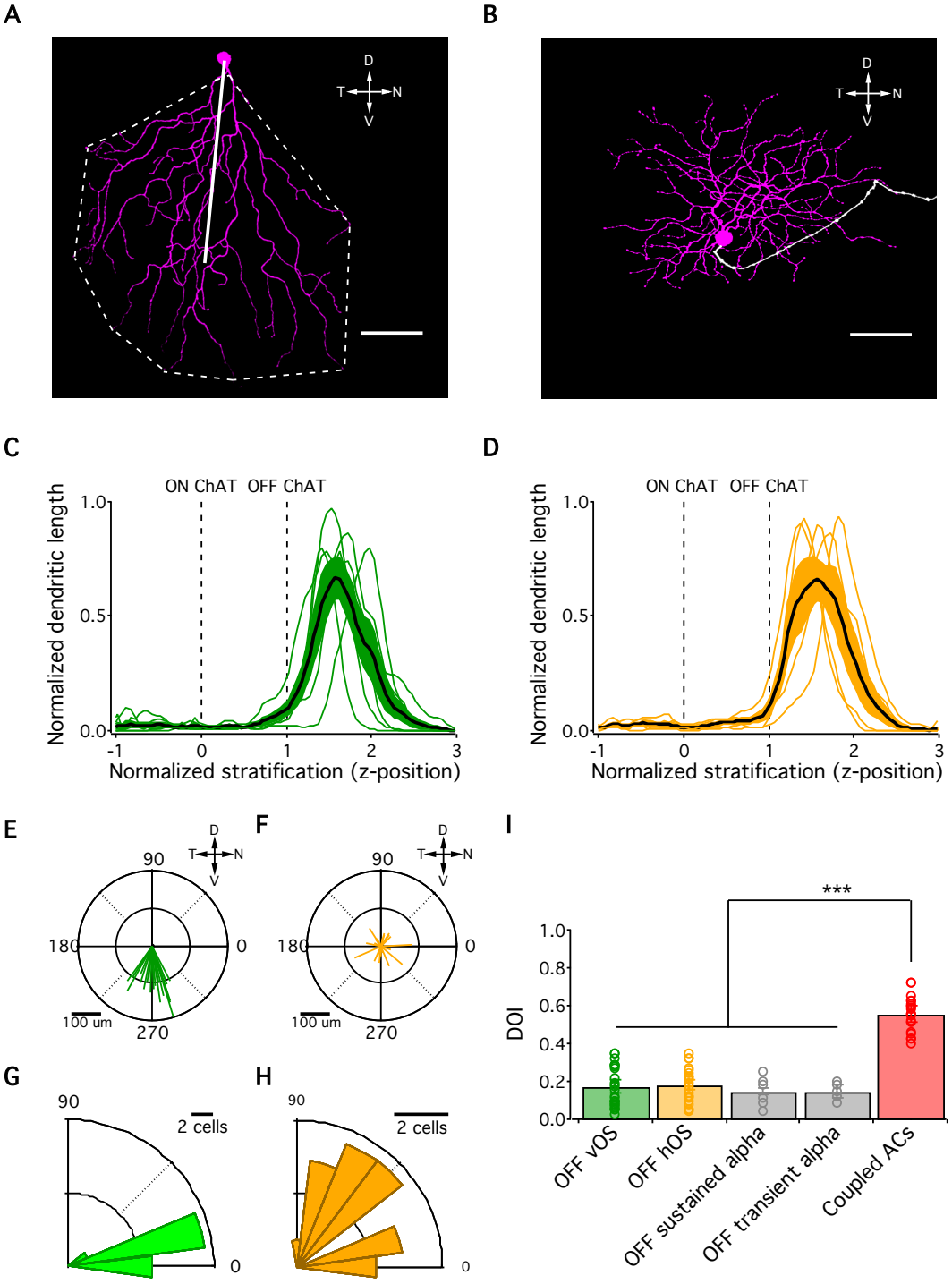

Figure 4. Morphology of OFF OS RGCs. (A, B) Dendritic morphologies of vertical OFF OS RGC **(A)** and horizontal OFF OS RGC **(B)**. OFF dendrites are represented in magenta and axons are in white. Scale bar = 50 µm. Dashed line in **(A)** shows outline of dendrites. Solid line is the vector from the soma to the center of mass (COM). **(C, D)** Z-profiles of OFF vOS **(C)** and OFF hOS **(D)** dendritic arbor stratification. Thin green and orange lines indicate profiles of individual OFF vOS and OFF hOS cells, respectively. Thick black lines represent mean for OFF

vOS (n = 6) and OFF hOS (n = 5). Dotted lines indicate ON and OFF starburst planes. The inner nuclear layer (INL) is located to the right and the ganglion cell layer (GCL) is located to the left. Shaded regions indicate SEM across cells. **(E, F)** Polar plots of COM vectors of OFF vOS (n = 24) **(E)** and OFF hOS (n = 22) **(F)** RGCs. Scale bar = 50 µm. **(G, H)** Rose plots of absolute differences between OS angle (θ_{OS}) and COM vector angle ($\theta_{COM\ vector}$) of ON vOS RGCs (n = 24) **(G)**, and OFF hOS RGCs (n = 22) **(H)**. **(I)** Dendritic orientation index (DOI) of OFF OS RGCs (n = 26 OFF vOS and 23 OFF hOS), OFF sustained alpha (n = 6), OFF transient alpha (n = 5) and amacrine cells coupled to OFF OS RGCs (n = 19). ***p < 0.001

(http://museum.eyewire.org; (Bae et al., 2017), we believe that the most likely matches are type '2aw' for OFF vOS RGCs and type '2i' for OFF hOS RGCs.

To quantify dendritic asymmetry, we fit polygons to the dendritic trees and calculated the area and the center of mass (COM) of the arborizations. OFF vOS RGCs had larger dendritic area than OFF hOS RGCs (4.48 ± 0.48 × 104 µm2, n = 26 vs. 3.93 ± 0.27 × 104 μm^2, n = 23, two-sample t test, p = 0.044). Vectors from the soma to the COM of the arborizations were significantly longer in OFF vOS cells than in OFF hOS RGCs (145.52 ± 8.09 µm vs. 50.09 ± 5.11 µm, two-sample t test, $p < 10^{-11}$) (Fig. 4E, F). These vectors were directed ventrally in OFF vOS RGCs (n = 26, $p < 10^{-6}$, Hodges–Ajne test) but pointed in random directions in OFF hOS RGCs (n = 23, p = 0.13, Hodges–Ajne test, Fig. 4E, F).

We measured the difference angle between the preferred orientation of the light response and the soma to dendritic COM vectors. In OFF vOS RGCs, the dendrites were well aligned to the preferred orientation (Fig. 4G). This relation was significantly different from a random uniform distribution (Hodges–Ajne test, p < 0.01). Due to the symmetric morphology of OFF hOS RGCs, there was no significant relationship between orientation preference and dendrites (Fig. 4H, Hodges–Ajne test, p = 0.61).

An asymmetry from soma to dendrites does not alone constitute a mechanism for OS. Since bipolar cell axons are small relative to the dendritic arbors of these RGCs and since they form tight mosaics (Wassle et al., 2009), the simple excitatory OS mechanism requires substantially oriented RGC dendrites with respect to their COM, not the soma (Discussion). We quantified the orientation of RGC dendrites relative to their COM using an index, dendritic orientation index (DOI), analogous to the vector sum orientation index we used to quantify the OS spike responses (Fig. 4I, Methods). Despite their soma-to-dendrites asymmetry, OFF vOS RGC dendrites were not significantly more oriented around their COM than those of OFF hOS RGCs or the two OFF alpha RGC types (two sample t test, $p = 0.64$). Moreover, DOIs of OFF OS RGCs were similar to that of well-known OFF RGCs with symmetric dendrites (Fig. 4I, two sample t test, $p > 0.2$ for all pairwise tests). In contrast with the lack of oriented dendrites in these RGCs, the coupled amacrine cells described below (see Fig. 5, 10) indeed had significantly higher DOI (Fig. 4I, two sample t test, $p < 10^{-3}$ for all pairwise tests). These results suggest that oriented dendrites alone cannot explain OS in either of the OFF OS RGC types, but oriented morphology is likely important in certain OS amacrine cells as has been shown in the rabbit retina (Bloomfield, 1994; Murphy-Baum and Taylor, 2015).

<u>OFF OS RGCs are coupled to ACs via Cx36 gap junctions.</u>

In the course of our morphology experiments, we noticed coupled cell bodies after filling OFF OS RGCs with neurobiotin. We traced the dendrites of some of the cells coupled to OFF vOS RGCs. These amacrine cells had somata in the inner nuclear layer (INL) and exhibited striking

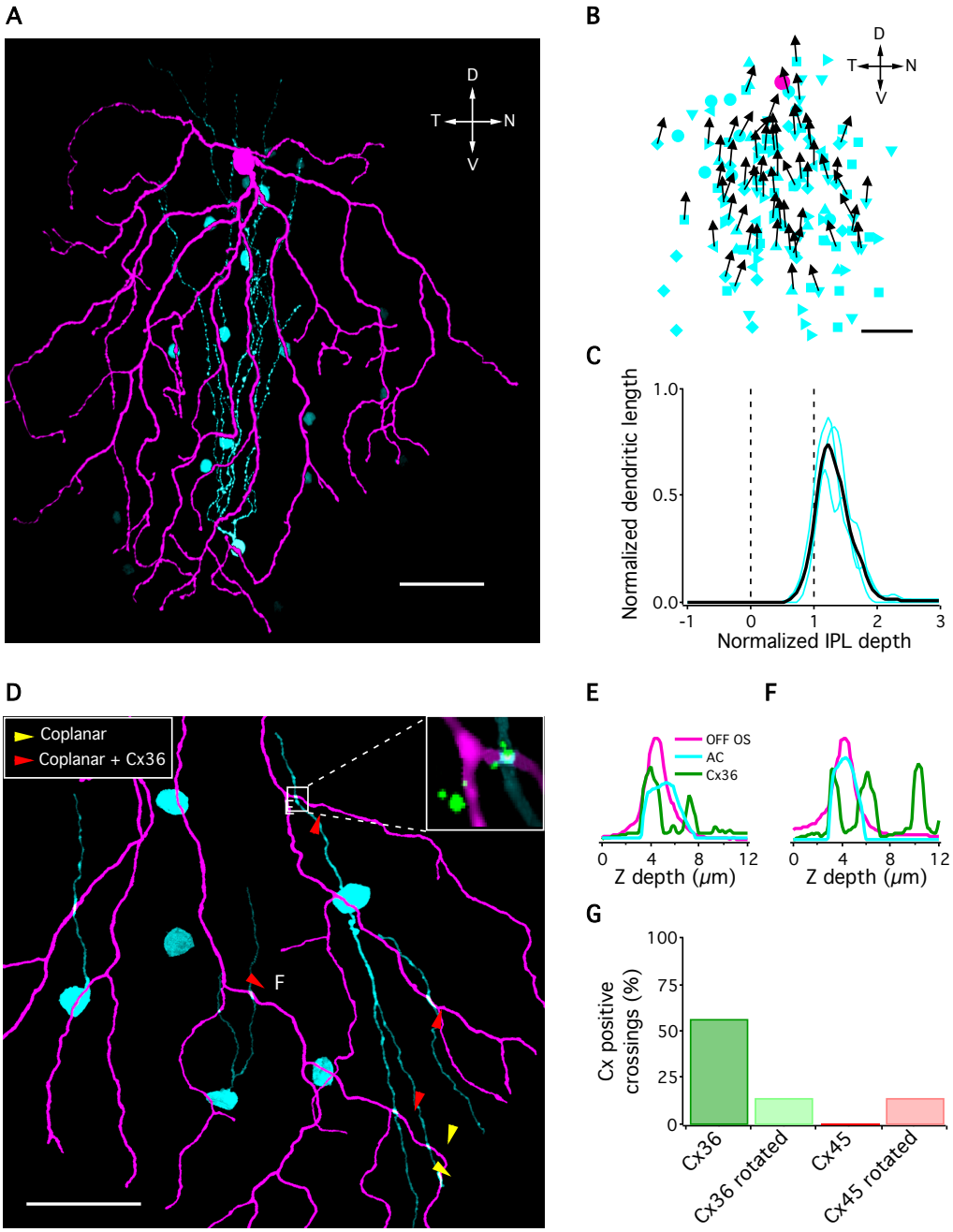

Figure 5. Electrical coupling between OFF OS RGCs and amacrine cells. (A) OFF OS RGC (magenta) and neurobiotin coupled amacrine cells (cyan). One of the coupled cells is traced. Scale bar = 50 µm. **(B)** Positions of amacrine cells coupled to OFF OS RGCs (cyan symbols). Different cyan symbols indicate cells from different experiments (n = 131 cells total from seven RGCs). Amacrine cells are plotted with respect to the RGC (magenta circle). Directions of primary dendrites are shown in black arrows when they were visible. Scale bar = 50 µm. **(C)**

Stratification of coupled amacrine cells dendrites in IPL. Cyan lines indicate profiles of individual amacrine cells. Black line represents mean across three cells. Dotted lines indicate ON and OFF starburst planes. The inner nuclear layer (INL) is located to the right and the ganglion cell layer (GCL) is located to the left. **(D)** Magnified view of an OFF OS (magenta) and amacrine cell (cyan) coupled network. Yellow and red arrowheads indicate coplanar dendrite crossings and coplanar dendrite crossings positive for connexin 36 (Cx36). Inset shows an example crossing with Cx36 puncta. Scale bar = 50 μm. **(E, F)** Z-axis profiles of fluorescent intensities for OFF OS, amacrine cell dendrites and Cx36 puncta. **(G)** Percentage of coplanar crossings that are connexin positive. A total of 58% (4/7) coplanar crossings were Cx36 positive and 0% (0/7) were Cx45 positive. A total of 14% (1/7) coplanar crossings were positive for either Cx36 or Cx45 when the connexin channels were rotated by 90°.

asymmetric morphology (Fig. 5A). All of their dendrites were aligned dorsally, opposite to the RGC dendrites (Fig. 5A, B). The coupled ACs stratified distal to the OFF ChAT band, overlapping OFF OS RGCs (Fig. 5C). On average a single OFF vOS RGC was coupled to 19 ± 2.3 cells in the INL (n = 7 RGCs). We observed weak coupling from OFF hOS RGCs to cells in the ganglion cell layer and INL, but we were unable to characterize their morphology (Discussion).

To identify the molecular identity of the connexin proteins forming the gap junctions, we stained a coupled network with different antibodies against connexin 36 (Cx36) and connexin 45 (Cx45) (Fig. 5D-G). We found that 57% of putative connections between OFF vOS RGCs and coupled amacrine cells colocalized with Cx36 puncta. Rotating the Cx36 channel by 90° eliminated most of the colocalization. The same analysis for Cx45 revealed no significant colocalization with putative crossings (Fig. 5G). We conclude that Cx36 is the predominant (possibly the only) connexin mediating gap junctions between OFF vOS RGCs and ACs.

Synaptic conductances in OFF OS RGCs

To understand the functional role of gap junctions in OFF OS RGCs, we searched for an electrophysiological signature of electrical synapses. Unlike synaptic currents from chemical

synapses, a source of current arising from electrical coupling remains constant in magnitude at different holding potentials and does not reverse polarity (Akrouh and Kerschensteiner, 2013; Kuo et al., 2016). A 200 μm diameter spot evoked currents with both transient and sustained components at light onset. The current reversed at −67 ± 4 mV (Fig. 6A, B, n = 15 cells), consistent with a source (mostly) from inhibitory chloride channels. Stimulation with much larger spots (1200μm diameter) produced slower currents with only a sustained component (Fig. 6C). We took advantage of the different time course of these currents to analyze their current-voltage (IV) relationships separately in different time windows (Fig. 6A-C). Unlike the inhibitory currents for smaller spots, the magnitude of these sustained currents remained constant and did not reverse at any holding potential tested (Fig. 6D). We attributed this current to electrical synapses, and we hypothesized that it was present for small stimuli as well, but was overwhelmed by the much larger inhibitory current. The peak outward current at light onset measured at the excitatory reversal potential was 757 ± 76 pA (Fig. 6F, n = 9 OFF vOS and OFF hOS cells). There was no significant difference between currents for OFF vOS and hOS RGCs ($p = 0.66$, Mann–Whitney U-test). The amplitude of gap junction currents was also similar between the two OFF OS RGC types (Fig. 6F, peak current=80 ± 12 pA, n = 6 OFF vOS and 72 ± 9 pA, n = 5 OFF hOS cells, $p = 0.54$, Mann–Whitney U-test).

To examine the spatial receptive field of the inhibition and the putative gap junction input, we presented spots of varying sizes while measuring the currents at either the excitatory or inhibitory reversal potential. These experiments revealed that inhibition acted upon narrow spatial scales, whereas the gap junction currents were more wide-field (Fig. 6E). For large spots, inhibition was absent in OFF OS RGCs, which helped us isolate the gap junction currents.

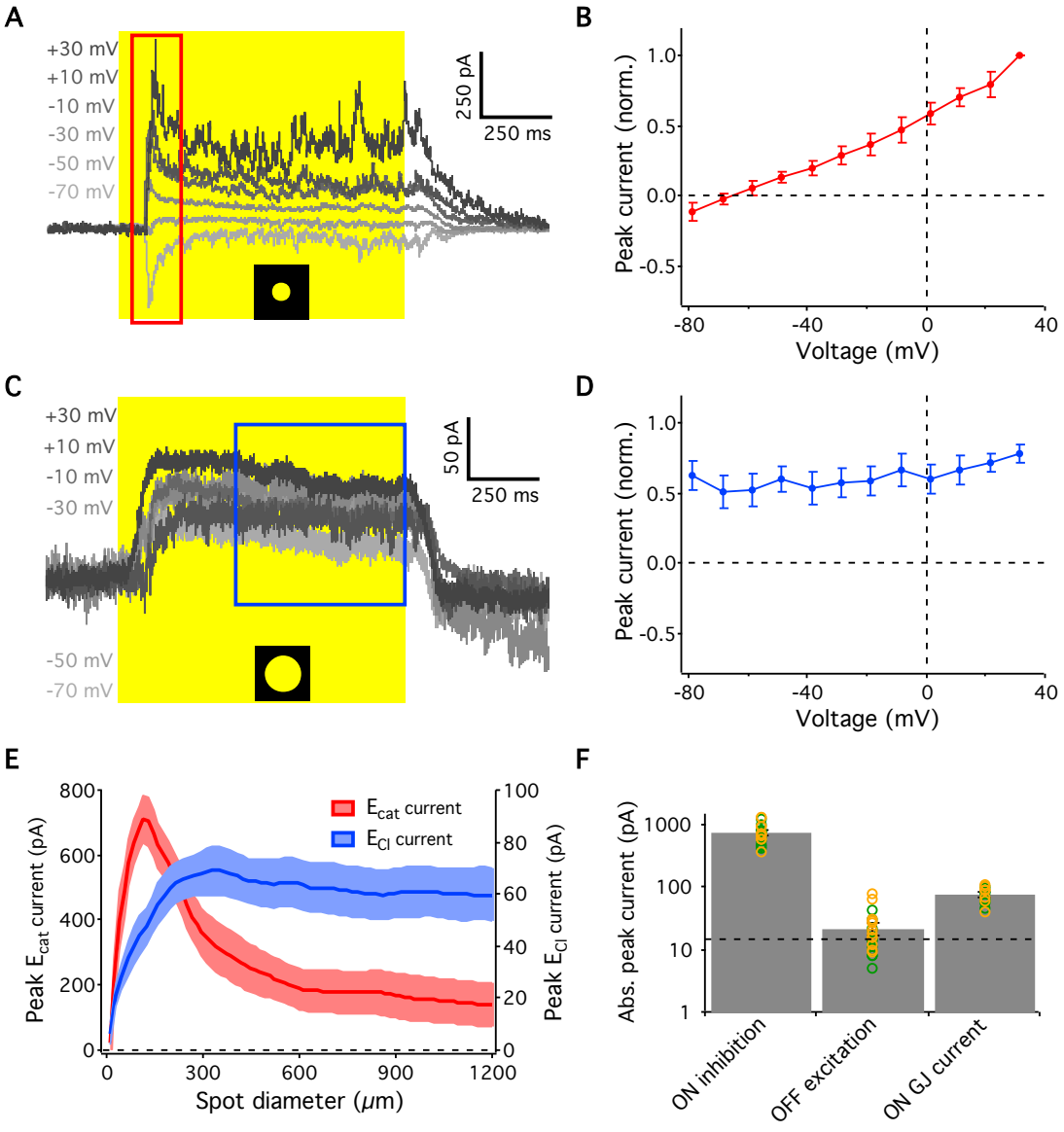

Figure 6. Synaptic inputs to OFF OS RGCs. (A) Current evoked in an OFF OS RGC by a light step (200 µm diameter) from darkness measured across a range of holding voltages. Yellow rectangle indicates light stimulus. **(B)** IV relationship for the stimulus in a. Error bars indicate SEM across n = 13 cells. Peak currents were measured in the temporal window (0–200 ms) indicated by red rectangle in **(A)**. (C) Current evoked in an OFF OS RGC by a light step (1200 µm diameter) from darkness measured across a range of holding voltages. Yellow rectangle indicates light stimulus. **(D)** IV relationship for the stimulus in **(C)**. Error bars indicate SEM across n = 13 cells. Peak currents were measured in the temporal window (500–1000 ms) indicated by blue rectangle in **(C)**. **(E)** Peak currents at excitatory reversal potential (red trace) and chloride reversal potential (blue trace) to spots of varying diameters for n = 13 cells. Currents were measured in a 0–200 ms temporal window at E_{cat} and 500–1000 ms temporal window at E_{Cl}. Shaded regions indicate SEM across cells. **(F)** Absolute peak currents evoked by a 200 µm diameter spot of light in OFF OS RGCs. Dotted line indicates peak baseline noise level. Note logarithmic scale.

Inhibition localized narrowly around the RGC dendrites is opposite to the dogma of its contribution to the receptive field surround, and we will return to this feature of our findings in the Discussion.

Pharmacology experiments revealed contributions of both GABA and glycine receptors to the inhibitory currents in OFF OS RGCs (Fig. 7A, B). GABAergic synapses account for most of the inhibition in these cells (Fig. 7C, 62% GABA, 25% glycine). In total inhibitory block, gap junction currents were still present and still showed a flat IV relationship (Fig. 7D). This result supports our interpretation of the flat IV as a sign of an electrical synapse.

Notably, we observed no excitatory current at light offset in OFF OS RGCs under our stimulus conditions. Peak currents at light offset measured at the inhibitory reversal potential were not significantly different from baseline noise before the light stimulus (Fig. 6F, −22.08 ± 4.74 pA, n = 18 cells, p = 0.09, Mann–Whitney U-test). A lack of excitation at light offset is consistent with the spiking patterns we observed in which firing was suppressed at light onset and returned only modestly above its baseline rate at light offset (Fig. 1A).

Two recent studies reported excitatory synapses onto JAM-B RGCs in voltage-clamp (Joesch and Meister, 2016) and by anatomical apposition with OFF bipolar cell ribbons in light microscopy (Neumann et al., 2016), so we performed additional experiments in an effort to reconcile our finding of a lack of OFF excitation with these reports. Presynaptic inhibition from amacrine cells onto bipolar cell terminals often has a powerful influence in suppressing excitatory transmission (Grimes, 2012; Zhang and McCall, 2012), so we analyzed the currents in OFF vOS RGCs with gabazine blocking $GABA_A$ receptors throughout the retina (Fig. 8). This

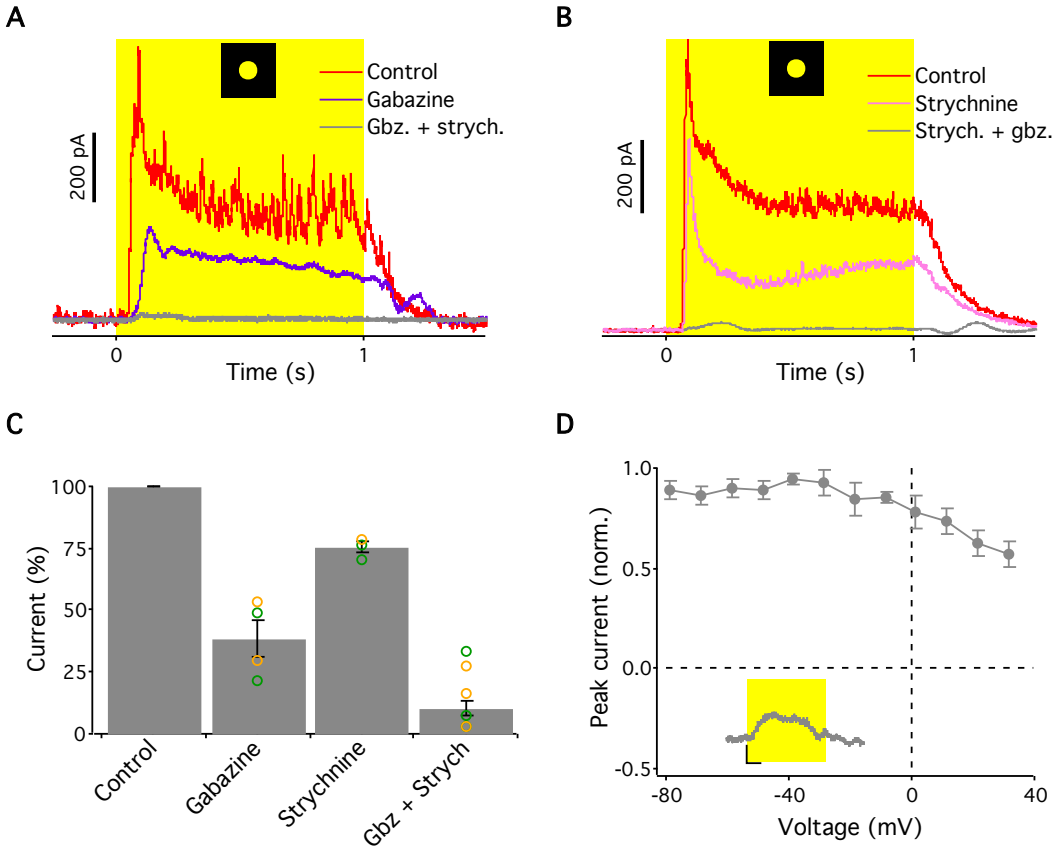

Figure 7. Pharmacology of inhibitory conductances in OFF OS RGCs. (A, B) Effect of gabazine and strychnine on light step responses (200 µm diameter) of example OFF OS RGCs from darkness. Gabazine and strychnine are bath applied first in **(A)** and **(B)** respectively. Cells are voltage clamped at E_{cat}. **(C)** Percentage change in peak currents measured at E_{cat} in inhibitory antagonists **(A, B)**. Error bars indicate SEM (n = 4 for gabazine, n = 4 for strychnine and n = 8 for both drugs). **(D)** IV relationship for the residual current in both inhibitory antagonists. Inset shows light step response (200 µm diameter) from darkness after application of both inhibitory blockers. Scale for inset: Y-axis = 100 pA, X-axis = 200 ms. Error bars indicate SEM across n = 8 cells.

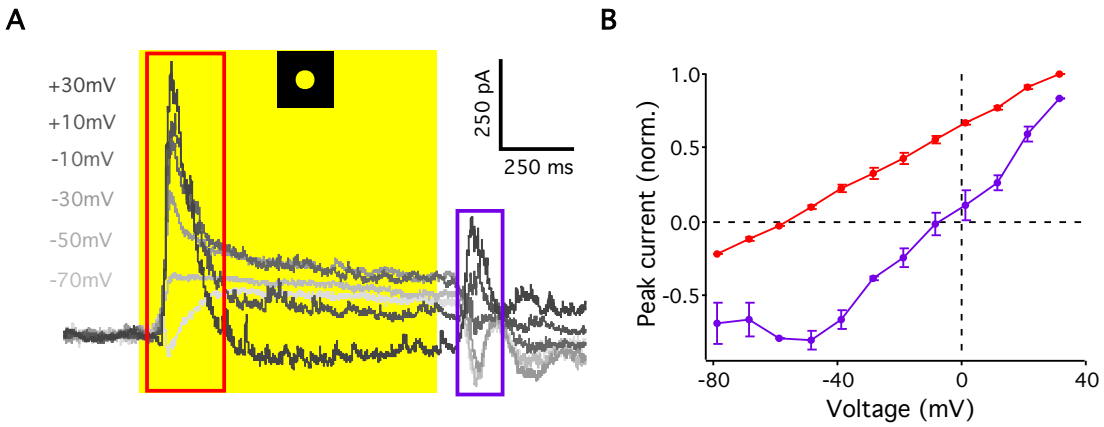

Figure 8. Removal of presynaptic inhibition reveals excitatory synaptic inputs to OFF OS RGCs. (A) Current evoked in an OFF OS RGC in presence of bath applied gabazine by a light step (200 µm diameter) from darkness measured across a range of holding voltages. Yellow rectangle indicates light stimulus. **(B)** IV relationship for the stimulus in (a). Error bars indicate SEM across n = 4 cells. Peak currents were measured in the temporal windows (0-200ms, red rectangle and 1000-1200ms, purple rectangle) indicated in **(A)**.

pharmacological manipulation indeed revealed a small inward current at light offset. IV analysis showed a J-shaped curve reversing near 0mV, consistent with a substantial contribution from NMDA receptors. Thus, excitatory synapses from OFF bipolar cells are present on OFF vOS RGCs, but they remained silent under the range of stimulus conditions we tested.

In summary, our voltage-clamp experiments coupled with pharmacology using inhibitory antagonists revealed three currents in OFF OS RGCs: (1) inhibition at light onset driven by $GABA_A$ and glycine receptors that is strongest for small stimuli, (2) an outward gap junction current at light onset that lacks surround suppression, and (3) an excitatory current that was unmasked after $GABA_A$ receptor blockade. We interpret these results in the form of a schematic circuit diagram in the Discussion.

Electrical synapses carry OS information

What are the relative contributions of electrical and chemical inhibitory synapses to OS in OFF OS RGCs? We measured the tuning curves of both currents in response to drifting gratings at different orientations (Fig. 9). While inhibition was similar at all orientations, gap junction currents had larger amplitude oscillations for drifting gratings in the preferred orientation than the null orientation. Importantly, the gap junction currents in the preferred orientation included substantial fluctuations below baseline, representing a net inward current, while currents were predominantly outward in the null orientation (Fig. 9B, C). We quantified grating responses by taking the cycle average current and measuring the peak inward current for gap junction currents and, correspondingly, the minimum outward current for inhibition. We

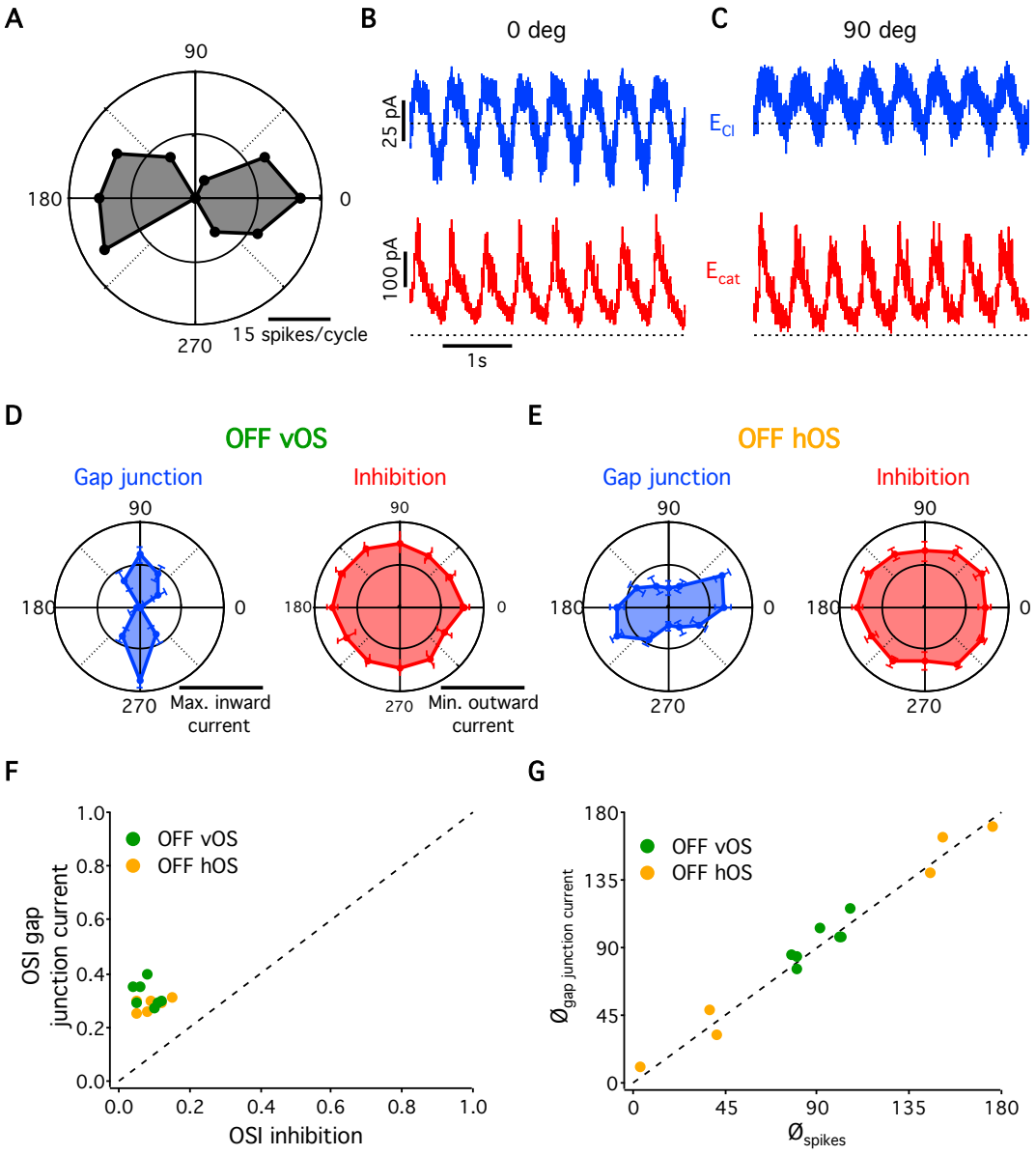

Figure 9. Synaptic responses to drifting gratings in OFF OS RGCs. (A) Polar plot of drifting grating responses of an example OFF OS RGC. **(B, C)** Raw traces of recorded currents at E_{Cl} (blue) and E_{cat} (red) currents at preferred **(B)** and null (C) orientations, respectively, for the cell in **(A)**. **(D, E)** Polar plots of population averaged normalized maximum inward gap junction (blue) and minimum outward inhibitory currents (red) for OFF vOS (n = 7, **D**) and OFF hOS (n = 6, **E**) RGCs. Error bars are SEM across cells. Inhibitory currents were obtained by subtracting the ECl current from Ecat current. (F) OSI of gap junction current plotted against OSI of inhibition for OFF vOS (n = 7) and OFF hOS (n = 6). **(G)** OS angle of gap junction ($\theta_{gap\ junction\ current}$) current plotted against OSI of cell attached spikes (θ_{spikes}) for OFF vOS (n = 7) and OFF hOS (n = 6).

chose this quantification because we sought to measure the influence of currents during the dark phase of the gratings, the period in which net depolarization causes OFF OS RGC's to spike in the preferred orientation. Population averages revealed OS gap junction currents and non-OS inhibition for both horizontal and vertical OFF OS RGC types (Fig. 9D-F, $OSI_{gap\ junction}$ significantly larger than OSI_{inh}, paired t test, $p < 10^{-4}$ for both OFF vOS and hOS). The tuning of gap junction input matched that of the spiking responses (Fig. 9G).

To measure directly the coupled OS amacrine cell type implicated in this circuit, we used a transgenic mouse line (Etv1), in which several amacrine cell types are sparsely labelled (Fig. 10). Coupling between OFF vOS RGCs and a labelled asymmetric amacrine cell was verified anatomically. Neurobiotin tracer injected in an OFF vOS RGC passed into the labelled amacrine cell, and Cx36 puncta were present at crossing points (Fig. 10A-C). An asymmetric AC recorded in this line hyperpolarized to a light spot (Fig. 10E), consistent with the outward gap junction currents recorded from OFF vOS RGCs (Fig. 6C), and it had OS responses to drifting grating stimuli aligned to the orientation of its neurites (Fig. 10F, G).

Next, we sought a causal manipulation to demonstrate the importance of electrical synapses in the computation of OS in OFF OS RGCs (Fig. 11). Meclofenamic acid (MFA) has been used to block gap junction-mediated signaling in the retina (Pan et al., 2007; Veruki and Hartveit, 2009). Bath application of MFA (100 μM) abolished spiking activity in OFF OS RGCs when presented with drifting gratings. We were able to record subthreshold responses in current clamp recordings. In MFA, subthreshold responses were still apparent for each cycle of the grating, but the responses were no longer OS (Fig. 11A-E, I, OSI Iclamp control = 0.33 ± 0.06, OSI MFA = 0.1 ± 0.01, p = 0.029, paired t test). While this result shows that gap junctions are

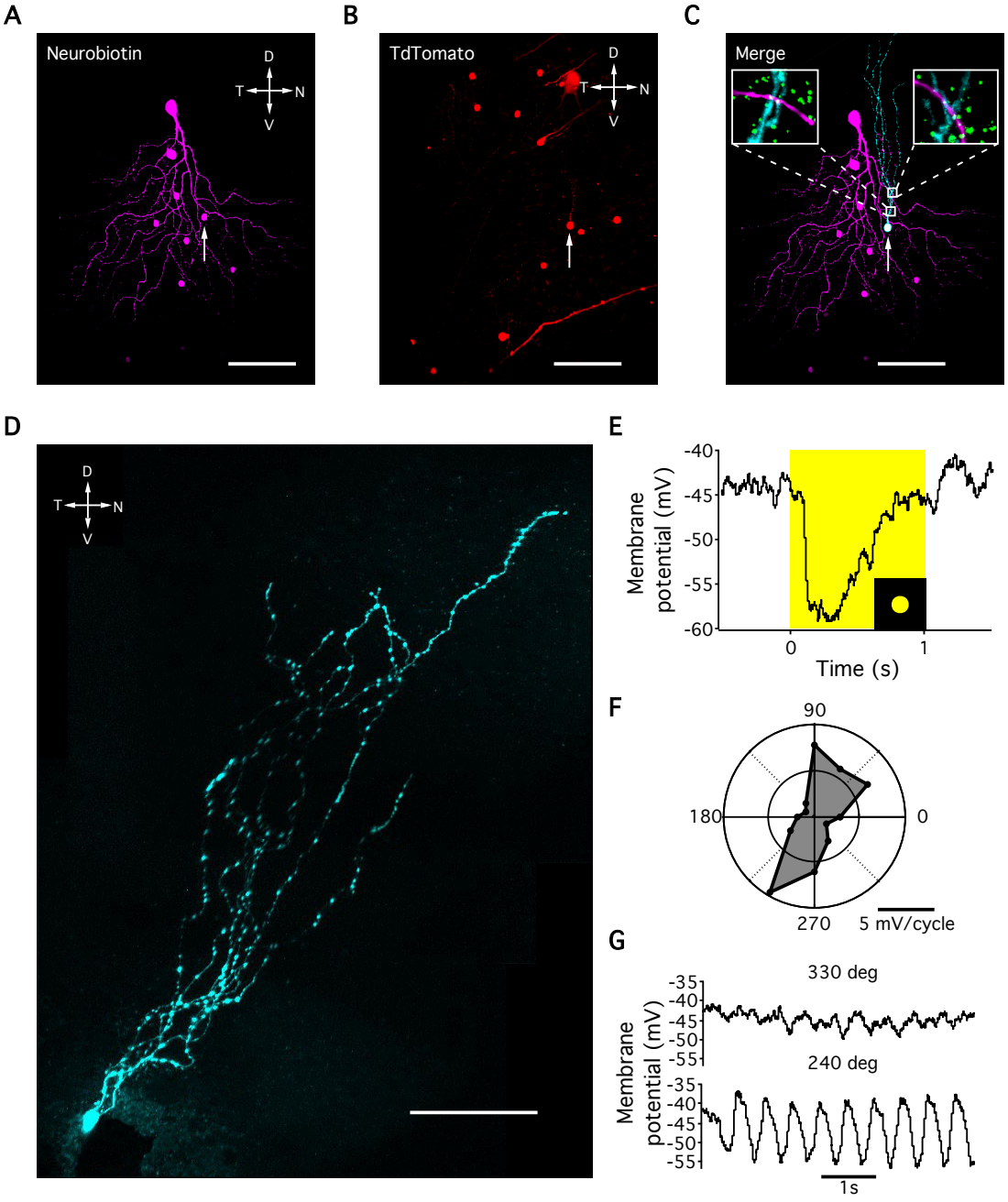

Figure 10. ACs coupled to OFF OS RGCs are OS. (A) Morphology of an OFF vOS RGC filled with neurobiotin in Etv1 transgenic retina. Coupled amacrine cells are also neurobiotin positive. **(B)** TdTomato labeled cell somas in Etv1 transgenic retina. **(C)** TdTomato fluorescence is present in the soma of one of the ACs coupled to OFF vOS RGC. The AC is traced and pseudocolored cyan. Insets show existence of Cx36 puncta (green) at crossings between ganglion cell (magenta) and amacrine cell (cyan) dendrites. Scale bars = 50 µm. **(D)** Morphology of a traced Etv1 OFF OS AC filled with Alexa 488 dye. Scale bar = 100 µm. **(E)** Response of Etv1 OFF OS AC to a 1s flash of 200 µm diameter circular light spot from darkness. Yellow rectangle indicates light stimulus. **(F)** Polar plot of drifting grating responses of Etv1 OFF OS AC. **(G)** Raw traces of recorded membrane potentials of the same cell in **(F)** along preferred and null orientations.

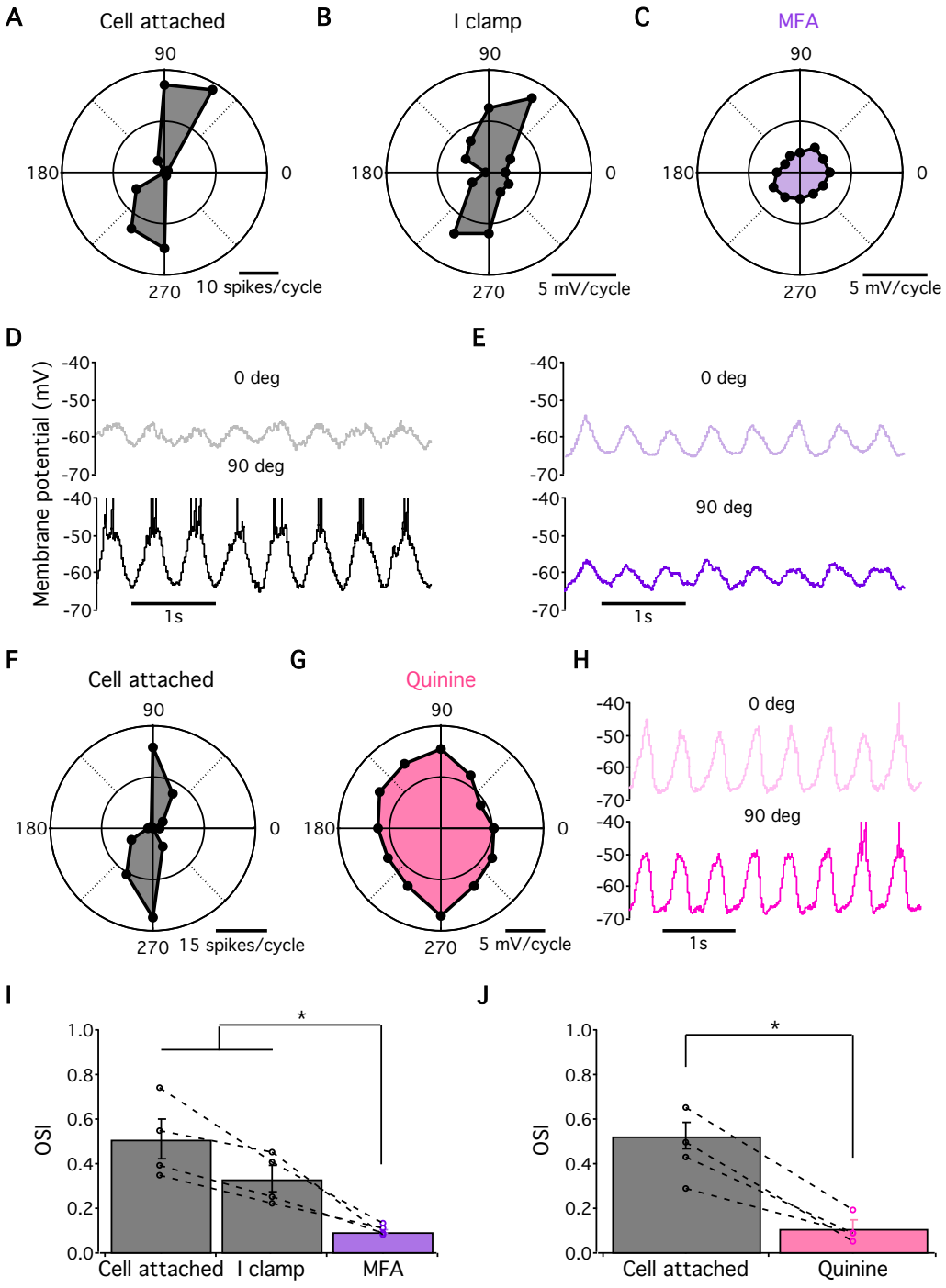

Figure 11. Electrical synaptic inputs are necessary for OS. (A) Polar plot of drifting grating responses of an example OFF OS RGC. **(B, C)** Polar plot of drifting grating responses of the same cell in a in current clamp before **(B)** and after **(C)** bath application of MFA. **(D, E)** Raw traces of recorded membrane potentials of the same cell in **(A)** along preferred and null orientations before **(D)** and after **(E)** bath application of MFA. **(F)** Polar plot of drifting

grating responses of an example OFF OS RGC. **(G)** Polar plot of drifting grating responses of the same cell in **(F)** in current clamp after intracellular application of quinine. **(H)** Raw traces of recorded membrane potentials of the same cell in **(F)** along preferred and null orientations after intracellular application of quinine. **(I)** OSI of drifting gratings responses in cell attached mode (grey) and in current clamp mode before (grey) and after (purple) MFA application. Error bars indicate SEM across n = 4 (n = 2 OFF hOS and n = 2 OFF vOS) cells. Dashed lines connect measurements from the same cell. **(J)** OSI of drifting gratings responses in cell attached mode (grey) and in current clamp mode after quinine application (pink). Error bars indicate SEM across n = 4 (n = 2 OFF hOS and n = 2 OFF vOS) cells. *$p < 0.05$

necessary for the OS computation in OFF OS RGCs, it does not prove that the essential gap junctions are in the RGC itself, since MFA blocks electrical synapses throughout the retina (Kuo et al., 2016). To achieve better specificity, we blocked Cx36 gap junctions intracellularly with quinine (800μM) (Srinivas et al., 2001). When we recorded responses to drifting gratings with quinine in the patch pipette, we observed reduced spiking activity and significantly decreased OS (Fig. 11F-H, J, OSI Iclamp control = 0.33 ± 0.06, OSI quinine = 0.11 ± 0.03, p = 0.019, unpaired t test). Since our quinine manipulation was specific for the single patched RGC, and the drug is selective for Cx36 gap junctions over the other types found in the inner retina (Bloomfield and Völgyi, 2009; Srinivas et al., 2001) it is likely that gap junctions essential for the OS computation were the same ones we identified anatomically (Fig. 5, Discussion). While quinine failed to eliminate all depolarization in OFF OS RGCs in response to drifting gratings possibly due to an incomplete block of gap junctions (Srinivas et al., 2001), the residual current was no longer OS, providing further evidence electrical synapses, rather than chemical synapses, carry OS information to these RGCs.

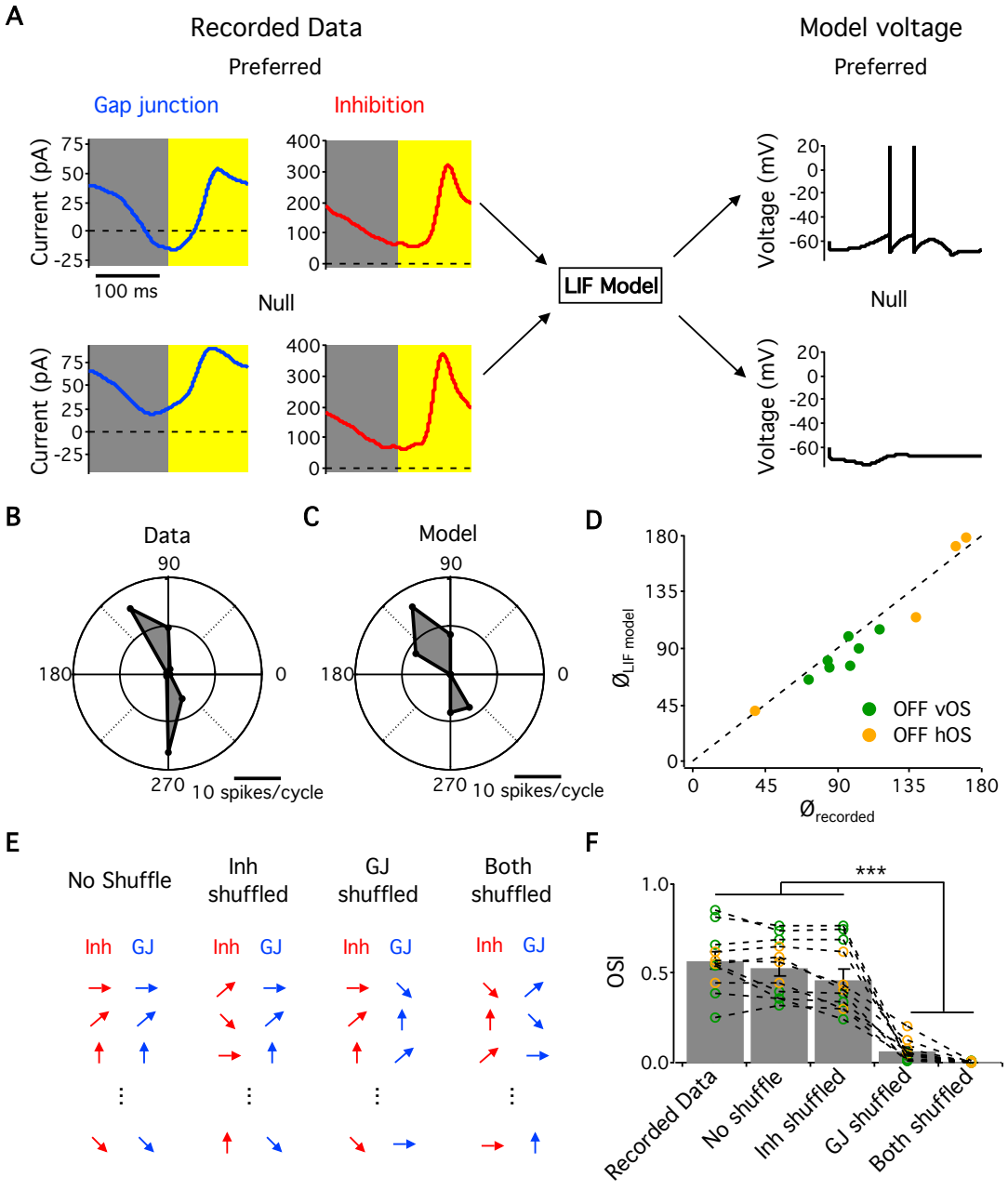

Figure 12. Leaky integrate and fire model of OFF OS RGCs. (A) Flowchart of the LIF model. Recorded cycle average gap junction and inhibitory currents measured in response to drifting grating stimuli were used as inputs in the LIF model to generate resulting membrane potential for different grating movement directions. **(B)** Polar plot of cell attached drifting grating responses of an example OFF OS RGC. **(C)** Simulated drifting grating response generated by the LIF model using the currents measured from the cell in **(B)**. **(D)** Scatter plot of recorded OS angles ($\theta_{recorded}$) vs. LIF model OS angles ($\theta_{LIF\ model}$). **(E)** Schematic showing the logic of different shuffling conditions of input currents. **(F)** OSI of the recorded data from four horizontal OFF OS RGCs (orange points) and seven vertical OFF OS RGCs (green points) along with OSI values from four different LIF model shuffling conditions. Dashed lines connect data and models from the same cells. Error bars indicate SEM across n = 11 cells. ***$p < 0.001$.

Modeling the OS computation in OFF OS RGCs

On the basis of our measurements of the synaptic currents in OFF OS RGCs, we constructed a conductance-based leaky integrate and fire (LIF) model of the circuit (Methods). The cycle average currents measured in whole-cell voltage clamp in response to drifting gratings were used as inputs to the model, and the model generated spiking behaviour for each grating angle (Fig. 12A). Recapitulating our experimental data, the model produced more spiking in the preferred orientation than in the null orientation. The LIF model was able to capture the shape of the orientation tuning curve (Fig. 12B, C), and the preferred orientations of individual cells (Fig. 12D).

To examine the necessity and sufficiency of electrical synaptic currents in generating OS, we shuffled synaptic currents between different grating angles (Fig. 12E). For all 11 cells (7 OFF vOS and 4 OFF hOS), the LIF model achieved nearly the same degree of OS as the recorded data, even with inhibitory currents recorded at different orientations randomly shuffled (Fig. 12F, two-sample t test, $p > 0.1$ for all pairwise tests). In contrast, shuffling the gap junction currents largely eliminated OS in the model (Fig. 12F, two-sample t test, $p < 10^{-4}$ for all pairwise tests). Our modelling results support the experimental result that OS in OFF OS RGCs is inherited from gap junctions with amacrine cells.

Discussion

Working model of the OFF OS circuit

A schematic circuit diagram for OFF OS RGCs based on our results is presented in Fig. 13. OFF bipolar cells form excitatory synapses with OFF OS RGCs (Neumann et al., 2016), however, under the range of stimulus conditions we tested, GABAergic inhibition prevents glutamate release from these synapses (Fig. 8). At light onset, OFF OS RGCs are inhibited by both GABAergic and glycinergic narrow-field amacrine cells (Figs. 4 and 5). Additionally, wide-field (oriented) OFF amacrine cells form electrical synapses with OFF OS RGCs (Figs. 5 and 6), and these synapses carry OS information to the RGC (Figs. 9, 11 and 12). The origin of OS in this circuit is presumably this coupled amacrine cell. Its highly asymmetric morphology (Figs. 4I, 5 and 10) suggests that, like other OS amacrine cells (Bloomfield, 1994; Murphy-Baum and Taylor, 2015), these cells might derive their OS simply from their asymmetric sampling of the bipolar cell mosaic (Fig. 13B), though other possibilities exist, including OS inhibition to the amacrine cell.

Similarities between OFF OS RGCs in mouse and rabbit retina

In this study, we report the presence of two OFF OS RGC types in the mouse retina and examine the circuit mechanisms of OS in these cells. OFF OS RGCs have been previously reported in the rabbit retina (Venkataramani and Taylor, 2010). Similar to mouse, the authors reported two types of rabbit OFF OS RGCs each preferring a cardinal orientation. Vertical-preferring rabbit OFF

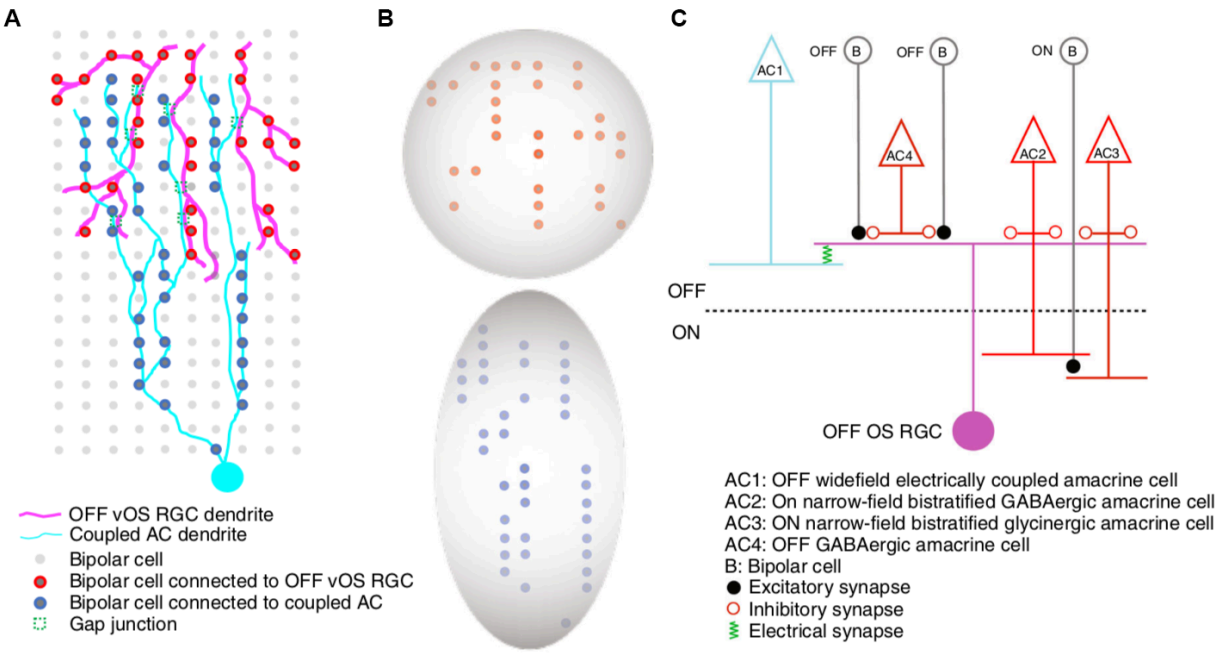

Figure 13. Schematic OFF OS RGC circuit model. (A) Top projection view of the OFF vOS RGC circuit. Dendrites of an OFF OS RGCs (magenta) are electrically coupled to an asymmetric amacrine cell (cyan). **(B)** Excitatory receptive fields for OFF vOS RGCs and coupled amacrine cells. The excitatory bipolar cell input to OFF vOS RGCs is predicted to be symmetric based on the cell's dendrites, whereas the excitatory input to the coupled cells is predicted to be asymmetric (Fig. 4). **(C)** Schematic model of neural circuit underlying the OS computation in OFF OS RGCs.

OS RGCs possess asymmetric dendritic morphology, whereas the horizontal-preferring RGCs have symmetric dendrites. Voltage-clamp recordings and pharmacology in rabbit OFF OS RGCs showed that OS relies on GABAergic inhibition. However, in our recordings, the combined inhibitory drive (consisting of both GABAergic and glycinergic components (Fig. 7) was found to be non-OS (Fig. 9).

Several morphological studies in teleost fish and rabbit retina report ACs similar to the ones coupled to OFF OS RGCs, all with dorsally pointing dendrites (Bloomfield, 1994; H. J. Wagner and E. Wagner, 1988)Famiglietti, 1989; Bloomfield, 1994; (Hoshi and Mills, 2009). One study in rabbit found these ACs tracer coupled to a RGC type called G3 (Hoshi and Mills, 2009). On the basis of morphological similarity, they proposed that the G3 RGC in rabbit was analogous to the JAM-B RGC in mouse. The authors went on to speculate that the anatomical circuit composed of prominent asymmetric ganglion and amacrine cell dendrites might result in orientation bias. Our imaging results also revealed oriented amacrine cells coupled to OFF vOS cells (Fig. 5A-C). Furthermore, similar to our findings in mouse, gap junctions between rabbit G3 RGCs and dorsally directed ACs also contained Cx36. A comprehensive electron microscopy study (Helmstaedter et al., 2013) reported a type of amacrine cell (ac 19–30) with oriented dendrites and a stratification profile matching the amacrine cells we observed coupled to OFF vOS RGCs.

A non-canonical complement of synaptic inputs

Our findings challenge the canonical organization of retinal circuits. Under a range of stimulus conditions, OFF OS RGCs lack excitatory currents. While spiking in RGCs is generally highly dependent on excitation from bipolar cells, there is precedent in the literature for RGCs in which inhibition is much larger than excitation and serves as the main driver modulating spiking (Jacoby et al., 2015; Murphy and Rieke, 2011; Sivyer et al., 2010). We were able to unmask excitatory synapses in $GABA_A$ receptor block (Fig. 8), but not in any of our stimulus conditions. It remains possible that different stimuli could unmask this excitatory current, and the search for those stimulus conditions remains an interesting target for future investigation.

Another way in which the OFF OS RGC circuit differs from canonical circuits is the spatial structure of inhibition. Unlike the wide-field OS input from electrical synapses, the inhibitory currents we recorded at light onset had strong surround suppression (Fig. 6E). This counters the common pattern of inhibition extending beyond the dendritic field of the RGC to contribute to its receptive field surround. Another mouse RGC was recently reported to have a similar receptive field structure in which inhibition has stronger surround suppression than excitation (Mani and Schwartz, 2017).

A novel role for gap junctions in the retina

The most striking way in which OFF OS RGCs differ from previously described RGCs is that gap junctions, rather than playing a supportive or modulatory role (Murphy and Rieke, 2011; Völgyi et al., 2013), are critical for the cell's feature selectivity. Currents transmitted by

electrical synapses are crucial for computing OS in OFF OS RGCs (Figs. 9, 11 and 12). This represents a new paradigm for thinking about the role of amacrine cell-RGC gap junctions. Though we observed no significant differences in the physiology or OS of gap junction currents between OFF vOS and OFF hOS RGCs, we were only able to trace the morphology of the amacrine cells coupled to OFF vOS RGCs. Perhaps a connexin other than Cx36 is present between amacrine cells and OFF hOS RGCs, and it is less permeable to neurobiotin. The electron microscopy study described only one highly oriented amacrine cell type (Helmstaedter et al., 2013). However, Famiglietti (Famiglietti, 1989) found four basic variants of dorsally directed amacrine cells in rabbit retina. Golgi staining of one of the types showed additional neurites branches with significant deviation from vertical orientations. It is possible that such branches are selectively coupled to OFF hOS cells and provide OS inputs. Identification of the electrical synaptic partner of OFF hOS RGCs remains a target for future experiments.

Dendritic morphology and OS

There have been conflicting reports in the literature as to whether OS RGCs have dendrites aligned along the preferred orientation of the light response and whether this feature is sufficient to account for their functional OS. For a RGC with asymmetric dendrites, the simplest mechanism by which it could achieve OS is by receiving a uniform distribution of excitatory synaptic inputs from bipolar cells along their dendritic arbors so that there is greater excitation for stimuli in the preferred orientation than for stimuli in the null orientation. In rabbit retina, both symmetric and asymmetric morphologies of OS RGCs (Amthor et al., 1989; Bloomfield, 1994; Venkataramani and Taylor, 2016; 2010) and OS amacrine cells (Bloomfield, 1994;

Murphy-Baum and Taylor, 2015) have been reported. Some studies have shown a correspondence between morphology and orientation preference (Amthor et al., 1989; Bloomfield, 1994; Murphy-Baum and Taylor, 2015; Venkataramani and Taylor, 2016), while others have not (Venkataramani and Taylor, 2010). A contribution of dendritic morphology has been implicated in the computation of direction selectivity within dendritic branches of starburst amacrine cells (J. S. Kim et al., 2014; S. Lee and Zhou, 2006) and in a subtype of ON-OFF DS RGCs (Trenholm et al., 2011). However, another study reported no correspondence between asymmetric morphology and direction preference in DS RGCs (Kay et al., 2011). A recent report of two additional speed-dependent DS RGCs in the mouse retina also noted the correspondence between dendritic morphology and direction preference (Rousso et al., 2016).

We found that OFF vOS RGCs have asymmetric dendrites with respect to their somata, and that this asymmetry is aligned with the orientation preference of their responses (Fig. 4). This is opposite to the case of ON OS RGCs where the asymmetric morphology of ON hOS RGCs is correlated with functional preference and ON vOS RGCs possess symmetric dendrites (Nath and Schwartz, 2016). However, several factors argue against dendritic asymmetry as a key determinant of OS in OFF OS RGCs. First, despite similar OS responses (Fig. 2), OFF hOS RGCs displayed no dendritic asymmetry (Fig. 4). Second, even the dendrites of OFF vOS RGCs were as symmetric as those of other OFF RGCs when measured from their COM rather than from the soma (Fig. 4I). Finally, an OS mechanism based on dendritic asymmetry would presumably involve OS excitation in the RGC (Fig. 13b). We observed no excitation in OFF OS RGCs with GABAergic signaling intact (Figs. 6, 7 and 8). Instead, OS relied on current transmitted by electrical synapses (Figs. 9, 11 and 12). The functional purpose of the soma-to-

dendrites asymmetry in OFF vOS RGCs remains unresolved. It may play a role in the DS that has been observed in these cells in certain conditions (I.-J. Kim et al., 2008) or it may be related to color opponency and the dorsoventral opsin gradient (Joesch and Meister, 2016).

Unlike OFF OS RGCs, the amacrine cells we found coupled to OFF vOS RGCs had strongly oriented dendrites (Figs. 4I, 5 and 10) in agreement with previous anatomical data from rabbit (Hoshi and Mills, 2009) and reconstructions from electron microscopy in mouse (Helmstaedter et al., 2013). Therefore, while it appears not to be a major factor in the computation of OS in the RGCs themselves, dendritic asymmetry is likely to play a role in OS in the coupled amacrine cells as has been previously suggested in other OS amacrine cell types (Bloomfield, 1994; Murphy-Baum and Taylor, 2015).

The relationship between OS and other functional properties in JAM-B RGCs

Previous reports have assigned JAM-B RGCs roles in direction selectivity, and colour opponency (Joesch and Meister, 2016; I.-J. Kim et al., 2008). Direction selectivity was weak in our conditions (Fig. 3F, G). Joesch and Meister (Joesch and Meister, 2016) reported inconsistent DS in JAM-B RGCs, and DS was eliminated altogether in photopic conditions. We found that OS is consistent across cells (Fig. 1F), and stable across a large range of spatial and temporal frequencies and light levels (Fig. 3). Though JAM-B RGCs were originally identified as DS RGCs, unlike ON-OFF and ON DS RGCs, their direction selectivity comes not from tuned synaptic input, but rather from a center-surround receptive field asymmetry (Joesch and Meister, 2016; I.-J. Kim et al., 2008). Thus, unlike the more robustly DS RGCs, their DS is highly

dependent on properties of a moving stimulus that could affect center-surround interactions, like color, speed, contrast, and background luminance.

Conversely, OS in these RGCs is robust (Fig. 3) and relies not on center-surround interactions but on electrical synaptic input (Figs. 9, 11 and 13). While it is undoubtedly an over-simplification to assign each RGC as a detector of a single feature in the visual world, we have shown that the representation of orientation is much more robust in these RGCs than that of direction. Nonetheless, JAM-B RGCs can code for orientation, direction, colour, and likely even combinations of these three features in different stimulus conditions. How multiplexed signals from RGCs are routed and decoded in the rest of the visual system is a general question of great importance for future research.

Methods

Animals: Wild-type mice (C57BL/6), JAM-B CreER/Thy1-stop-YFP and Etv1-CreERT2/Ai14(tdT) transgenic mice of either sex (22 males WT, 3 males JAM-B, 1 male Etv1 and 9 females WT, 1 female JAM-B) between ages 6 weeks and 4 months were dark-adapted overnight. Animals were sacrificed following animal protocols approved by Center for Comparative Medicine (CCM), Northwestern University.

Electrophysiology: Retina dissections were conducted under IR light (940 nm) with assistance from IR visible light converter (night vision) goggles and separate IR dissection scope attachments (BE Meyers). Cardinal directions were identified using scleral landmarks (Wei et

al., 2010). Relieving cuts were made along cardinal directions and the whole retina was mounted ganglion cell side upon a 12-mm poly-D-lysine- coated glass coverslip (BioCoat Cellware, Corning), which was secured to a recording dish via grease. The dish was placed on the electrophysiology rig (SliceScope Pro 6000, Scientifica, UK) and superfused with carbogenated Ames medium (US Biological Life Sciences, A-1372-25; 9 mL per min) warmed to 32 °C. Tissue was illuminated at 950 nm for visualization. Cell attached recordings were obtained with a 2-channel patch-clamp amplifier (MultiClamp 700B, Molecular Devices) using pipettes (2–3 MΩ) filled with Ames solution. 2-photon illumination (960 nm, MaiTai HP, SpectraPhysics) was used for targeting fluorescently labelled somas in JAM-B transgenic mice retinas. For voltage-clamp experiments, pipettes (4–6 MΩ) were filled with an intracellular solution composed of (in mM): 104.7 Cs methanesulfonate, 10 TEA-Cl, 20 HEPES, 10 EGTA, 2 QX-314, 5 Mg-ATP and 0.5 Tris-GTP (~277 mOsm; pH ~7.32 with CsOH). To isolate excitatory and inhibitory synaptic inputs, each ganglion cell was held at the reversal potential for inhibition (~−60 mV) and excitation (~10 mV), respectively. Absolute voltage values were corrected for a liquid junction potential of −8.58 mV in the Cs-based intracellular solution. For calculation of E_{Cl-}, we calculated the [Cl−] in Ames (105 mM) and used the Nernst equation. It was assumed that during voltage-clamp recordings, the intracellular chloride concentration was equal to the [Cl−] in Cs internal solution. For current clamp experiments, pipettes (4–6 MΩ) were filled with an intracellular solution composed of (in mM): 125 K-aspartate, 10 KCl, 1 MgCl2, 10 HEPES, 1 CaCl2, 2 EGTA, 4 Mg-ATP and 0.5 Tris-GTP (277 mOsm; pH ~7.15 with KOH). Pharmacological reagents were purchased from Sigma-Aldrich (gabazine, strychnine, MFA,

quinine). Drug concentrations: strychnine, 1 μM; gabazine, 10 μM; MFA, 100 μM; quinine 800 μM.

Visual stimuli: A custom-designed light projection device (DLP LightCrafter, Texas Instruments) was used to display visual stimuli. All spatial stimuli patterns were displayed on a 1280 × 800 pixel array with pixel size of 2–3 μm and were focused onto the photoreceptor layer through the microscope condenser. Most experiments used blue LED illumination having peak spectral output at 450 nm. Photon flux was attenuated to suitable levels using neutral density filters (Thor Labs) and light intensity values were calibrated and measured in rhodopsin isomerizations per rod per second (R*/rod/s). During cell attached recordings, the RGC's response to horizontal and vertical bars (200 × 40 μm) across 13 locations along each axis spaced by 40 μm were measured to obtain the spatial position of receptive field (RF) center. Subsequent stimuli were delivered at the RF center. Circular spots of 200 μm diameter on dark background were used to identify light step profiles of RGCs. Spots of diameters ranging from 10–1200 μm were used to characterize the spatial dynamics of RGC responses. Moving bar stimuli consisted of rectangular bars (600 × 50 μm) moving at 1000 μm/s for 3 s across the RF of RGCs. All such stimuli were presented at 200 R*/rod/s. Full-field sine wave drifting gratings are presented from a background intensity of 500 R*/rod/s at a Weber contrast of 100% for 5 s to identify OFF OS RGCs. Spatial and temporal frequencies of drifting gratings are varied between 0.025, 0.05, 0.1 and 0.2 cycles per degree (cpd) under the approximation of 1 cycle per 30 microns on the retina, and 1, 2, 4, and 8 Hz, respectively. Dark bars were flashed from a mean illuminance level of 500 R*/rod/s. All stimuli with varying parameters were presented in pseudorandom order.

Immunohistochemistry: Tissues were fixed for 30 min in 4% paraformaldehyde (Electron Microscopy Sciences) and incubated in 0.1 M phosphate buffer (PB) overnight at 4 °C. Fixed retinas were incubated in PBS containing 3% normal donkey serum (blocking agent), 0.05% sodium azide, 0.5% Triton X-100 for 2 h. This was followed by incubation in blocking solution and primary antibody against ChAT (Millipore, AB144P, goat anti-ChAT, 1:500 v/v) for five nights at 4 °C. Afterwards, tissues were rinsed in 0.1 M PB and incubated for two nights at 4 °C with secondary antibody against goat IgG (Jackson ImmunoResearch, 711-605-152, donkey anti-goat Alexa 647, 1:500 v/v) and streptavidin (Thermo Scientific, DyLight 488, 1:500 v/v). Following immunostaining, retinas were mounted on slides with Vectashield Antifade mounting (Vector Labs) medium.

Imaging: Prior to whole-cell recordings, patch pipettes were filed with AlexaFluor 488 or AlexaFluor 568. After recording, RGC morphology was imaged using two photon microscopy (920 or 760 nm, MaiTai HP, SpectraPhysics) under a 60x water immersion objective (Olympus LUMPLan FLN 60x/1.00 NA). Emission was collected by a 520–540 nm bandpass filter.

For dendritic stratification, target RGCs were injected via patch pipettes containing Neurobiotin tracer (Vector Laboratories, SP-1150, ~3% w/v and ~280 mOsm in potassium aspartate internal solution). To improve our ability to resolve the morphology of the coupled cells, we maintained the preparation in bright light (~10^6 R*/rod/s) for 4 h after the neurobiotin fill before fixation. Light has been reported to increase coupling among RGCs and between RGCs and amacrine cells (Hu et al., 2010).

Fixed tissues were imaged on a Nikon A1R laser scanning confocal microscope mounted on a Nikon Ti ZDrive PerfectFocus microscope stand equipped with an inverted 40x and 60x oil immersion objective (Nikon Plan Apo VC 40x/60x/1.4 NA). RGC dendrites and ChAT labelling were imaged at 488 and 647 nm excitation, respectively. All confocal images were collected with spacing of 0.2 μm in the z-axis. Dendritic arbors were traced using Fiji software Simple Neurite Tracer plugin. For dendritic stratification profiles similar program and methods were used as described in (Sümbül et al., 2014).

Data analysis: The baseline firing rates of OFF OS RGCs and other OFF RGCs were calculated in a 500 ms time window before a light step and averaged across 10 epochs. Peak firing rates at light offset were calculated from peri-stimulus time histograms of light step responses. OSI, direction selectivity index and preferred orientation and direction angles were calculated based on a standard metric of the circular variance. Vector sum of the responses across orientations is given by:

$$\frac{\sum R(\theta)e^{2i\theta}}{\sum R(\theta)} \text{ for OSI and } \frac{\sum R(\theta)e^{i\theta}}{\sum R(\theta)} \text{ for DSI}$$

where R(θ) is the response for 'θ' orientation across the entire stimulus time window for both drifting gratings. Absolute amplitude gives the value of this index and the phase of the resultant complex number (or half the phase) gives the value of preferred direction/orientation.

For computing center of mass (COM), the RGC dendritic field was fitted with a polygon using a custom written Matlab script (http://www.github.com/SchwartzNU/ SymphonyAnalysis). The polygon perimeter was resampled into 1000 points and the centroid or COM was computed.

Vectors were constructed from the COM to the RGC somas and COM vector lengths and angles were measured with respect to the soma as the origin. For measuring dendritic orientation index (DOI), vectors were constructed from the centroid to the perimeter points and the vector sum calculated similarly using the above equation. Half of the complex phase of the sum gives the preferred orientation of the dendrites.

Population averaged IV curves were generated by normalizing currents across all voltages to the maximum current for each cell followed by averaging across cells. For population averages of maximum inward and minimum outward currents, the currents were normalized by the absolute value of the currents and then averaged across cells.

Spikes in current clamp recordings were removed using a sliding window average (25 ms window, 250 data points) and subthreshold oscillations were analyzed subsequently.

All electrophysiological data were analyzed with a custom open-source Matlab analysis package (http://www.github.com/SchwartzNU/SymphonyAnalysis), and figures were constructed in Igor 6.36 (Wavemetrics, Portland, OR).

Modeling: To model the membrane voltage response of OFF OS RGCs to drifting gratings, a leaky integrate-and-fire (LIF) neuronal model was used (Fig. 12). The sub-threshold voltage across the membrane is given by the differential equation:

$$\tau \frac{dV}{dt} = (V_{rest} - V(t) - RI_{ext}(t))$$

where V is the membrane voltage, V_{rest} the resting potential, R the leak resistance, and τ is the

membrane time constant. I_{ext} (t) represents the 'external' current which is equal to the sum of excitatory and inhibitory synaptic currents and is given by

$$I_{ext}(t) = I_{gj} + \left(V(t) - V_{rev,inh}\right)g_{inh}(t)$$

where I_{gj} is the gap junction current and $V_{rev,inh}$ and $g_{inh}(t)$ are the inhibitory reversal potential

and synaptic conductance respectively. The inhibitory conductance was calculated by dividing currents measured in voltage clamp by the difference between the clamped voltage and the inhibitory reversal potential. It was assumed in this model that all inhibitory currents are carried by Cl^- ions. Spiking is incorporated into the model by resetting the voltage to a constant value Vreset once it has crossed a threshold V_{th}. Following a spike, τ was increased temporarily ($\tau_{refractory}$) to mimic a refractory period. Cycle average gap junction and inhibitory currents were randomly permuted between different grating angles and bootstrapped 10000 times using a custom written MATLAB script to generate an average OSI for shuffling conditions.

Statistical Analysis: Data sets were compared using a Student's t-test (two-sided), Wilcoxon signed rank test or the Mann–Whitney U-test, Hodges-Ajne test, Hartigan's dip test with the test selected according to data structure. Statistical significance was accepted at $p < 0.05$. No statistical methods were used to predetermine sample sizes. Data collection and analysis were randomized or performed blind to the conditions of the experiments. Numerical values are presented as mean ± s.e.m.

Chapter 4. Discussion

Mouse OS cells are selective for cardinal orientations

Orientation tuning of OS cells in primary visual cortex is a continuous, fairly uniform distribution (i.e. all orientations are represented). In mouse LGN, the data are more complicated. (Marshel et al., 2012) report only horizontal OS cells in superficial dLGN, (Piscopo et al., 2013) report horizontal and vertical OS cells throughout the dLGN, and (Zhao et al., 2013) report a fairly uniform distribution of orientation selectivity in LGN. Previous MEA studies of mouse OS RGCs did not report the distribution of orientation preference. The distribution of orientation preference in SC and its relationship to the retinotopic map also remains somewhat controversial(Ahmadlou and Heimel, 2015; Feinberg and Meister, 2015).

In this context, it is an important discovery that mice have both horizontal and vertical OS cells each of ON and OFF polarities and that their distribution throughout the retina appears random (i.e. not a coordinated orientation and position map as reported in SC). While cardinal orientation selectivity has been reported in the retinas of other species(Amthor et al., 1989; He et al., 1998; Levick, 1967; Venkataramani and Taylor, 2016; 2010), the context of recent high-profile reports of OS in retino-recipient brain areas in mouse makes this a timely and crucial piece of information.

Contribution of dendritic morphology to OS computation.

This work helps to answer two key questions about the relationship between RGC dendritic morphology and function:

2A. Are oriented dendrites required for retinal OS?

There have been conflicting reports in the literature as to whether OS RGCs have dendrites aligned along the preferred orientation of the light response and whether this feature is sufficient to account for their functional OS(Amthor et al., 1989; Bloomfield, 1994; Venkataramani and Taylor, 2016; 2010). Similarly, while many ON-OFF direction selective RGCs have symmetric dendrites, at least one class of them has asymmetric dendrites pointing from the soma toward the preferred direction(Trenholm et al., 2011). We show that horizontal ON OS cells indeed have asymmetric dendrites aligned to the horizontal axis (though they also have orthogonally tuned inhibition, so the dendrites are not the whole mechanism), while vertical ON OS cells have symmetric dendrites. Moreover, analogous to horizontal ON OS, vertical OFF OS RGCs also have asymmetric dendrites along the preferred orientation. Nevertheless, OFF OS cells do not receive oriented excitation suggesting that asymmetric morphology is not necessary for OS computation. Oriented dendrites might play a role in sharpening an already existing OS tuning as in case of ON hOS RGCs.

2B. Do dendrites in the outer half of the IPL always receive input from OFF bipolar cells?

One notable exception to the segregation of ON and OFF bipolar inputs into the inner and outer halves of the IPL, respectively, is the M1 ipRGC which receives ON bipolar input in the outer (typically OFF) sublamina of the IPL. This study provides another example of this atypical outer IPL stratification, because we failed to measure any spikes or excitatory input currents at light offset in ON OS RGCs. Taken together, these findings may cause us to revise the standard picture of ON/OFF segregation in the IPL or at least appreciate that the exceptions go beyond the

M1 ipRGC which is an atypical RGC in many other ways as well.

A novel role for gap junctions in the retina.

Gap junctions are ubiquitous in all layers of the vertebrate retina. The most notable function of gap junctions in the outer retina is to establish parallel channels of signal transmission via rod-cone electrical coupling (Bloomfield and Dacheux, 2001; Raviola and Gilula, 1973). In the inner retina, information flows from the primary rod pathway to the cone circuitry via AII amacrine cell-ON cone bipolar axon electrical synapses (Kolb, 1977) which regulate the rectification of cone bipolar to On RGC synapses (Grimes et al., 2014). This is one of most immensely investigated gap junctions in the nervous system (Deans et al., 2002; Demb and Singer, 2012; Grimes et al., 2014; Han and Massey, 2005; Ke et al., 2014). Electrical synapses have also been implicated to play important roles in RGC computations such as approach sensitivity (Münch et al., 2009), lag normalization (Trenholm et al., 2013b) and motion processing (Kuo et al., 2016).

In our study, we demonstrate morphological and physiological evidence of coupling between OFF OS RGCs and amacrine cells in the INL. The currents via these gap junctions seem to be crucial for OS computation in OFF OS RGCs. Thus, we uncover yet another important role of gap junctions in the inner vertebrate retina.

Importance to the broader systems neuroscience community

Two of the central goals of systems neuroscience are (1) to describe neural computations at the level of synaptic connectivity between well-defined cell types, and (2) to trace neural circuits

through the brain and, ultimately, to behavior. This project lays the foundation for future research that can achieve these lofty goals.

A new model system for circuit computation

For over 30 years, the direction-selective (DS) circuit in the retina (particularly in the mouse retina within the last decade) has been one of the premier model systems for detailed studies of neural computation at the levels of individual cells, synapses, development, and circuits (Briggman et al., 2011; Demb, 2007; Vaney et al., 2012; Wei and Feller, 2011). Our discovery of OS circuits in the mouse retina offers a new model system in which we can ask many of the same questions. Which interneurons contribute to OS? Is selective wiring established in development? How does neuronal structure influence function? Comparisons with the canonical DS circuit will be particularly informative.

A new model system for linking defined cell types to behavior

Optogenetics and chemogenetics have opened the door to well-controlled, reversible perturbations of specific cell types in behaving animals. Essential to the success of these methods is the identification of a cell type likely to play a role in a particular task. Our identification of OS RGCs is the first step in this line of research. Future studies are underway in our lab and others (Macosko et al., 2015) promise to identify molecular markers for each RGC type. Soon we will be able to activate or silence ON and OFF OS RGCs to determine how this retinal OS pathway influences perception and behavior.

References

Ackert, J.M., Wu, S.H., Lee, J.C., Abrams, J., Hu, E.H., Perlman, I., Bloomfield, S.A., 2006. Light-induced changes in spike synchronization between coupled ON direction selective ganglion cells in the mammalian retina. J. Neurosci. 26, 4206–4215.

Adorján, P., Levitt, J.B., Lund, J.S., Obermayer, K., 1999. A model for the intracortical origin of orientation preference and tuning in macaque striate cortex. Vis. Neurosci. 16, 303–318.

Ahmadlou, M., Heimel, J.A., 2015. Preference for concentric orientations in the mouse superior colliculus. Nat Commun 6, 6773.

Akrouh, A., Kerschensteiner, D., 2013. Intersecting circuits generate precisely patterned retinal waves. Neuron 79, 322–334.

Ala-Laurila, P., Greschner, M., Chichilnisky, E.J., Rieke, F., 2011. Cone photoreceptor contributions to noise and correlations in the retinal output. Nat Neurosci 14, 1309–1316.

Amthor, F.R., Takahashi, E.S., Oyster, C.W., 1989. Morphologies of rabbit retinal ganglion cells with complex receptive fields. J. Comp. Neurol. 280, 97–121.

Antinucci, P., Nikolaou, N., Meyer, M.P., Hindges, R., 2013. Teneurin-3 Specifies Morphological and Functional Connectivity of Retinal Ganglion Cells in the Vertebrate Visual System. Cell Reports 5, 582–592.

Antinucci, P., Suleyman, O., Monfries, C., Hindges, R., 2016. Neural Mechanisms Generating Orientation Selectivity in the Retina. Current Biology 26, 1802–1815.

Apostolides, P.F., Trussell, L.O., 2013. Regulation of interneuron excitability by gap junction coupling with principal cells. Nat Neurosci 16, 1764–1772.

Badea, T.C., Nathans, J., 2004. Quantitative analysis of neuronal morphologies in the mouse retina visualized by using a genetically directed reporter. J. Comp. Neurol. 480, 331–351.

Baden, T., Berens, P., Franke, K., Román Rosón, M., Bethge, M., Euler, T., 2016. The functional diversity of retinal ganglion cells in the mouse. Nature 529, 345–350.

Bae, J.A., Mu, S., Kim, J.S., Turner, N.L., Tartavull, I., Kemnitz, N., Jordan, C.S., Norton, A.D., Silversmith, W.M., Prentki, R., Sorek, M., David, C., Jones, D.L., Bland, D., Sterling, A.L.R., Park, J., Briggman, K.L., Seung, H.S., the EyeWirers, 2017. Digital museum of retinal ganglion cells with dense anatomy and physiology. bioRxiv 182758.

Ben-Yishai, R., Bar-Or, R.L., Sompolinsky, H., 1995. Theory of orientation tuning in visual cortex. Proceedings of the National Academy of Sciences 92, 3844–3848.

Ben-Yishai, R., Hansel, D., Sompolinsky, H., 1997. Traveling waves and the processing of weakly tuned inputs in a cortical network module. J Comput Neurosci 4, 57–77.

Berntson, A., Taylor, W.R., 2000. Response characteristics and receptive field widths of on-bipolar cells in the mouse retina. The Journal of Physiology 524, 879–889.

Bickford, M.E., Zhou, N., Krahe, T.E., Govindaiah, G., Guido, W., 2015. Retinal and Tectal "Driver-Like" Inputs Converge in the Shell of the Mouse Dorsal Lateral Geniculate Nucleus. J. Neurosci. 35, 10523–10534.

Blasdel, G.G., Salama, G., 1986. Voltage-sensitive dyes reveal a modular organization in monkey striate cortex. Nature 321, 579–585.

Bloomfield, S.A., 1994. Orientation-sensitive amacrine and ganglion cells in the rabbit retina. Journal of Neurophysiology 71, 1672–1691.

Bloomfield, S.A., 1991. Two types of orientation-sensitive responses of amacrine cells in the mammalian retina. Nature 350, 347–350.

Bloomfield, S.A., Völgyi, B., 2009. The diverse functional roles and regulation of neuronal gap junctions in the retina. Nat Rev Neurosci 10, 495–506.

Bonds, A.B., 1989. Role of inhibition in the specification of orientation selectivity of cells in the cat striate cortex. Vis. Neurosci. 2, 41–55.

Briggman, K.L., Helmstaedter, M., Denk, W., 2011. Wiring specificity in the direction-selectivity circuit of the retina. Nature 471, 183–188.

Brivanlou, I.H., Warland, D.K., Meister, M., 1998. Mechanisms of Concerted Firing among Retinal Ganglion Cells. Neuron 20, 527–539.

Caldwell, J.H., Daw, N.W., 1978. Effects of picrotoxin and strychnine on rabbit retinal ganglion cells: changes in centre surround receptive fields. The Journal of Physiology 276, 1–12. doi:10.1113/jphysiol.1978.sp012234

Chapman, B., Zahs, K.R., Stryker, M.P., 1991. Relation of cortical cell orientation selectivity to alignment of receptive fields of the geniculocortical afferents that arborize within a single orientation column in ferret visual cortex. Journal of Neuroscience 11, 1347–1358.

Chen, C., Regehr, W.G., 2000. Developmental remodeling of the retinogeniculate synapse. Neuron 28, 955–966.

Chen, H., Liu, X., Tian, N., 2014. Subtype-dependent postnatal development of direction- and orientation-selective retinal ganglion cells in mice. Journal of Neurophysiology 112, 2092–2101.

Cheong, S.K., Tailby, C., Solomon, S.G., Martin, P.R., 2013. Cortical-like receptive fields in the lateral geniculate nucleus of marmoset monkeys. J. Neurosci. 33, 6864–6876.

Christie, J.M., Westbrook, G.L., 2006. Lateral excitation within the olfactory bulb. J. Neurosci. 26, 2269–2277.

Coombs, J., van der List, D., Wang, G.Y., Chalupa, L.M., 2006. Morphological properties of mouse retinal ganglion cells. Neuroscience 140, 123–136.

Crook, J.M., Kisvárday, Z.F., Eysel, U.T., 1997. GABA-induced inactivation of functionally characterized sites in cat striate cortex: effects on orientation tuning and direction selectivity. Vis. Neurosci. 14, 141–158.

Cruz-Martín, A., El-Danaf, R.N., Osakada, F., Sriram, B., Dhande, O.S., Nguyen, P.L., Callaway, E.M., Ghosh, A., Huberman, A.D., 2014. A dedicated circuit links direction-selective retinal ganglion cells to the primary visual cortex. Nature 507, 358–361.

Damjanović, I., Maximova, E., Maximov, P., Maximov, V., 2012. Cardinal difference between the orientation-selective retinal ganglion cells projecting to the fish tectum and the orientation-selective complex cells of the mammalian striate cortex. Journal of Integrative Neuroscience 11, 169–182.

Damjanović, I., Maximova, E., Maximov, V., 2011. On The Organization Of Receptive Fields Of Orientation-Selective Units Recorded In The Fish Tectum. Journal of Integrative Neuroscience 08, 323–344.

Demb, J.B., 2007. Cellular Mechanisms for Direction Selectivity in the Retina. Neuron 55, 179–186.

Detwiler, P.B., Hodgkin, A.L., 1979. Electrical coupling between cones in turtle retina. The Journal of Physiology 291, 75–100.

DeVries, S.H., 1999. Correlated firing in rabbit retinal ganglion cells. Journal of Neurophysiology 81, 908–920.

DeVries, S.H., Qi, X., Smith, R., Makous, W., Sterling, P., 2002. Electrical coupling between mammalian cones. Curr. Biol. 12, 1900–1907.

Ding, H., Smith, R.G., Poleg-Polsky, A., Diamond, J.S., and Briggman, K.L., 2016. Species-specific wiring for direction selectivity in the mammalian retina. Nature 535, 105–110.

Doi, M., Uji, Y., Yamamura, H., 1995. Morphological classification of retinal ganglion cells in mice. J. Comp. Neurol. 356, 368–386.

Elyada, Y.M., Haag, J., Borst, A., 2009. Different receptive fields in axons and dendrites underlie robust coding in motion-sensitive neurons. Nat Neurosci 12, 327–332.

Euler, T., Detwiler, P.B., Denk, W., 2002. Directionally selective calcium signals in dendrites of starburst amacrine cells. Nature 418, 845–852.

Eysel, U.T., Crook, J.M., Machemer, H.F., 1990. GABA-induced remote inactivation reveals cross-orientation inhibition in the cat striate cortex. Exp Brain Res 80, 626–630.

Famiglietti, E. V. in Neurobiology of the Inner Retina (eds Weiler, R. & Osborne, N. N.). 169–180 (Springer, Berlin, 1989).

Farajian, R., Pan, F., Akopian, A., Völgyi, B., Bloomfield, S.A., 2011. Masked excitatory crosstalk between the ON and OFF visual pathways in the mammalian retina. The Journal of Physiology 589, 4473–4489.

Farrow, K., Masland, R.H., 2011. Physiological clustering of visual channels in the mouse retina 105, 1516–1530.

Feinberg, E.H., Meister, M., 2015. Orientation columns in the mouse superior colliculus. Nature 519, 229–232.

Ferster, D., 1987. Origin of orientation-selective EPSPs in simple cells of cat visual cortex. Journal of Neuroscience 7, 1780–1791.

Ferster, D., Chung, S., Wheat, H., 1996. Orientation selectivity of thalamic input to simple cells of cat visual cortex. Nature 380, 249–252.

Ferster, D., Koch, C., 1987. Neuronal connections underlying orientation selectivity in cat visual cortex. Trends in Neurosciences 10, 487–492.

Fried, S.I., Münch, T.A., Werblin, F.S., 2002. Mechanisms and circuitry underlying directional selectivity in the retina. Nature 420, 411–414.

Galarreta, M., Hestrin, S., 2001. Electrical synapses between GABA-releasing interneurons. Nat Rev Neurosci 2, 425–433.

Greene, M.J., Kim, J.S., Seung, H.S., and EyeWirers. (2016). Analogous Convergence of Sustained and Transient Inputs in Parallel On and Off Pathways for Retinal Motion Computation. Cell Rep. 14, 1892–1900.

Grimes, W.N., 2012. Amacrine cell-mediated input to bipolar cells: Variations on a common mechanistic theme. Vis. Neurosci. 29, 41–49.

Hansel, D., Sompolinsky, H., 1996. Chaos and synchrony in a model of a hypercolumn in visual cortex. J Comput Neurosci 3, 7–34.

Hartline, H.K., 1940. The Receptive Fields Of Optic Nerve Fibers. American Journal of Physiology-Legacy Content 130, 690–699.

He, S., Levick, W.R., Vaney, D.I., 1998. Distinguishing direction selectivity from orientation selectivity in the rabbit retina. Vis. Neurosci. 15, 439–447.

Helmstaedter, M., Briggman, K.L., Turaga, S.C., Jain, V., Seung, H.S., Denk, W., 2013. Connectomic reconstruction of the inner plexiform layer in the mouse retina. Nature 500, 168–174.

Herberholz, J., Antonsen, B.L., Edwards, D.H., 2002. A lateral excitatory network in the escape circuit of crayfish. J. Neurosci. 22, 9078–9085.

Hoshi, H., Mills, S.L., 2009. Components and properties of the G3 ganglion cell circuit in the rabbit retina. J. Comp. Neurol. 513, 69–82.

Hu, E.H., Bloomfield, S.A., 2003. Gap junctional coupling underlies the short-latency spike synchrony of retinal alpha ganglion cells. J. Neurosci. 23, 6768–6777.

Hu, E.H., Pan, F., Völgyi, B., Bloomfield, S.A., 2010. Light increases the gap junctional coupling of retinal ganglion cells. The Journal of Physiology 588, 4145–4163.

Hubel, D.H., Wiesel, T.N., 1974. Sequence regularity and geometry of orientation columns in the monkey striate cortex. J. Comp. Neurol. 158, 267–293.

Hubel, D.H., Wiesel, T.N., 1968. Receptive fields and functional architecture of monkey striate cortex. The Journal of Physiology 195, 215–243.

Hubel, D.H., Wiesel, T.N., 1962. Receptive fields, binocular interaction and functional architecture in the cat's visual cortex. The Journal of Physiology 160, 106–154.

Hunter, P.R., Lowe, A.S., Thompson, I.D., Meyer, M.P., 2013. Emergent properties of the optic tectum revealed by population analysis of direction and orientation selectivity. J. Neurosci. 33, 13940–13945.

Jacoby, J., Zhu, Y., DeVries, S.H., Schwartz, G.W., 2015. An Amacrine Cell Circuit for Signaling Steady Illumination in the Retina. Cell Reports 13, 2663–2670.

Jia, H., Rochefort, N.L., Chen, X., Konnerth, A., 2010. Dendritic organization of sensory input to cortical neurons in vivo. Nature 464, 1307–1312.

Joesch, M., Meister, M., 2016. A neuronal circuit for colour vision based on rod-cone opponency. Nature 532, 236–239.

Johnston, J., Ding, H., Seibel, S.H., Esposti, F., Lagnado, L., 2014. Rapid mapping of visual receptive fields by filtered back-projection: application to multi-neuronal electrophysiology and imaging. The Journal of Physiology 592, 4839–4854.

Johnston, J., Lagnado, L., 2015. General features of the retinal connectome determine the computation of motion anticipation. Elife 4, e06250.

Kay, J.N., la Huerta, De, I., Kim, I.J., Zhang, Y., Yamagata, M., Chu, M.W., Meister, M., Sanes, J.R., 2011. Retinal Ganglion Cells with Distinct Directional Preferences Differ in Molecular Identity, Structure, and Central Projections. Journal of Neuroscience 31, 7753–7762.

Kier, C.K., Buchsbaum, G., Sterling, P., 1995. How retinal microcircuits scale for ganglion cells of different size. Journal of Neuroscience 15, 7673–7683.

Kim, I.-J., Zhang, Y., Yamagata, M., Meister, M., Sanes, J.R., 2008. Molecular identification of a retinal cell type that responds to upward motion. Nature 452, 478–482.

Kim, J.S., Greene, M.J., Zlateski, A., Lee, K., Richardson, M., Turaga, S.C., Purcaro, M., Balkam, M., Robinson, A., Behabadi, B.F., Campos, M., Denk, W., Seung, H.S., EyeWirers, 2014. Space-time wiring specificity supports direction selectivity in the retina. Nature 509, 331–336.

Kong, J.-H., Fish, D.R., Rockhill, R.L., Masland, R.H., 2005. Diversity of ganglion cells in the mouse retina: Unsupervised morphological classification and its limits. J. Comp. Neurol. 489, 293–310.

Kuffler, S.W., 1953. Discharge patterns and functional organization of mammalian retina. Journal of Neurophysiology 16, 37–68.

Kuo, S.P., Schwartz, G.W., Rieke, F., 2016. Nonlinear Spatiotemporal Integration by Electrical and Chemical Synapses in the Retina. Neuron 90, 320–332.

Lee, S., Chen, L., Chen, M., Ye, M., SEAL, R.P., Zhou, Z.J., 2014. An Unconventional Glutamatergic Circuit in the Retina Formed by vGluT3 Amacrine Cells. Neuron 84, 708–715.

Lee, S., Kim, K., Zhou, Z.J., 2010. Role of ACh-GABA cotransmission in detecting image motion and motion direction. Neuron 68, 1159–1172.

Lee, S., Zhou, Z.J., 2006. The synaptic mechanism of direction selectivity in distal processes of starburst amacrine cells. Neuron 51, 787–799.

Lee, S.-H., Kwan, A.C., Zhang, S., Phoumthipphavong, V., Flannery, J.G., Masmanidis, S.C., Taniguchi, H., Huang, Z.J., Zhang, F., Boyden, E.S., Deisseroth, K., Dan, Y., 2012. Activation of specific interneurons improves V1 feature selectivity and visual perception. Nature 488, 379–383.

Levick, W.R., 1967. Receptive fields and trigger features of ganglion cells in the visual streak of the rabbits retina. The Journal of Physiology 188, 285–307.

Levick, W.R., Thibos, L.N., 1982. Analysis of orientation bias in cat retina. The Journal of Physiology 329, 243–261.

Levick, W.R., Thibos, L.N., 1980. Orientation bias of cat retinal ganglion cells. Nature 286, 389–390.

Lien, A.D., Scanziani, M., 2013. Tuned thalamic excitation is amplified by visual cortical circuits. Nature Neuroscience 16, 1315–1323.

Lowe, A.S., Nikolaou, N., Hunter, P.R., Thompson, I.D., Meyer, M.P., 2013. A systems-based dissection of retinal inputs to the zebrafish tectum reveals different rules for different functional classes during development. J. Neurosci. 33, 13946–13956.

Mani, A., Schwartz, G.W., 2017. Circuit Mechanisms of a Retinal Ganglion Cell with Stimulus-Dependent Response Latency and Activation Beyond Its Dendrites. Curr. Biol.

Marshel, J.H., Kaye, A.P., Nauhaus, I., Callaway, E.M., 2012. Anterior-Posterior Direction Opponency in the Superficial Mouse Lateral Geniculate Nucleus. Neuron 76, 713–720.

Martersteck, E.M., Hirokawa, K.E., Evarts, M., Bernard, A., Duan, X., Li, Y., Ng, L., Oh, S.W., Ouellette, B., Royall, J.J., et al., 2017. Diverse Central Projection Patterns of Retinal Ganglion Cells. Cell Reports 18, 2058–2072.

Mastronarde, D.N., 1983. Interactions between ganglion cells in cat retina. Journal of Neurophysiology 49, 350–365.

Maturana, H.R., Frenk, S., 1963. Directional Movement And Horizontal Edge Detectors In The Pigeon Retina. Science 142, 977–979.

Livingstone, M.S., 1998. Mechanisms of Direction Selectivity in Macaque V1. Neuron 20, 509–526.

Murphy, G.J., Rieke, F., 2011. Electrical synaptic input to ganglion cells underlies differences in the output and absolute sensitivity of parallel retinal circuits. J. Neurosci. 31, 12218–12228.

Murphy-Baum, B.L., Taylor, W.R., 2015. The Synaptic and Morphological Basis of Orientation Selectivity in a Polyaxonal Amacrine Cell of the Rabbit Retina. J. Neurosci. 35, 13336–13350.

Nath, A., Schwartz, G.W., 2017. Electrical synapses convey orientation selectivity in the mouse retina. Nat Commun 8, 2025.

Nath, A., Schwartz, G.W., 2016. Cardinal Orientation Selectivity Is Represented by Two Distinct Ganglion Cell Types in Mouse Retina. J. Neurosci. 36, 3208–3221.

Neumann, S., Hüser, L., Ondreka, K., Auler, N., Haverkamp, S., 2016. Cell type-specific bipolar cell input to ganglion cells in the mouse retina. Neuroscience 316, 420–432.

Niell, C.M., Stryker, M.P., 2008. Highly selective receptive fields in mouse visual cortex. J. Neurosci. 28, 7520–7536.

Oesch, N., Euler, T., Taylor, W.R., 2005. Direction-Selective Dendritic Action Potentials in Rabbit Retina. Neuron 47, 739–750.

Oyster, C.W., Barlow, H.B., 1967. Direction-Selective Units in Rabbit Retina: Distribution of Preferred Directions. Science 155, 841–842.

Pan, F., Mills, S.L., Massey, S.C., 2007. Screening of gap junction antagonists on dye coupling in the rabbit retina. Vis. Neurosci. 24, 609–618.

Nikolaou, N., Lowe, A.S., Walker, A.S., Abbas, F., Hunter, P.R., Thompson, I.D., and Meyer, M.P., 2012. Parametric Functional Maps of Visual Inputs to the Tectum. Neuron 76, 317–324.

Atallah, B.V., Bruns, W., Carandini, M., and Scanziani, M., 2012. Parvalbumin-Expressing Interneurons Linearly Transform Cortical Responses to Visual Stimuli. Neuron 73, 159–170.

Passaglia, C.L., Troy, J.B., Rüttiger, L., Lee, B.B., 2002. Orientation sensitivity of ganglion cells in primate retina. Vision Research 42, 683–694.

Pearson, J.T., Kerschensteiner, D., 2015. Ambient illumination switches contrast preference of specific retinal processing streams. Journal of Neurophysiology 114, 540–550.

Pei, Z., Chen, Q., Koren, D., Giammarinaro, B., Acaron Ledesma, H., Wei, W., 2015. Conditional Knock-Out of Vesicular GABA Transporter Gene from Starburst Amacrine Cells Reveals the Contributions of Multiple Synaptic Mechanisms Underlying Direction Selectivity in the Retina. J. Neurosci. 35, 13219–13232.

Pereda, A.E., 2014. Electrical synapses and their functional interactions with chemical synapses. Nat Rev Neurosci 15, 250–263.

Pereda, A.E., Bell, T.D., Faber, D.S., 1995. Retrograde synaptic communication via gap junctions coupling auditory afferents to the Mauthner cell. Journal of Neuroscience 15, 5943–5955.

Perry, V.H., Oehler, R., Cowey, A., 1984. Retinal ganglion cells that project to the dorsal lateral geniculate nucleus in the macaque monkey. Neuroscience 12, 1101–1123.

Pfleger, B., Bonds, A.B., 1995. Dynamic differentiation of GABAA-sensitive influences on orientation selectivity of complex cells in the cat striate cortex. Exp Brain Res 104, 81–88.

Piscopo, D.M., El-Danaf, R.N., Huberman, A.D., Niell, C.M., 2013. Diverse Visual Features Encoded in Mouse Lateral Geniculate Nucleus. Journal of Neuroscience 33, 4642–4656.

Reid, R.C., Alonso, J.M., 1995. Specificity of monosynaptic connections from thalamus to visual cortex. Nature 378, 281–284.

Rodieck, R.W., 1991. The density recovery profile: a method for the analysis of points in the plane applicable to retinal studies. Vis. Neurosci. 6, 95–111.

Rompani, S.B., Mu€llner, F.E., Wanner, A., Zhang, C., Roth, C.N., Yonehara, K., and Roska, B. (2017). Different Modes of Visual Integration in the Lateral Geniculate Nucleus Revealed by Single-Cell-Initiated Transsynaptic Tracing. Neuron 93, 767–776.e6.

Rousso, D.L., Qiao, M., Kagan, R.D., Yamagata, M., Palmiter, R.D., Sanes, J.R., 2016. Two Pairs of ON and OFF Retinal Ganglion Cells Are Defined by Intersectional Patterns of Transcription Factor Expression. Cell Reports 15, 1930–1944.

Sanes, J.R., Masland, R.H., 2015. The Types of Retinal Ganglion Cells: Current Status and Implications for Neuronal Classification. Annu. Rev. Neurosci. 38, 221–246.

Santina, L.D., Kuo, S.P., Yoshimatsu, T., Okawa, H., Suzuki, S.C., Hoon, M., Tsuboyama, K., Rieke, F., and Wong, R.O.L., 2016. Glutamatergic monopolar interneurons provide a novel pathway of excitation in the mouse retina. Curr. Biol. 26, 2070–2077.

Schwartz, G.W., Okawa, H., Dunn, F.A., Morgan, J.L., Kerschensteiner, D., Wong, R.O., Rieke, F., 2012. The spatial structure of a nonlinear receptive field. Nat Neurosci 15, 1572–1580.

Sclar, G., Freeman, R.D., 1982. Orientation selectivity in the cat's striate cortex is invariant with stimulus contrast. Exp Brain Res 46, 457–461.

Sernagor, E., Grzywacz, N.M., 1995. Emergence of complex receptive field properties of ganglion cells in the developing turtle retina. Journal of Neurophysiology 73, 1355–1364.

Sheffield, M.E.J., Best, T.K., Mensh, B.D., Kath, W.L., 2011. Slow integration leads to persistent action potential firing in distal axons of coupled interneurons. Nat Neurosci 14, 200–207.

Shlens, J., Rieke, F., Chichilnisky, E.J., 2008. Synchronized firing in the retina. Current Opinion in Neurobiology 18, 396–402.

Shou, T., Leventhal, A.G., Thompson, K.G., Zhou, Y., 1995. Direction biases of X and Y type retinal ganglion cells in the cat. Journal of Neurophysiology 73, 1414–1421.

Sillito, A.M., 1975. The contribution of inhibitory mechanisms to the receptive field properties of neurones in the striate cortex of the cat. The Journal of Physiology 250, 305–329.

Sillito, A.M., Kemp, J.A., Patel, H., 1980. Inhibitory interactions contributing to the ocular dominance of monocularly dominated cells in the normal cat striate cortex. Exp Brain Res 41, 1–10.

Sivyer, B., Taylor, W.R., Vaney, D.I., 2010. Uniformity detector retinal ganglion cells fire complex spikes and receive only light-evoked inhibition. Proc. Natl. Acad. Sci. U.S.A. 107, 5628–5633.

Skottun, B.C., Bradley, A., Sclar, G., Ohzawa, I., Freeman, R.D., 1987. The effects of contrast on visual orientation and spatial frequency discrimination: a comparison of single cells and behavior. Journal of Neurophysiology 57, 773–786.

Smith, E.L., Chino, Y.M., Ridder, W.H., Kitagawa, K., Langston, A., 1990. Orientation bias of neurons in the lateral geniculate nucleus of macaque monkeys. Vis. Neurosci. 5, 525–545.

Somers, D.C., Nelson, S.B., Sur, M., 1995. An emergent model of orientation selectivity in cat visual cortical simple cells. Journal of Neuroscience 15, 5448–5465.

Srinivas, M., Hopperstad, M.G., Spray, D.C., 2001. Quinine blocks specific gap junction channel subtypes. Proceedings of the National Academy of Sciences 98, 10942–10947.

Sun, W., Li, N., He, S., 2002. Large-scale morphological survey of mouse retinal ganglion cells. J. Comp. Neurol. 451, 115–126.

Sümbül, U., Song, Sen, McCulloch, K., Becker, M., Bin Lin, Sanes, J.R., Masland, R.H., Seung, H.S., 2014. A genetic and computational approach to structurally classify neuronal types. Nat Commun 5, 3512.

Swindale, N.V., Shoham, D., Grinvald, A., Bonhoeffer, T., Hübener, M., 2000. Visual cortex maps are optimized for uniform coverage. Nat Neurosci 3, 822–826.

Tanaka, K., 1985. Organization of geniculate inputs to visual cortical cells in the cat. Vision Research 25, 357–364.

Tanaka, K., 1983. Cross-correlation analysis of geniculostriate neuronal relationships in cats. Journal of Neurophysiology 49, 1303–1318.

Trenholm, S., Johnson, K., Li, X., Smith, R.G., Awatramani, G.B., 2011. Parallel Mechanisms Encode Direction in the Retina. Neuron 71, 683–694.

Trenholm, S., McLaughlin, A.J., Schwab, D.J., Awatramani, G.B., 2013a. Dynamic Tuning of Electrical and Chemical Synaptic Transmission in a Network of Motion Coding Retinal Neurons. Journal of Neuroscience 33, 14927–14938.

Trenholm, S., Schwab, D.J., Balasubramanian, V., Awatramani, G.B., 2013b. Lag normalization in an electrically coupled neural network. Nat Neurosci 16, 154–156.

Tsumoto, T., Eckart, W., Creutzfeldt, O.D., 1979. Modification of orientation sensitivity of cat visual cortex neurons by removal of GABA-mediated inhibition. Exp Brain Res 34, 351–363.

Vaney, D.I., 1991. Many diverse types of retinal neurons show tracer coupling when injected with biocytin or Neurobiotin. Neuroscience Letters 125, 187–190.

Vaney, D.I., Sivyer, B., Taylor, W.R., 2012. Direction selectivity in the retina: symmetry and asymmetry in structure and function. Nat Rev Neurosci 13, 194–208.

Venkataramani, S., Taylor, W.R., 2016. Synaptic Mechanisms Generating Orientation Selectivity in the ON Pathway of the Rabbit Retina. J. Neurosci. 36, 3336–3349.

Venkataramani, S., Taylor, W.R., 2010. Orientation selectivity in rabbit retinal ganglion cells is mediated by presynaptic inhibition. J. Neurosci. 30, 15664–15676.

Veruki, M.L., Hartveit, E., 2009. Meclofenamic acid blocks electrical synapses of retinal AII amacrine and on-cone bipolar cells. Journal of Neurophysiology 101, 2339–2347.

Vervaeke, K., Lorincz, A., Nusser, Z., Silver, R.A., 2012. Gap junctions compensate for sublinear dendritic integration in an inhibitory network. Science 335, 1624–1628.

Vidyasagar, T.R., 1984. Contribution of inhibitory mechanisms to the orientation sensitivity of cat dLGN Neurones. Exp Brain Res 55, 192–195.

Vidyasagar, T.R., Urbas, J.V., 1982. Orientation sensitivity of cat LGN neurones with and without inputs from visual cortical areas 17 and 18. Exp Brain Res 46, 157–169.

Vlasits, A.L., Bos, R., Morrie, R.D., Fortuny, C., Flannery, J.G., Feller, M.B., Rivlin-Etzion, M., 2014. Visual stimulation switches the polarity of excitatory input to starburst amacrine cells. Neuron 83, 1172–1184.

Völgyi, B., Abrams, J., Paul, D.L., Bloomfield, S.A., 2005. Morphology and tracer coupling pattern of alpha ganglion cells in the mouse retina. J. Comp. Neurol. 492, 66–77.

Völgyi, B., Chheda, S., Bloomfield, S.A., 2009. Tracer coupling patterns of the ganglion cell subtypes in the mouse retina. J. Comp. Neurol. 512, 664–687.

Völgyi, B., Pan, F., Paul, D.L., Wang, J.T., Huberman, A.D., Bloomfield, S.A., 2013. Gap junctions are essential for generating the correlated spike activity of neighboring retinal ganglion cells. PLoS ONE 8, e69426.

Wagner, H.J., Wagner, E., 1988. Amacrine cells in the retina of a teleost fish, the roach (Rutilus rutilus): a Golgi study on differentiation and layering. Philosophical Transactions of the Royal Society B: Biological Sciences 321, 263–324.

Wang, L., Sarnaik, R., Rangarajan, K., Liu, X., Cang, J., 2010. Visual Receptive Field Properties of Neurons in the Superficial Superior Colliculus of the Mouse. Journal of Neuroscience 30, 16573–16584.

Wassle, H., Peichl, L., Boycott, B.B., 1981. Dendritic territories of cat retinal ganglion cells. Nature 292, 344–345.

Wassle, H., Puller, C., Muller, F., Haverkamp, S., 2009. Cone Contacts, Mosaics, and Territories of Bipolar Cells in the Mouse Retina. Journal of Neuroscience 29, 106–117.

Wei, W., Elstrott, J., Feller, M.B., 2010. Two-photon targeted recording of GFP-expressing neurons for light responses and live-cell imaging in the mouse retina. Nat Protoc 5, 1347–1352.

Weliky, M., Bosking, W.H., Fitzpatrick, D., 1996. A systematic map of direction preference in primary visual cortex. Nature 379, 725–728.

White, A.J., Wilder, H.D., Goodchild, A.K., Sefton, A.J., Martin, P.R., 1998. Segregation of receptive field properties in the lateral geniculate nucleus of a New-World monkey, the marmoset Callithrix jacchus. Journal of Neurophysiology 80, 2063–2076.

Xin, D., Bloomfield, S.A., 1997. Tracer coupling pattern of amacrine and ganglion cells in the rabbit retina. J. Comp. Neurol. 383, 512–528.

Xu, X., Ichida, J., Shostak, Y., Bonds, A.B., Casagrande, V.A., 2002. Are primate lateral geniculate nucleus (LGN) cells really sensitive to orientation or direction? Vis. Neurosci. 19, 97–108.

Yacoub, E., Harel, N., Ugurbil, K., 2008. High-field fMRI unveils orientation columns in humans. Proc. Natl. Acad. Sci. U.S.A. 105, 10607–10612.

Yonehara, K., Balint, K., Noda, M., Nagel, G., Bamberg, E., Roska, B., 2011. Spatially asymmetric reorganization of inhibition establishes a motion-sensitive circuit. Nature 469, 407–410.

Zhang, C., McCall, M.A., 2012. Receptor targets of amacrine cells. Vis. Neurosci. 29, 11–29.

Zhao, X., Chen, H., Liu, X., Cang, J., 2013. Orientation-selective Responses in the Mouse Lateral Geniculate Nucleus. Journal of Neuroscience 33, 12751–12763.